Characterization of the Human Plasma Macrolipidome using Standard Reference Material 1950 – Metabolites in frozen human plasma

by

Klaudia Elisabeth Steckel

A thesis

presented to the University of Waterloo

in fulfillment of the

thesis requirement for the degree of

Master of Science

in

Kinesiology

Waterloo, Ontario, Canada, 2021

Author's Declaration

This thesis consists of material all of which I authored or co-authored: see Statement of Contributions included in the thesis. This is a true copy of the thesis, including any required final revisions, as accepted by my examiners.

I understand that my thesis may be made electronically available to the public

Statement of Contributions

The experiment was designed by the author of this thesis, Klaudia Steckel with feedback from Dr. Ken Stark. Samples were analysed on the quadrupole time of flight and quadrupole orbitrap mass spectrometry platforms at the University of Waterloo Mass Spectrometry Facility by Dr. Juan Jose Aristizabal Henao. The sample was also shipped to Bruker Daltonics in Billerica, MA USA and analyzed on the trapped ion mobility-quadrupole-time of flight mass spectrometry platform by Dr. Heino Heyman with assistance from Dr. Xuejun Peng. The raw mass spectrometry data was processed and analysed by the author of this thesis, Klaudia Steckel.

Abstract

Standard Reference Material (SRM) 1950 Metabolites in frozen human plasma is a pooled plasma sample created by the National Institute of Standards and Technology (NIST) to be representative of plasma from the population of the United States of America. Attempts to characterize the lipidome of SRM 1950 have been done mainly at the sum compositional or "brutto" level but fatty acyl compositional or "medio" level information is limited. The "medio" level of information of lipids is necessary to link biological lipids to dietary intakes of fatty acids. An untargeted approach (data dependent acquisition) to characterize lipids of high abundance (the macrolipidome) in SRM 1950 at the medio level was used across three ultra-high performance liquid chromatography tandem mass spectrometers that included a Quadrupole-Orbitrap (qOrbi), a Quadrupole-Time of Flight (QToF) and a Trapped Ion Mobility Spectrometry-Quadrupole-Time of Flight (timsToF). Both positive and negative electrospray ionization modes were used in each instrument. Unique medio level characterizations were completed for 120 lipids in the qOrbi, 130 in the QToF and 108 in the timsToF across positive and negative polarity analyses. Quantitation of the top 20 medio lipids showed similar trends across the three platforms and represented 59% of the lipidome in the qOrbi and timsToF and 51% in the QToF. Phosphatidylcholine was consistently identified as the lipid class with the highest abundance, with a minimum of 20% abundance. Cholesterol ester 18:2 was consistently the lipid of highest concentration, with phosphatidylcholine 16:0_18:2 as the glycerophospholipid of highest concentration. The most concentrated triacylglycerol (TG) was TG 16:0_18:1_18:2 in the timsToF or TG 16:0_18:1_18:1 in the QToF while in the qOrbi there was coelution for both these TG species (isomers containing 16:1). Concentrations of lipids determined across the platforms were relatively similar although several of the concentrations

determined with the QToF platform were lower in positive polarity. The medio level lipidomic characterization of SRM 1950 provides information on the fatty acyl composition of the most abundant lipid species in human plasma that can serve as a reference for future studies. Specifically, the lipids identified can be used for the development of mass spectrometry inclusions lists to develop routine targeted analyses of plasma to enable nutritional insights into the effects on health and disease on lipid metabolism in clinical studies.

Acknowledgements

I would like to start by thanking my supervisor, Dr. Ken Stark for his guidance and time over the past two years. Besides all the lipidomic knowledge I have gained, you have taught me how to be more confident in my abilities.

I would also like to thank my committee members, Dr. Robin Duncan and Dr. Michaela Devries-Aboud for their support. I also have Dr. Robin Duncan to thank for introducing me to the Stark lab. I would also like to thank Dr. Richard Smith for all of my mass spec training.

This project would not have been possible without the contributions from Dr. Juan Jose Arisitizabal Henao and his continued eagerness to help me even when in a different country. This project would also not have been completed without the knowledge and support of Dan Chalil. Thank you for always being there, regardless of the time. I would also like to thank the Duncan lab for making my time more enjoyable.

Lastly, I would like to thank my friends and family, meine Mama und Papa, Karl, Dylan and of course Felix. I could not have done it without you.

Table of Contents

List of Figures

List of Tables

List of Abbreviations

APCI - atmospheric pressure chemical ionization
CE - collisional energy OR cholesterol ester
CER - ceramide
CCS - collisional cross section
CM - chylomicron
DAG - diacylglycerol
DBU - 1,8-Diazabicyclo[5.4.0]undec-7-ene
DDA - data-dependent acquisition
DIA - data-independent acquisition
DHA - docosahexaenoic acid
DSDMA - Distearyldimethylammonium chloride
EPA - eicosapentaenoic acid
ESI - electrospray ionization
FA - fatty acyls
FFA - free fatty acid
GL - glycerolipid
GP – glycerophospholipid
HexCer - hexosylceramide
HCD - higher-energy collisional dissociation
HDL - high-density lipoprotein
HPLC - high-performance liquid chromatography
IM - ion mobility
IMMS - ion mobility mass spectrometry
Lipid Maps - Lipid Metabolites and Pathways Strategy
LPC - lysophosphatidylcholine
LPL - lysophospholipid
LDL - low-density lipoprotein
MS - mass spectrometry
MS/MS - tandem mass spectrometry
m/z - mass to charge ratio
NIDDK - National Institute of Diabetes and Digestive and Kidney Diseases
NIST - National Institute of Standards and Technology
PA – phosphatidic acid
PASEF - Parallel Accumulation-Serial Fragmentation
PC – phosphatidylcholine
PE - phosphatidylethanolamine
PG - phosphatidylglycerol
PI - phosphatidylinositol
PK - polyketide
PR - prenol lipid
PS - phosphatidylserine
PUFA - polyunsaturated fatty acid
Q - quadrupole mass spectrometer

QE - Q-Exactive quadrupole orbitrap mass spectrometer by Thermo Fisher
qOrbi - quadrupole orbitrap hybrid mass spectrometer
QQQ - triple quadrupole mass spectrometer
QToF - quadrupole time-of-flight hybrid mass spectrometer
SL - saccharolipid
SM - sphingomyelin
SP - sphingolipid
SRM - standard reference material
ST - sterol lipid
TG - triacylglycerol
TIMS - trapped ion mobility spectrometry
timsToF Pro - trapped ion mobility-quadrupole-time of flight mass spectrometer by Bruker
ToF - time of flight mass spectrometer
UHPLC - ultra-high performance liquid chromatography
UHPLC-MS/MS - ultra-high performance liquid chromatography/tandem mass spectrometry
VLDL - very low-density lipoprotein

Chapter 1
Introduction

The field of lipidomics has expanded exponentially since 2001 when only a single publication regarding the "lipidome" or "lipidomics" existed on PubMed. In the year 2015, over 500 studies were published and over 1500 studies were published in the year 2020. In principle, lipidomics is the attempt to characterize all lipids in a sample. In practice, numerous lipids are identified typically qualitatively and there is some analytical bias towards certain types or classes of lipids. While various tissue and sample matrices have been reported, examinations of the plasma lipidome to identify possible biomarkers of health and disease are the most common types of studies, and have been applied to various health research studies examining biomarkers for indications of disease such as diabetes[1], heart disease[2], obesity,[3] Alzheimer's disease[4,5,6,7] and cancer[8]. Lipidomics has also been used to examine the role of lipids in human disease using various tissues and cells as lipids can provide insight on disorders related to energy dysregulation such as diabetes, lipid signalling in inflammation and cell death, lipid-protein interactions in neurological disorders, and host-pathogen interactions during infection and invasion of bacteria, viruses and parasites. [9] In addition to human based analyses, various tissues of animals, plants, and microorganisms such as yeast and algae have been analyzed as models for disease and/or enhanced understanding of lipid metabolism.[10] Complex food matrices can also be analyzed for lipid composition determinations but also for food traceability and adulteration monitoring.[11] The level of structural lipid information reported between studies varies, with some studies identifying the overall lipid class, number of carbons and double bonds, and others defining the lipid complex with corresponding fatty acyl constituents. Previous knowledge of the disease also typically dictates the lipid class of focus for analysis. Lipidomics remains an evolving field.

There are now multiple international consortiums in place such as the Lipid Metabolites and Pathways Strategy (Lipid Maps) Consortium (http://www.lipidmaps.org), the Lipidomics Standards Initiative (https://lipidomics-standards-initiative.org/), LipidomicNet (https://www.lipidomicnet.org/index.php/Main_Page), and Lipidomics Informatics for Life Sciences (LIFS) (https://lifs-tools.org/) which aim to provide resources and help standardize the field.

Standardization is an ongoing challenge in the field of lipidomics.[12] Different types of mass spectrometry instruments with different settings are constantly being used. Initially, low resolution triple quadrupole mass spectrometers were used for lipidomic analyses, but high resolution Orbitrap and Time of Flight instruments with accurate mass capabilities to several decimal places have become preferred as they became commercially available. Within an instrument, samples can be introduced by direct infusion to rapidly run numerous samples in "shotgun" approaches or by using upfront separation techniques to spread the mass spectra of the lipids across different retentions times to reduce complexity and enable a higher degree of confidence when identifying the chemical structures. After introducing the sample within the instrument, data is collected using different modes such as full-scan, data-dependent and data-independent acquisition that can have distinct outputs[13] and then processing of the raw data can vary depending on software platforms, chemical compound databases and the reliance on automated identifications versus manual inspections. The lack of harmonization in lipidomic analyses has been demonstrated in an interlaboratory comparison where 31 different laboratories were sent a plasma Standard Reference Material (SRM) to analyze, and the results were quite inconsistent.[14]

SRM 1950 Metabolites in Frozen Human Plasma is pooled human plasma from 100 individuals representing the population of the United States of America. It was created by the National Institute of Standards and Technology (NIST) and National Institute of Diabetes and Digestive and Kidney Diseases (NIDDK) in collaboration with the Centers for Disease Control and Prevention (CDC) for metabolic analyses. The Lipid Maps consortium has also systematically profiled SRM 1950 previously.[15] Due to the wide availability of the sample, it provides the opportunity for a cross-platform analysis to identify potential variations in lipidomic workflows. While lipidomic profiling of SRM 1950 is not a novel concept, the previous reports that were available during the design of this thesis were limited to data at the sum compositional, or "brutto" level.[14,15] Brutto level identifications are not specific and can represent multiple different fatty acyl species that can be difficult to integrate into existing nutritional and food composition data and knowledge. For example, a lipid identified as PC 36:2 cannot be confirmed as containing saturates, monounsaturates or polyunsaturates since it could be PC 18:0_18:2 or PC 18:1_18:1. Identifying the fatty acyls within a lipid is known as the medio level of information while PC 18:0/18:2 and PC 18:1/18:1 indicate genio level where the positional isomers of fatty acyls have been determined.[16] Determining higher levels of information are associated with increased analytical burden and more advanced analytical platforms.

Characterizing the lipidome is challenging due to the sheer number of lipids, the complex fatty acyl isomers and the large dynamic range in the abundances of individual species. Defining the human plasma lipidome at the "medio" level is required to consolidate lipidomic findings with the large body of fatty acid-based research, but the analytical burden of defining the entire lipidome of samples used for nutritional research at the medio level is tremendous. However, these analyses can be made feasible if the analysis focuses on lipids of relatively high abundance

or the “macrolipidome”. The macrolipidome of a sample is relatively stable during sample handling as it is based on the main structural lipids, and the macrolipidome can provide insight into basic lipid metabolism and dietary habits.[16] The macrolipidome of a sample can be defined by identifying and quantifying a percentage of the total lipid signal (ie. 85%) and/or a cut-off for the individual contribution of a lipid to the total (ie. 0.1%). In contrast to the macrolipidome, the microlipidome is made of low abundant lipids, many of which are bioactive. Characterizing the microlipidome often requires specialized care in handling and preparing the sample due to the stability of many of these lipids and several different targeted analytical procedures may be required due to the diversity in the types of these lipids. As such, quantitative screening of the macrolipidome of plasma in the future is a feasible endeavour while quantitative profiling of the microlipidome remains a daunting task.

High quality medio level lipidomic information requires the use of LC-MS/MS. Specifically, the use of tandem mass spectrometry is critical as inspection of analyte fragmentations patterns at the MS/MS level is necessary to confirm medio level information. Both positive and negative ionization modes must be used to achieve a full coverage of the lipid classes as some lipid classes will preferentially become protonated while others prefer to become deprotonated.[15] The upfront LC is also necessary for increasing the separation of lipid species by retention time and improving the quality of identifications. Without retention time separation in the mass spectrometer, the bias towards identifying the most abundant lipids and lipids that ionize more readily can significantly impact quantitation efforts. Ion suppression or enhancement is common in mass spectrometry and can be influenced by endogenous matrix components within a sample.[17] For lipidomics, both reversed phase and hydrophilic interaction liquid chromatography (HILIC) can be used depending on the analytical goal. HILIC tends to

preferentially separate lipids by their lipid class while reversed phase tends to preferentially separate by the fatty acid compositions of the lipids.[18] In this thesis, reversed phase is used exclusively due to the main interest in determining medio information that includes fatty acyl species. Ion mobility is another separation technique that is being used either alone or in combination with LC for lipidomics increasing to aid in lipid species and isomer separations.[12] In this thesis, a platform that includes trapped ion mobility spectrometry coupled to LC separation will also be used.

Incorporating specific fatty acyl information into lipidomics will greatly improve the ability to understand lipid metabolism and how diet impacts health. The importance of essential fatty acids and their impact on physiology has been examined extensively for over 50 years.[19,20] In addition, examining the fatty acid compositions of blood has revealed biomarkers that can be used to estimate dietary intakes and to indicate potential disease risk. [4,15,21,22] For example, increased blood levels of the omega-3 polyunsaturated fatty acids (PUFA) eicosapentaenoic and docosahexaenoic acid have been associated with a decreased risk of cardiovascular diseases, may support fetal neural development, and may reduce inflammation.[23,24,25] However, conventional fatty acid analyses results in a loss of information as fatty acids are chemically removed from their parent lipid in blood and then derivatized to form fatty acid methyl esters for gas chromatographic analysis.[26] The use of liquid chromatography coupled to tandem mass spectrometry (LC-MS/MS) can allow for the determination of the fatty acyl species of these original complex lipids. This level of information has been labelled as the “medio level” and determining lipidomic data at this level would allow the comparison and validation of new lipidomic data to existing fatty acid literature[27] and food and nutrient databases.[28]

The medio level macrolipidome of human plasma SRM 1950 was examined in this thesis. Lipids were extracted from SRM 1950 and analyzed on three different ultra-high performance liquid chromatography (UHPLC) MS/MS instruments using an untargeted approach. These cross-platform analyses were completed utilizing: A Dionex UltiMate 3000 UHPLC system (Dionex Corporation, Bannockburn, IL, USA) coupled to a Thermo Q-Exactive Quadrupole-Orbitrap MS/MS (QORBI; Thermo-Fisher Scientific, Waltham, Ma, USA), a Waters Acquity UHPLC system coupled to a Waters Synapt G2Si Quadrupole-Time-of-Flight MS/MS (QToF; Waters Corporation, Milford, MA, USA) and a Bruker Elute UHPLC coupled to a Bruker specific trapped ion mobility-quadrupole-time of flight MS/MS (timsToF Pro; Bruker Scientific, MA, USA). Instruments were operated in both positive and negative ion polarities to encompass the entire spectrum of complex lipids and data dependent acquisition was used to characterize the macrolipidome of the plasma samples. This research is important for standardization of analysis and reporting in the lipidomic field as the medio level lipid information of SRM 1950 generated can be used as a reference for studies examining the plasma lipidome.

Chapter 2
Background - Lipidomics

2.1 Lipidomics

Lipidomics involves identifying lipids in their natural state to characterize the lipid composition of a biological system. Understanding the lipid profile of a biological sample can provide great insight into the physiological impacts of diet and disease as lipids play key roles in energy storage, membrane structures, and in signalling pathways. There are eight main parent classes of lipids established off of their biochemical properties: fatty acyls (FA), glycerolipids (GL), glycerophospholipids (GP), sphingolipids (SP), sterol lipids (ST), prenol lipids (PR), saccharolipids (SL), and polyketides (PK).[29] Biological samples are prone to variation in both the concentration of lipid species and complexity of lipid structures leading to difficulties in the separation and identification of lipids within a biological sample.[15]

Attempting to characterize all lipid species present in a biological sample can require multiple analytical approaches due to the complexity and variation in lipid structures. Mass spectrometry (MS) is the most common platform used in identifying lipid molecules since they can be analyzed in their native form.[14] The analytical technique can be tailored and refined when combined with upfront separation techniques such as liquid chromatography (LC), ion mobility (IM) and different MS modalities. High resolution MS extends the accuracy of mass determinations and tandem mass spectrometry (MS/MS) provides additional characterization of fragments from a compound to aid in the chemical characterization and identification of analytes. Different analytical approaches are ideal for different research goals. There are rapid, high throughput techniques such as “shotgun lipidomics” that quickly screen lipidomic profiles versus upfront separation techniques used prior to the mass spectrometer such as chromatography that can isolate lipids and enable precise characterization and quantitation of individual lipids. As

such, there is a range of "untargeted" and "targeted" approaches that can provide different levels of chemical structure information about a molecule.

2.2 Untargeted and Targeted Lipidomics

Establishing the goal of a lipidomic analysis directly influences the analytical workflow to be used, which directly impacts the type and quality of the data. When analyzing a sample of unknown composition with the goal of characterizing the lipidome, an untargeted, or global approach is often used. This provides a general overview of the entire lipidome of a sample but will be limited in the number of correct identifications of each lipid and limit the ability to quantitate. Untargeted analysis is typically done through data independent analysis (DIA) and data dependent analysis (DDA) where no prior inclusion lists, or parameters are used to target the analysis towards specified ions. Untargeted approaches are biased for characterizing the lipids of high abundance or ions that have been enhanced as ions with higher recorded intensities or responses are prioritized and selected by the detection process. For example, top 5 DDA is a common approach where five lipids with the highest signal at the MS level at a time point are selected for fragmentation and MS/MS characterization. However, these global approaches are amenable for analyzing the macrolipidome of a sample when the goal is to characterize a subset of high abundant lipids as compared with characterizing the entire lipidome with a very large number of low abundant lipids.[16] A focus on lipids of high abundance limits the number of analytes measured, and limits the dynamic range to be used and thus allows a generalized analytical workflow to be created that has a higher potential to be standardized across platforms and laboratories.

Targeted lipidomics are used when the analytes to be measured are specified by the analyst prior to the analytical process. An inclusion list of the masses of the analytes to be measured is defined as part of the acquisition parameters of the instrument. Targeted approaches can result in controlled and manageable data outputs as lipid species of interest are examined and data processing routines can be established.[30,31] Lipidomic profiling of samples can be completed using targeted approaches through the development of large inclusions lists that generate comparable datasets which can be examined for insight in large clinical studies.[32] Targeted approaches can also include tailoring for the analytes of interest by using specific solvents, standards, and instrument parameters. This level of targeting is are often required to measure low abundant lipids in a sample that are part of the "microlipidome".[16] Lipid molecules in the microlipidome are often considered "bioactive" as they are involved in acute lipid metabolism and lipid signalling, so sample stability is also a concern.[16] Diacylglycerols (DAG), phosphatidylinositols (PI), ceramides (CER), and oxylipins are low abundant lipids that would be considered part of the microlipidome.[16]

2.3 "BMGI" System for Indicating the Level of Information in Lipidomics

The level of information determined for each lipid is an important and well recognized aspect of lipidomics.[33, 34, 35] However, describing the different levels of information can be cumbersome, therefore the terms *brutto, medio, genio* and *infinio* have been proposed as the BMGI system, to quickly convey the level of information that was determined for lipid structures.[16] Brutto or sum compositional information pertains to the method of indicating the complex lipid class and the overall number of carbons and carbon-carbon double bonds of the fatty acyls components. This is the most common level of information reported, as it can be

confidently identified using parent ion mass alone without tandem mass spectrometry. In the example in **Figure 1**, PC 38:6 represents a phosphatidylcholine with fatty acyls combining for 38 carbons and 6 carbon-carbon double bonds. The next level of information, medio, provides insight into both the parent lipid class and the specific individual fatty acyl constituents without determining the location of the fatty acyls on the lipid structure. This is typically achieved by identifying MS/MS fragments that match the specific fatty acyl (or the loss of the specific fatty acyl). This provides information about the fatty acyls in the lipid that were not defined at the brutto level, so PC 38:6 could be identified at the medio level as PC 16:0_22:6 (**Figure 1**) with the underscore indicating that the stereospecific numbering *sn*-1 and *sn*-2 positions of the fatty acyls are unknown. The increase in structural value obtained between the brutto and medio level is further portrayed in **Figure 1** as PC 38:6 could represent five biologically relevant unique lipid species while medio identification could only represent two. Genio level information then provides the *sn* of the fatty acyl constituents allowing the regioisomers of complex lipids to be distinguished. This information is denoted using a forward slash so the medio level PC 16:0_22:6 would be denoted as either PC 16:0/22:6 or PC 22:6/16:0. Genio level determinations increase the analytical burden either through more stringent or advanced separation approaches and requires additional data processing. Infinio level of information is used when the location and geometry of the carbon-carbon double bonds within the fatty acyl chains are defined. This is depicted in **Figure 1** as PC 16:0/22:6 (4Z,7Z,10Z,13Z,16Z,19Z) indicates one completely unique and resolved lipid structure. While ideal, this level of information requires separate workflows prior to sample injection such as the use of benzene or in-line instrument modifications such as ozone introduction to create different adducts based on the double bonds.[36] This creates an

extreme burden with extensive sample preparation and data processing but is viewed as the gold standard for the future of the field.

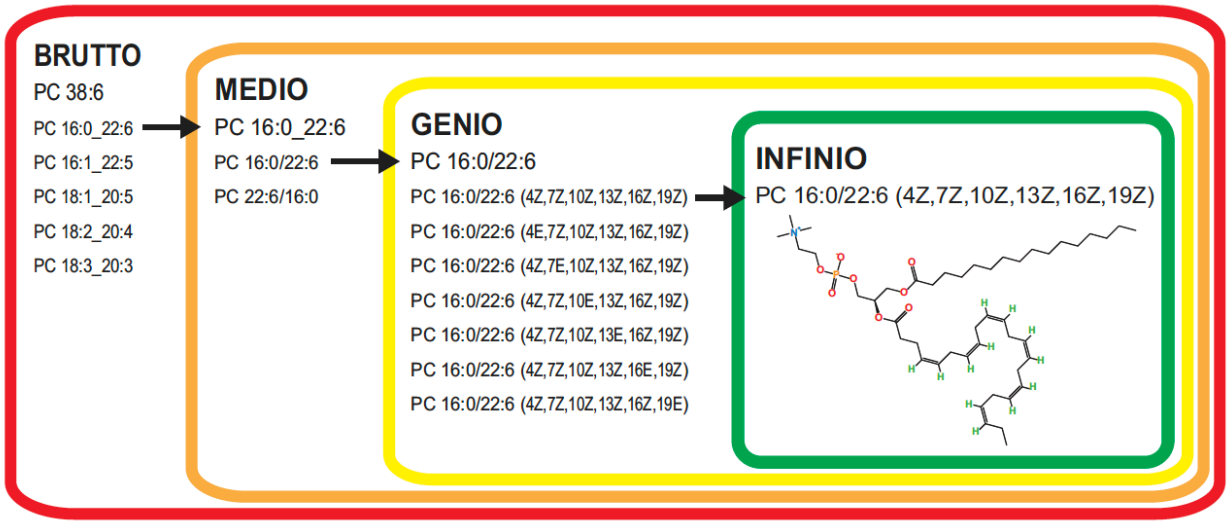

Fig 1. The BMGI system for indicating the level of structural information using 1-hexadecanoyl-2-(4Z,7Z,10Z,13Z,16Z,19Z-docosahexaenoyl)-sn-glycero-3-phosphocoline as an example.[37]

2.4 Sample Introduction into a Mass Spectrometer

When a sample is directly injected into a mass spectrometer using a syringe, it is termed *shotgun* lipidomics. Shotgun lipidomics is a quicker and relatively less extensive process compared to the alternative use of chromatographic separation beforehand. Time is saved since chromatography parameters do not need to be established and maintained and each analytical run is considerably shorter without the chromatographic column run time. Overall, this leads to rapid sample analysis. This direct infusion can also increase analytical throughput in a targeted approach when identifying an ion of interest within a sample. However, since the entire sample contents are analyzed concurrently and potentially fragmented at the same time, shotgun lipidomics can produce noisy spectrums and isomer separation is often not possible. This option is typically done for less concentrated and complex samples. Ion suppression and matrix effects also act as large obstacles that can lead to the analyte of interest not being observed in complex

biological samples.[38] More complex lipidomes benefit from prior separation using chromatography or other techniques prior to introduction into the mass spectrometer.

2.4.1 Principles of High-Performance Liquid Chromatography for Separation

High-performance liquid chromatography (HPLC) is an analytical technique that is commonly used in lipidomics to separate compounds in a sample prior to mass spectrometry to improve identification and quantification. Liquid chromatography separates lipids by differences in their physical and chemical properties to introduce the ions gradually into the mass spectrometer and obtain less noisy spectra. This improves the identification of lipid isobars (different lipids with identical mass to charge ratios [m/z]) and isomers. Separation is achieved through the use of two phases: one that is fixed in place, or the stationary phase, and another that moves past it, the mobile phase. The instrument operates utilizing high pressure, up to 6000 psi, to push a sample through a narrow column that is lined with the stationary phase.[39] Packed columns are typically used with particle sizes ranging from 1.7 to 5 μm which requires high pressures for the sample to flow through. Smaller particle sizes provide better resolution but require higher pressure. Newer ultra-high performance liquid chromatography (UHPLC) instruments operate upwards 15000 psi and can use columns with smaller particles.[39] The stationary phase is typically made from silica beads of various sizes with bonded chemicals with a polarity that is selected for the type of separation being conducted.[39] A solvent system is used to introduce the sample into one end of the column. Pressure is applied to pump the solvents either isostatically or via a gradient, through the column where components of the sample will then interact more strongly with either the mobile or the stationary phase depending on its

polarity. The more the solute interacts with the stationary phase, the later that compound will elute out of the column.

HPLC methods are named after the polarity of the stationary phase. When a polar stationary phase is used with a non-polar solvent system, this is called normal-phase chromatography.[39, 40] While normal phase chromatography is rarely used due to the requirement for 100% organic solvents, a variant method, hydrophilic interaction liquid chromatography (HILIC) has gained popularity in lipidomics as they provide similar separations to normal-phase chromatography with a lower organic solvent requirement. The polar stationary phase of HILIC columns separate lipids based on the polarity, or hydrophobicity of the lipid head groups and can provide good separation of lipids that may have poor retention in the reverse-phase.[40] However, separation based on fatty acyl chain composition within the lipid can be limited with HILIC which may prevent medio level characterizations.[41] Reverse-phase chromatography is a very common HPLC technique that uses a non-polar stationary phase with a polar mobile phase.[39, 40] C18 columns are commonly used for reverse-phased chromatography in lipidomics, which indicates that 18 long hydrocarbon chains are bonded to the silica beads to form the stationary phase.[40] The 18C stationary phase can therefore interact with the hydrocarbon carbon chains of the fatty acyls in lipids to provide effective fatty acyl species separation in addition to general lipid class separations that is necessary for acquiring medio levels of information.

2.4.2 Sample Ionization via Electrospray Ionization

The ionization of analytes within the sample is critical before entry into the mass spectrometer regardless of direct infusion or prior separation. This process was typically applied after separation using a GC as the molecules in the gas phase can be electrically ionized directly

or through less aggressive indirect chemical ionization using a reagent gas. The ionization of liquid samples was revolutionary.[42] These techniques included Electrospray Ionization (ESI) or Atmospheric Pressure Chemical Ionization (APCI) and are considered soft ionization techniques. ESI is the most popular and operates by vaporizing the sample over a voltage to create a plume of charged droplets.[43,44] A heated capillary supports the droplet formation and will evaporate the solvent until one charged ion molecule is left.[43,44] These ions are then attracted to the entrance of the mass spectrometer since the entrance is a counter electrode to the capillary. In ESI, the compound of interest must be present as an ion in solution, so it is important to consider the pH of the mobile phase along with the presence of ions (ie. ammonium, NH_4^+) which can aid in the formation of ionized chemical adducts for analysis.[44] The composition of the running buffer is also important to consider when trying to counter ion suppression and matrix effects which is a common obstacle in ESI.[38] Competition of available charges and interfering compounds at high concentrations from both the sample and mobile phase can lead to difficulties in detecting the analyte of interest.[38]

Depending on the sample and solvent system used, the analytes will prefer to form either positive or negative ions. The MS can operate under both positive and negative modes, but the setting is usually established before analysis and in many MS platforms it cannot be operated to detect positive and negative ions concurrently. While there are some MS instruments that have the capability of fast polarity switching, a compatible running buffer composition must be used which does not allow for optimization of the running buffer for the positive (acidic buffer preferred) and negative (basic buffer preferred) polarities. Not all lipids can be detected using one polarity alone, therefore it is important to consider ESI-polarity in lipidomics since lipids vary in polarity and will ionize differently depending on their structure.

2.4.3 Separation of Ions via Ion Mobility

Ion mobility (IM) is an electrophoretic gas-phase technique that offers an additional layer of separation of ions in the millisecond timeframe, prior to analysis of the mass of a compound.[45] IM separates ions based on their mobility through an inert gas as the force from an electric field is applied.[45,46,47] This process separates ions based on their charge, shape and size which can be beneficial for isobar, and isomer separation often encountered in lipidomics.[45,46,47] Combination of IM with mass spectrometry (IMMS) has evolved over the past 20 years.[48] This can be used in addition to LC techniques for further separation and will produce signals with less interference for a reduction in chemical noise. When mobility is combined with the m/z obtained from a mass analyzer, a shape-to-charge ratio can be calculated to determine a unique collisional cross section (CCS) value of a compound. The CCS value can be used in combination with MS data to improve confidence of lipid identifications. There are different types and forms of IM largely based on the configuration of the separation space with drift tube, travelling wave, and trapped ion mobility spectrometry being incorporated into commercial mass spectrometers by different manufacturers.

2.5 Principles of Mass Spectrometry

Mass spectrometry is a powerful instrument that is used to determine the mass of an unknown compound. It is a desirable detector when coupled with chromatography given it can differentiate compounds with identical retention times. Mass spectrometry works under a high vacuum by accelerating ions through an electric field so that they can be differentiated by their mass to charge ratio (m/z).[39] If the charge of the ion is +1, then the m/z value is equal to that of its mass since z=1. As mentioned previously in **Section 2.4.2**, an MS can operate under positive

or negative conditions and the polarity of ion detection must match the ionization tendencies of the lipid that is to be analyzed. For example, non-polar lipids such as triacylglycerols (TG) and cholesterol esters (CE) are detected only in positive polarity mode while some polar lipids such free fatty acids and phosphatidylinositols are detected only in negative mode.

There have been great advancements in the field of lipidomics which can be attributed to the improvements in resolution and mass accuracy of MS instruments. Mass spectrometers were first developed as a tool to separate ions of differing m/z. A quadrupole (Q) was an early example of an instrument that was able to filter ions based on their mass by varying the voltage between 4 parallel rods of opposite polarity so that only specified ions would pass through the field.[39] The instrument was relatively small, light, inexpensive and easy to operate. Even more potential applications became available when utilizing three of these quadrupoles in tandem as a triple-quadrupole (QQQ). The QQQ enabled tandem mass spectrometry (MS/MS) where the first Q is used to isolate the ion of interest, the second Q is used to fragment the ion of interest and the third Q is used to identify the fragment ions produced from the parent ion. Through applying knowledge of bond strengths within chemical structures, common fragment ions can be predicted to confirm the analyte ion of interest. A large obstacle with these Q mass analyzers however were that they can only provide unit or nominal mass resolution, meaning that each mass can only be separated from the next whole integer. This low resolution is problematic as single unit masses can be shared by various compounds with different elemental compositions (isobars). For example, N_2 and C_2H_4 share the same nominal mass (28 u) despite having different accurate masses (28.00614 u and 28.03139 u, respectively). With high levels of mass accuracy, compounds sharing accurate masses will have the same elemental composition, but with

different arrangements (isomers), although some isomers can be isolated with separation techniques.

The development of high-resolution mass spectrometers allows for high mass accuracy measurements capable of distinguishing ions with different elemental compositions but the same nominal mass. High resolution analyzers include Time of Flight (ToF) instruments and various types of ion traps including the Orbitrap. However, accurate mass cannot distinguish compounds with different arrangements of the same elemental composition (isomers) and MS/MS measurements of fragments are usually necessary. Hybrid instruments were developed with Q mass analyzer utilized as the first mass analyzer to select ions for fragmentation in a collision cell that are then detected with a higher resolution analyzer. The Mass Spectrometry Facility at the University of Waterloo has two high resolution hybrid platforms: a Quadrupole-Orbitrap (qOrbi) and a Quadrupole-Time of Flight (QToF) instrument. For this thesis, a collaboration with Bruker Daltonics also allowed for samples to be analyzed on a Trapped Ion Mobility Spectrometry-Quadrupole-Time of Flight (timsToF) instrument. These instruments are described in more detail below.

2.5.1 UHPLC – ESI Quadrupole-Orbitrap Mass Spectrometry

The Thermo Q-Exactive (QE; Thermo-Fisher Scientific, Waltham, Ma, USA) is a Quadrupole-Orbitrap (qOrbi) hybrid mass spectrometer that is coupled with a UHPLC. Analyte ions will start to separate in the UHPLC column. As they elute from the column, they will enter the ESI source and become a single gas molecule as described earlier in **Section 2.4.2.** From here, the ions will enter the quadrupole mass analyzer. It consists of 4 parallel rods of opposite polarity.[39] Depending on the applied voltage, some ions will not have a stable trajectory and

therefore will not reach the detector. The quadrupole can also act as a mass filter to isolate ions of interest. In untargeted experiments, the allowed mass range is set to correspond to the known range of most lipids (50-1200m/z). The ions leave the quadrupole and enter the Orbitrap, where they will oscillate around the centre electrode at a unique frequency that is equivalent to its m/z. A current is produced through a split in the outer electrode as the ions oscillate, which can be Fourier transformed to produce a spectrum. If a MS/MS experiment is being conducted, the ions will leave the Orbitrap and enter a higher-energy collisional dissociation (HCD) cell for fragmentation and then re-enter the Orbitrap for m/z detection. The quadrupole itself can only detect nominal mass resolution but due to the repeated measurements of the ions during the oscillation, the Orbitrap provides extremely high mass accuracy relative to other mass spectrometry detectors. However, the requirement for ions to oscillate around the detector requires time and limits scan speeds of orbitrap instruments.

2.5.2 UHPLC-ESI Quadrupole-Time of Flight Mass Spectrometry

The QToF is also coupled to a UHPLC so after chromatographic separation the ions first enter the quadrupole region. In data dependent acquisition, the quadrupole allows a set number of ions by abundance to proceed further into the instrument. The Waters Synapt G2Si QToF (Waters Corporation, Milford, MA, USA) instrument has the capability for travelling wave IM separation after the quadrupole. This includes a trap section before the IM section and a transfer section after which are both capable of further fragmenting ions. IM was not used for any of the analyses based on previous experiments[49] therefore this region was used only as a HCD cell in the present thesis. The ToF detector works by applying a voltage to a backplate behind the ion source giving ions the same kinetic energy before accelerating the ions through a drift region,

which has no electric or magnetic field.[39] As a result, the velocity of the ions and the time required to reach the detector is largely dictated by the mass of the compound. The Synapt G2Si QToF is a reflectron instrument which means the flight path of the ions to the detector are not direct but involve reflection back towards the detector. This instrument is also capable of single-pass (increased sensitivity) and double-pass (enhanced resolution) options. For tandem mass spectrometry experiments, the ions are exposed to rapidly alternating low and high collision energies in the HCD cell (after the quadrupole and before the ToF analyzer). The ToF method of m/z determination allows for very rapid scan times but in older instruments resolution was poor. Ion beam focusing, reflectron designs, reference mass infusion (lock mass) configurations and strategies in modern ToF instruments has improved mass accuracy and resolution dramatically, such that they approach that of Orbitrap instruments.

2.5.3 UHPLC-ESI Trapped Ion Mobility Spectrometry - Quadrupole-Time of Flight Mass Spectrometry

Recently, Bruker Daltonics has incorporated trapped ion mobility spectrometry (TIMS) into a QToF instrument.[50] The instrument can still be coupled to upfront UHPLC with the TIMS region of the instrument receiving the ions immediately after introduction by the electrospray source. The TIMS traps ions by holding them stationary in a moving column of gas through the use of an electric field, in contrast to conventional IM where ions move through a stationary gas under an uniform electric field within a drift tube[50,51] or by an electrical peak potential oscillation in travelling wave IM. The TIMS uses an electrical field to counter the drag of the gas flow entering the ion source to isolate ions within the trap tube. The electrical field holds the highly mobile ions close to the ion source end of the trap, while the gas drag force moves the less

mobile ions towards the quadrupole end of the trap. Lowering the electrical field gradient allows ions to leave the trap and enter the quadrupole. The parent ions can then be selected in the quadrupole and then pass through a collision cell where MS/MS fragmentation can occur prior to entering the ion pusher of the single pass reflectron ToF. In summary, the TIMS is used for additional separation of ions after the UHPLC separation, the quadrupole filters the parent ions, the collision cell can oscillate to produce MS/MS fragments and the precursor and fragment m/z are detected by the ToF mass analyzer. In this thesis samples were sent to Bruker Daltonics, MA, USA to be run on a timsToF Pro platform coupled to a Bruker Elute UHPLC.

2.6 Standardization in the Field of Lipidomics

As lipidomic data became available, considerable variation in both the results and reporting has created a challenge to understand and establish consensus in the field of lipidomics.[14] The large diversity of lipids and their structures is a challenge for both analysis and reporting. Multiple components within a lipidomic workflow can vary including sample collection and storage, lipid extraction, separation technique, instrumentation and instrumentation parameters, analyst, and within data processing and lipid annotation.[35,52,53,54] The initial lipidomic method setup has a large impact on the outcome of the analysis and can lead to variation in results. Generating lipidomic data sets is a large analytical burden, especially for complex biological lipidomes. Thousands of features, or ions with a unique m/z and retention time, may be detected by the mass spectrometer. Targeted and untargeted approaches are both employed, and data acquisition approaches can differ. For untargeted approaches, automated software is often used to identify potential lipids and help with this burden to eliminate false positives. This automation relies heavily on pre-existing databases and the amount of manual confirmation of lipid

identifications required will vary between user and workflow. Quantification of lipid species is also challenging, as commercial internal standards for each potential lipid molecule are not available or even feasible.[55] Care must be taken in selecting the correct internal standard for the lipid to be quantitated. Differences among researchers with both the identification and reporting of lipid molecules also contributes to the lack of standardization in the field. Differences in reporting units, such as relative percent versus absolute amounts also creates difficulty in comparing what is already present in the literature.[35] It is also important that only the appropriate level of structural information is reported based on what is provided from a MS versus MS/MS workflow.[35] The BMGI system is one example of efforts being utilized to help standardize the field, and provide guidelines on the reporting of structural lipid information.[16]

Over 15 years ago, a large contribution to enhance the field of lipidomics was established through a "comprehensive classification system for lipids".[56] This was a universal classification system that divided lipids into eight main categories, providing researchers with an organisation tool for comprehension and reporting. Lipid Maps (LIPID Metabolites And Pathways Strategy; http://www.lipidmaps.org) was key in progressing this initiative and continues to be a large open-source gateway for databases, tools, webinars and resources for the lipidomic research community.[29,57] It currently holds the largest curated lipid structure database and is an extremely useful platform to communicate the current state of the lipidomic field. Lipid Maps has helped immensely in standardizing the field and creating resources and guidelines for the lipidomic community. A key contribution from Lipid Maps included a collaboration with other institutions to create standard reference materials to try to establish consensus within the field of lipidomics. Large interlaboratory studies have since been published and provide valuable insight into methodologies while continuing to highlight improvement within the field.[14,58] Of specific

interest is standard reference material (SRM) 1950, frozen metabolites in human plasma, which acts as an average pooled human plasma reference. Lipid profiling of this sample includes fatty acid analysis and complex lipid analysis which has mostly been reported at the brutto level. Efforts and calls to standardize lipidomics are now common[35,52,53,54] and with improvements in mass spectrometry platforms and software, characterization of the macrolipidome of SRM 1950 at the medio level should be completed.

Chapter 3
The Human Plasma Lipidome

3.1 Using Human Plasma for Clinical and Dietary Insights

Reliable measurements of dietary fat intakes are required to determine the impact fatty acids have on health and disease. There are different types of dietary assessment, but each technique has limitations in capturing precise data on dietary intakes. Most techniques rely on self-reporting that is prone for errors such as sub-consciously altering ones diet during the assessment period, under reporting of food items and amounts, and incomplete or outdated nutrient information in food databases which can lead to improper estimates of the dietary fats consumed.[59,60] Analytical analysis of human adipose tissue and human plasma lipid composition grew as a tool to characterize dietary lipid intakes without self-report bias.[61,62] As the major storage site of dietary fat, adipose tissue provides insight on long-term patterns of fatty acid intake, but it is comprised of mainly triacylglycerols (TG) that do not reflect the fatty acid composition of cell membranes from where many physiological effects mediate. Obtaining adipose samples by biopsies are also invasive and not suitable for routine screening. Human plasma contains a mix of circulating lipids that can reflect dietary intake and physiological conditions[62,63] and human plasma and serum is routinely collected in various clinical settings. For lipidomics, human plasma reflects *in vivo* physiological lipids best and provides greater reproducibility than serum-based analysis.[30,53,54,64,65] The coagulation process during the collection of human serum leads to changes particularly in low abundant lipids of the microlipidome through both generation and degradation of some lipid species. The isolation of human serum has been found to most strongly affect the concentrations of lysophospholipids (LPL), sphingomyelins (SM), some free fatty acids (FFA) and other oxylipins.[64]

3.2 The Lipidome of Human Plasma

Human plasma lipids and the chemical composition of plasma have been studied for over 50 years in an attempt to better understand physiology and disease.[66,67,68] In human plasma there are thousands of distinct lipid species, but they fall into 6 main categories: free fatty acyls (FFA), glycerolipids (GL), glycerophospholipids (GP), sphingolipids (SP), sterols (ST), and prenols (PR).[15] The plasma lipidome is however, largely dictated by the contents of lipoproteins which are utilized to help transport lipids throughout the body. The four main classes of lipoproteins are: chylomicrons (CM), very low-density lipoproteins (VLDL), low-density lipoproteins (LDL) and high-density lipoprotein (HDL). Lipoproteins are made up of a single layer of polar lipids (mainly phospholipids and cholesterol) with various associated proteins on the exterior with an interior core of non-polar lipids such as TG and cholesterol esters (CE). The ratio of non-polar to polar lipids vary across the types of lipoproteins with CM and VLDL being the largest in diameter and having large non-polar cores that are mainly TG and the particles distribute fatty acids in TG to tissues throughout the body via the circulation.[69] For lipoproteins that are smaller in diameter, the interior amount of TG is less, resulting in higher densities. The interior core of LDL and HDL is mostly CE with little TG and a greater proportion of GP with HDL particles having the smallest diameter and a relatively high amount of protein.[69] LDL and HDL lipoproteins are involved in cholesterol and reverse cholesterol transport. In addition to lipoproteins, the plasma protein albumin has a non-polar cleft and can transport various lipids such as non-esterified fatty acids throughout the blood stream and there is a very small pool of unbound or soluble fatty acids in plasma that are free in the circulation.[70]

Half of the plasma lipidome on a molar (nmol/ml) basis is ST lipids (cholesterol and CE) followed by GP and GL.[14,15] However, when based on weight (mg/dl), GP are the most abundant

lipids.[15] In general, these three lipid classes constitute about 90% of the human plasma lipidome. With over 45 distinct fatty acids in human plasma, the potential fatty acid compositions of the CE, GP and GL lipid classes are in the thousands of unique lipid species. However, given that 16:0 (palmitic acid), 18:1 n-9 (oleic acid) and 18:2 n-6 (linoleic acid) constitute about 65% of the fatty acids in plasma total lipids, many of the these fatty acyl species combinations are of relatively low abundance.[61,71]

3.2.1 Lipid Biomarkers as a window to Metabolic Health

Levels of cholesterol and TG in human plasma have been uses as lipid biomarkers for cardiovascular disease risk for over 50 years. These measurements are based on indirect spectrophotometry assays that allow reliable quantitative estimates, but provide limited structural information.[72] Previously, lipid profiling was difficult due to the complexity of the lipids which required multiple purification and analytical techniques.[73] The evolution of lipidomic research to achieve characterization of both the parent lipid class and the corresponding fatty acyl constituents was possible through the improvement in technology of mass spectrometers. Liquid chromatography coupled to high resolution mass spectrometers provided a single platform that could analyze a variety of lipid species in a single analytical run despite the complexity and varying polarities of human plasma lipids. These advancements in lipidomic techniques has allowed plasma lipid biomarker research for indications of disease such as diabetes[1], heart disease[2], obesity,[3] Alzheimer's disease[4,5,6,7] and cancer[8] although much of this work has been done using brutto level identifications.

In 1035 women with gestational diabetes, 311 lipids were associated with increased risk of developing type 2 diabetes within 10 years and over 70 lipids were associated with a decreased

risk out of 1000 identified lipids.[1] TG with 50 to 54 carbons and 0 to 4 double bonds were the major lipid species contributing to an increased risk of type 2 diabetes while SP and PC GP were the major species associated with a decreased risk of onset.[1] The four PC lipids associated with a decreased risk that were defined at the medio level were PC 17:0_18:1, PC 17:0_18:2, PC 18:1_20:4, PC 18:2_16:1.[1] In patients diagnosed with a ST-segment elevation myocardial infarction (STEMI), increases of 16 lipids were identified as markers of myocardial injury.[2] These were all FFA ranging from myristic acid to docosahexaenoic acid which can be identified through accurate mass in negative mode alone. Obesity biomarkers have also been explored using the plasma lipidome with lysophosphatidylcholine (LPC) species being negatively associated with obesity in 100 male adolescents ranging from normal to obese weight.[3] Specifically, LPC 18:2, LPC 18:1, LPC 20:2, LPC 20:1 and LPC 20:0 were significantly lower in obese individuals.[3] Several lipidomic studies have also identified that increases of plasma ceramide species with either 16, 21 and 24 carbons in length increase the risk of developing Alzheimer's disease, as reviewed recently.[4] A higher risk of developing Alzheimer's disease has also been associated with decreased levels of several plasma phospholipids including PC 36:6, PC 38:0, PC 38:6, PC 40:1, PC 40:2, PC 40:6 and LPC 18:2 [7] and PC 16:0_20:5, PC 16:0_22:6 and PC 18:0_22:6.[6] In cancer research, lipidomic biomarkers largely at the brutto level have been investigated in 19 different types of cancers suggesting cancer is involved in specific perturbations in membrane lipids.[8] As an example, increases in PC 32:1, PC 34:1, PC 36:1 and SM 34:1 and decreases in PC 38:4, PC 38:6, phosphatidic acid (PA) 40:5, PA 38:3, Phosphatidylethanolamine (PE) 38:4 and PI 38:4 were associated with increased risk of the onset of colon cancer.[8] However, some studies have identified cancer biomarkers at the medio level,

such as increases in phosphatidylserine (PS) 18:0_18:1 and PI 18:0_20:4 as indicators of bladder cancer.[8]

Measuring the lipidome provides a metabolomic phenotype that can provide insights into health and disease status. Adding the medio level of information to these biomarker endeavours will allow the fatty acyl information of the corresponding lipid class to be used to identify very specific metabolic pathways and link physiological mechanisms to dietary intake and fatty acid metabolism.

3.3 Human Plasma Standard Reference Material 1950 Lipidomics

Characterization of the human plasma lipidome has been greatly benefitted by the creation and use of a standard reference material as interlaboratory results can be compared. Standard Reference Material (SRM) 1950 was created by the National Institute of Standards (NIST) and National Institute of Diabetes and Digestive and Kidney Diseases (NIDDK).[74] SRM 1950 was created from pooling human plasma from 100 individuals whose ethnicity reflected that of the US population and it was originally created for interlaboratory metabolomics analysis and to hopefully aid in the identification of potential biomarkers of disease.[74,75] This SRM is ideal for characterizing the human plasma lipidome as it was made to reflect the typical lipid profile of the US population.

A variety of metabolites found in SRM 1950, and the analytical methods to quantify them are well understood.[75] These metabolites are reported on the certificate of analysis provided by NIST which includes the fatty acid profile as determined by gas chromatography.[74] There have been several attempts to characterize the lipidome of SRM 1950 to date.[15,14,41,58,76] Quehenberger et al. provided the first assessment and they established an understanding of the lipid class

breakdown of plasma.[15] They used multiple lipidomic workflows that included multiple different MS platforms and eight different extraction methods.[15] Most of the lipids were identified at the brutto level and there was a large focus on eicosanoid identification due to their bioactivity as they contribute less than 0.001% to the sample by concentration or weight.[15] With the brutto identification approach, the number of glycerolipids identified was quite low. More recently, SRM 1950 was used in an interlaboratory study from over 31 laboratories by Bowden et al. which identified a large number (1,527) of unique lipid species, but there were problems in consistent identifications as only 339 lipid species were reported by at least 5 laboratories.[14] This study highlighted the lack of standardization within the field of lipidomics, and the presented results were again limited to brutto level identifications.

Other studies have also used MS based workflows to analyze lipids within SRM 1950 but the focus was to establish workflows or software for lipidomics and not on the characterization of the lipidome itself.[41,58,77–80,80–83] Summarizing the results of these studies (**Table 1)** indicate that most researchers are identifying the highest number of lipid species in the GP class in comparison to the other lipid classes in SRM 1950, but there is still considerable variation across studies which is often dictated by the expertise and research interest of the analysts. This is highlighted in the original work of Quehenberger at al., where 107 FA species that were mainly eicosanoids and 204 SP species were identified.[15] These lipid classes are of low abundance and can be considered microlipidomic in plasma. The relatively low number of TG species identified by most groups examining SRM 1950, indicates that fatty acyl profiling the macrolipidome is not a common approach. Characterizing lipids at the brutto level also limits the characterization of the GL and GP classes. When quantitation is attempted rather than just identification, most studies are limited to brutto level identifications. The quantitative values obtained from

Quehenberger et al., and Bowden et al., are summarized in **Table 2**.[37] Obtaining the medio level of information of lipid species in SRM 1950 is a valuable contribution to characterizing the lipidomic profile of human plasma in order to identify potential key fatty acyl lipid species of importance and link them to human nutrition and metabolic pathways.

Table 1. Number of Lipid Species identified by Lipid Class in SRM 1950 in Literature

		Number of Species Identified								
Author	**Year**	**FA**	**GL**	**GP**	**SP**	**ST**	**PR**	**Total**	**Q**	**Notes**
Bowden et al.[14]	2017	14	83	150	58	34		339	Yes	Consensus in 5 or more labs (31 labs total)
Quehenberger et al.[15]	2010	107	73	160	204	36	8	588	Yes	Large FA (eicosanoid) focus
Koelmel et al.[83]	2019		18	54	14			86	Yes	Lipids found by both Quehenberger et al., and Bowden et al.
Ulmer et al.[76]	2017	8	47	127	42	30		254	Yes	Confirmed lipids established by Bowden et al. with a MEDM > 40%
Wolrab et al.[78]	2020		49	50	14				Yes	HILIC-UHPLC/MS
			68	37	19				Yes	UHP SFC chromatography/MS
Schwaiger et al.[80]	2018	14	49	143	58	5		269	AUC	RP Liquid chromatography
		14	55	135	61	3		268	AUC	Dual HILIC and RP chromatography
		21	85	167	92	7		372	AUC	Use of a developed exclusion list
Lange & Fedorova[41]	2020			155	36			191	Yes	Dual HILIC and RP chromatography
Schoeny et al.[81]	2020		166	258	45	39		508	Yes*	Positive polarity only
				299	111			410	Yes*	Negative polarity only
Triebl et al.[79]	2020		24	44	7			75	Yes*	Common lipids between 3 different MS workflows
Tsugawa et al.[58]	2020	52	106	109	24	14		305	Yes	Agilent 6546 QTOF with SPLASH quantitation

Some current literature of the number SRM 1950 lipid class species identified in the presented studies and supplementary data. Not all studies focused on all lipid classes, and workflows between studies vary. FA, fatty acids; GL, glycerolipids; GP, glycerophospholipids; SP, sphingolipids; ST, sterols; PR, prenols; Q, quantitation; MEDM, median of means methods to generate a consensus value from laboratory values; HILIC, Hydrophilic Interaction Liquid Chromatography; UHPLC, ultra-high performance liquid chromatography; MS, mass spectrometry; SFC, supercritical flow chromatography; AUC, Area Under the Curve provides arbitrary units for the abundance of a lipid; RP, reverse phase; YES* indicates only some lipids of interest were quantified and included only quantification of lipids also present in the Bowden et al.,[14] study; QTOF, quadrupole time-of-flight.

Table 2. Lipids in Standard Reference Material 1950 from the Literature

Lipid Category	Defining the plasma lipidome, 2010[15]		Interlaboratory Harmonizing Exercise, 2017[14]		
			All labs	Consensus (5+ labs)	
	Species (number)	Sum (mg/dL)	Species (number)	Species (number)	MEDM[c] (mg/dL)
Fatty acyls	107	6	177	14	7
Glycerolipids	73	94	317	83	54
Glycerophospholipids	160	201	679	150	108
Sphingolipids	204	24	236	58	26
Sterol lipids	36	146	118	34	230
Prenol lipids	8	0.4	-	-	-
Total	588	471	1527	339	424

Unique lipid species found in Quehenberger et al.[15], using multiple analyses and Bowden et al.[14], by multiple laboratories by number of identifications and concentration. Analysis from multiple workflows were combined in both studies to obtain these values. MEDM, median of means methods to generate a consensus value from laboratory values.

Chapter 4
General Methods

4.1 Design

This thesis utilized three ultra-high performance liquid chromatography/tandem mass spectrometry (UHPLC-MS/MS) platforms to characterize the macrolipidome of SRM 1950 at the medio level. The platforms included: A Dionex UltiMate 3000 UHPLC system (Dionex Corporation, Bannockburn, IL, USA) coupled to a Thermo Q-Exactive Quadrupole-Orbitrap mass spectrometer (qOrbi; Thermo-Fisher Scientific, Waltham, Ma, USA), a Waters Acquity UHPLC system coupled to a Waters Synapt G2Si Quadrupole-Time-of-Flight mass spectrometer (QToF; Waters Corporation, Milford, MA, USA) and a Bruker Elute UHPLC coupled to a Bruker trapped ion mobility spectrometry Time-of-Flight Pro mass spectrometer (timsToF; Bruker Scientific, MA, USA). The chromatography protocols and the MS acquisitions modes were similar. The processing of raw data was completed manually with the aid of automated software and compared across instruments and current literature.

4.2 General Hypotheses

- Manual inspection of mass spectra will improve the quality of identifications as compared with software-based identifications.
- TG, GP, and CE species will constitute the majority of the SRM 1950 macrolipidome.
- Positive ESI-polarity will provide the greatest overview of the macrolipidome since majority of the lipidome consists of positive ionizing lipids.
- Negative ESI-polarity will produce more confident identification of lipids species at the medio level since acyl fragments can be detected directly in this mode.
- Medio level identifications of SRM 1950 will be possible for the most abundant lipids.

4.3 Chemicals and Materials

Solvents including chloroform, methanol, isopropanol, n-butanol, acetonitrile and hexane (HPLC grade or higher) were purchased from Thermo Fisher Scientific (Mississauga, ON, Canada). Citric acid, disodium phosphate, ammonium formate, and formic acid were purchased from Sigma-Aldrich (Oakville, ON, Canada). The SPLASH LIPIDOMIX standard used for quantitation was purchased from Avanti Polar Lipids (Alabaster, AL, USA) and contains one deuterated internal standard for each lipid class.[84] SRM 1950 was obtained from the National Institute of Standards and Technology (NIST).[74]

4.4 Lipid Extraction

Lipid extraction was completed according to a modified Folch method.[85] In summary, lipids were extracted from a 300 µL aliquot of SRM using 2:1 chloroform:methanol that contained 100 µL of deuterated internal standards (SPLASH LIPIDOMIX, Avanti) per 1 mL of 2:1 chloroform:methanol. This was vortexed for 1 min. Afterwards, the addition of 500 µL of 0.2 M sodium-phosphate buffer, inversion and centrifugation at 1734 rcf at room temperature for 5 min was used to produce two distinct layers. The organic phase containing the lipids was collected. The remaining aqueous phase were then re-extracted by adding 2 mL of chloroform. Samples were re-vortexed, re-centrifuged and the organic layer was collected once again and combined with the initial collection. The lipid extracts were then dried under nitrogen gas and stored in chloroform at -80°C. Aliquots for analyses by each instrument were taken from this original lipid extraction.

4.5 Lipidomic Analysis

The lipid extract of the SRM 1950 with internal standard added (as prepared according to **Section 4.4**) was analyzed by three UHPLC-MS/MS platforms in positive and negative mode in quadruplicate (**Fig 2**, Flowchart). The total lipid extracts were dried under nitrogen gas and reconstituted to 1500 µL using 65:30:5 acetonitrile:isopropanol:water +0.1% formic acid. The UHPLC chromatography protocol was the same for all three platforms. The mobile phase consisted of (A) 60:40 acetonitrile/water (v/v) +10 mM ammonium formate +0.1% formic acid (pH 4.3), and (B) 90:10 isopropanol/acetonitrile (v/v) +10 mM ammonium formate +0.1% formic acid (pH 5.8). A Waters Acquity UHPLC Charged Surface Hybrid (CSH) C18 150mm x 2.1mm x 1.7µm column with a VanGuard CSH 1.7 m pre-column (Waters Corporation, Milford, MA, USA) was also used for all instruments. The multi-step gradient used was as follows: solvent B was 32% from 0-1.5min, followed by a linear increase to 45% B from 1.5-4 min, 50% B from 4-8 min, 55% B from 8-18min, 60% B from 18-20 min, 70% B from 20-35 min, 95% B from 35-40 min, 95% B from 40-45 min, a decrease to 32% B at 45.1 min and a hold at 32% B until 48 min. A flowrate of 250 µL/min was used with a compartment temperature of 45 °C and an injection volume of 5 µL. The samples were analyzed on the qOrbi and QToF platforms at the University of Waterloo Mass Spectrometry Facility and timsToF at Bruker Daltonics in Billerica, MA, USA. The specific MS/MS positive and negative polarity settings for each instrument differed slightly and are given in detail in the platform specific **Sections 5.3.2, 6.3.2** and **7.3.2**.

All data was acquired using untargeted top-5 data-dependent acquisitions (DDA). Initial data processing was completed using *Progenesis QI* data treatment software (v2.3, Nonlinear Dynamics, UK). The workflow for data processing began by importing the raw data files produced from the UHPLC-MS/MS analysis into the Progenesis software. The initial data

processing was then completed using the software which combined the raw data files of the quadruplicate analyses and processed peak picking. Chemical adducts of interest and the quadruplicate experimental design setup was manually selected. The ChemSpider and LipidBlast[86] databases containing structural and fragmentation patterns of lipids were imported into Progenesis QI with a 25 ppm precursor and a 5 ppm product mass tolerance. Progenesis then generated a list of features, which are ions with a unique m/z and retention time (RT) found within the sample. Possible identifications, also called a raw identification (ID), were generated for review based on spectrum matching with the imported databases with an associated feature when available. Within Progenesis, the list of features was sorted by descending abundance which is calculated by the software based on the signal intensity of a given ion detected by the mass spectrometer. An automated lipid annotation program within Progenesis was then used to automatically accept a raw ID when only one possible raw ID had a fragmentation score >50 which was termed an automated ID. The fragmentation score was calculated by Progenesis based on how well the experimental spectrum matched that of the reference database. The automated medio ID annotations were saved and exported for comparison with the manual lipid annotation approach.

The list of features and possible raw ID were then confirmed manually to identify lipids within the sample at the brutto level and the medio level when MS/MS scans were available. This was completed for the highly abundant features until a cumulative abundance of 85%, or the 'top 85%' of features had been reviewed in the sample. A manual inspection of the fragmentation patterns was completed within either the data treatment software (Progenesis) or the data acquisition software of the respective instrument (see below) to confirm fatty acyl chains when present. The data acquisition software included XCalibur QualBrowser (version 2.1;

Thermo-Fisher Scientific, Waltham, MA, USA) for the qOrbi, MassLynx (version 4.1; Waters, Milford, MA, USA) for the QToF and Compass DataAnalysis (version 5.3; Bruker Scientific, MA, USA) for the timsToF. The data acquisition software was used to view the fragmentation MS/MS in the raw chromatograms using the software for the associated platform when spectra appeared noisy, had co-elution of species, or potential in-source fragmentation. A manual approach allowed contaminants and background ions within the samples to be identified. LIPID MAPS® Online Tools (www.lipidmaps.org) was also utilized to assist with determination of potential IDs based upon given m/z values and fragmentation patterns during a manual approach. The associated platform software was also utilized for manual peak integrations to obtain area under the curve (AUC) values for quantitation of the 20 lipids of highest abundance. This was completed by normalizing the peak intensities in the total ion chromatograms from the lipid of interest to that of the appropriate internal standard of the same lipid subclass within all replicates.

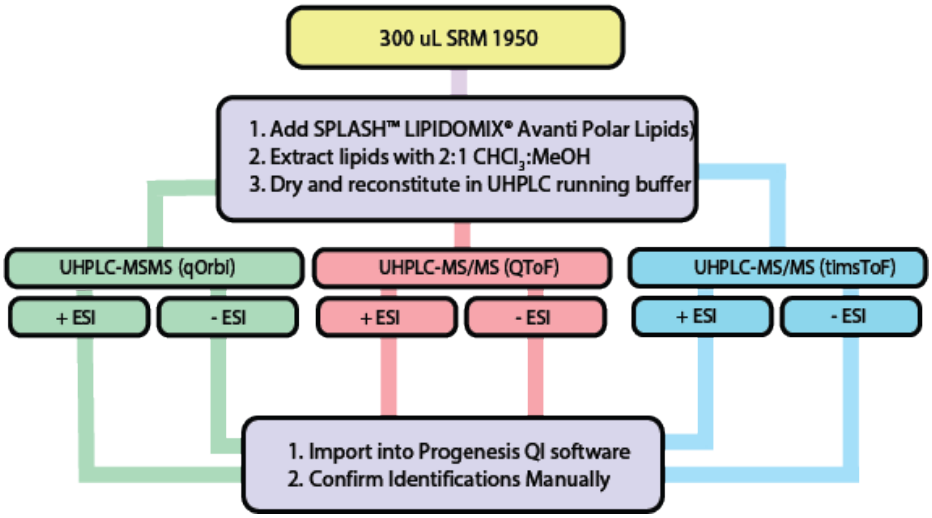

Fig 2. Summary flowchart depicting the lipidomic workflow of SRM 1950 throughout the three UHPLC-MS/MS platforms.

Chapter 5
SRM 1950 Macrolipidomics using Quadrupole-Orbitrap MS/MS

5.1 Rational and Objectives

Analysis of the plasma SRM 1950 prepared by NIST provides an overview of the plasma lipidome found in the general adult North American population in a single sample. The results of which can be utilized to identify potential lipid biomarkers for more targeted clinical analyses. The Q-Exactive by Thermo Fisher is a Quadrupole-Orbitrap (qOrbi) hybrid mass spectrometer and is the first platform used in this thesis to establish initial analytical results for the macrolipidome of SRM 1950 at the medio level utilizing an untargeted approach that would be adapted to the other platforms. The Q-Exactive is a high-resolution accurate mass instrument with very high mass accuracy and resolving power (more details in **Section 2.5.1**) that has been used in the past by our laboratory to identify lipids of high abundance in various types of biological samples.[49] Although it requires more time to resolve ions, it is capable of DDA with high sensitivity when combined with an UHPLC that separates the lipid species prior to ionization. The qOrbi provides a user-friendly interface and raw data outputs that are compatible with Progenesis QI software that supported the first attempt at characterizing SRM 1950.

5.2 Hypotheses

- The qOrbi platform will produce fragmentation for identification of lipids of high abundance at the medio level due to operation and functionality of DDA.
- The features will have a low number of false positives during the identification process, as the Orbitrap requires longer scan times to oscillate ions to achieve high resolution and sensitivity.

5.3 Methods, Materials and Study Design

5.3.1 Sample Collection and Lipid Extraction

SRM 1950 was obtained from NIST (as previously described in **Section 4.3**). Lipids were extracted via a modified Folch procedure and stored in chloroform at -80°C until analysis (as previously described in **Section 4.4**). For analysis, the SRM 1950 lipid extract was dried under nitrogen gas and reconstituted to 1500 µL using 65:30:5 acetonitrile:isopropanol:water +0.1% formic acid.

5.3.2 Macrolipidomic Profiling

A Dionex UltiMate 3000 UHPLC system (Dionex Corporation, Bannockburn, IL, USA) was used to introduce the sample into the qOrbi instrument. More information can be found in **Chapter 4** on the LC gradient, column, and other general methods used. Ion formation was completed using an ESI source. The qOrbi was operated in quadruplicate for both positive and negative polarity modes.

For the positive and negative ESI modes, the experiment was operated with a spray voltage of +/- 2.5 kV, 35,000 resolution in MS and 17,5000 resolution in MS/MS, scan range m/z 70 to 1000, sheath gas flow rate 35 and capillary temperature 300 °C. DDA for top-5 ions with a ± 1.0 Da isolation window and a normalized collision energy of 17.5 units was used. Positive spectra were lock mass-corrected using di-isooctyl phthalate (m/z 391.28429 $[M+H]^+$) which was present in the mobile phase. Negative spectra were lock mass corrected using trifluoroacetic acid that was present in the mobile phase (m/z 112.98559 $[M-H]^-$).

All data was analyzed using Progenesis QI Software (v2.3, Nonlinear Dynamics, UK) as described in detail in **Section 4.5**. This included raw data for four replicates in positive mode and three replicates in negative mode. A list of features in descending abundance was created through Progenesis QI software and the data was automatically processed to accept lipid annotations where only one of the possible raw ID had a fragmentation score >50. The automated ID lipid annotations were compared with the manual lipid annotation approach. The features were then manually inspected to identify lipids within the Progenesis data treatment software and raw chromatograms were viewed for confirmation using XCalibur QualBrowser data acquisition software (Version 2.1; Thermo-Fisher Scientific, Waltham, MA, USA) when necessary. Brutto lipid identifications were made based off the mass and retention time of a feature, and medio identifications were made if corresponding MS/MS spectra was available. Features were manually inspected until 85% of the cumulative abundance within the sample, or the top 85% most abundant compounds, were reviewed. XCalibur QualBrowser was also utilized for manual peak integrations to obtain area under the curve (AUC) values for quantitation of the 20 lipids of highest abundance.

5.4 Results

5.4.1 Number of Features and Raw Identifications using Progenesis

In positive mode, Progenesis generated 13039 features, which are ions with a unique mass and retention time (RT) found in the sample. Of these features, 11428 had at least one raw identification (ID) produced by Progenesis which was based on the imported databases using the mass of the ion and a fragmentation score when available. A total of 467 features were fragmented and generated corresponding MS/MS data, of which 419 were assigned at least one

raw ID. In negative mode, Progenesis generated 25647 features, with 22178 having at least one raw ID. From these, 157 features were fragmented to produce MS/MS data and 117 of these had at least one raw ID.

5.4.2 Fully Automated Lipid Annotation process via Progenesis QI Software

Automated identifications were limited and largely problematic. The automated lipid annotation process only generated four automated ID (raw ID with fragmentation score >50) in positive mode (**Table 3**) and three in negative mode (**Table 4**) within the top 85%. Manual inspection indicated that many of these automated ID were not correct. In positive mode, TG 16:0_16:1_18:2, TG 16:0_18:2_18:3 and TG 16:0_16:1_17:1 were correctly identified, but other TG fatty acyl isomers co-eluted, so the automated ID was considered partial. The other automated ID indicated the feature at 32.88 min RT with 690.6181 m/z was a cholesterol derivative with 20:3 ester, when it was CE 20:4. In negative mode, SM 18:2_24:1 was correctly identified through the automated ID process but the deuterated ISTD, PC 15:0_18:1(d7) was incorrectly identified as a contaminant. The third automated ID was N,N'-Ethylenebisstearamide, but this contaminant could not be confirmed manually.

5.4.3 Lipid contribution to the Top 85% of Cumulative Abundance

Features from each run (positive and negative) were ordered by decreasing abundance and the MS mass spectra of features that were in the top 85% of the total cumulative abundance were examined manually. The abundance rank, m/z, RT, brutto and medio ID when possible, relative abundance and cumulative abundance were recorded (**Appendix A.1 & A.2**).

In the positive mode, there were 147 features contributing to 85% of the total abundance of the sample, also referred to as the 'top 85%' (**Figure 3**). Within the top 85%, the feature with the smallest abundance contributed 0.080% to the total signal. Of the 147 features, 130 were manually inspected at the brutto level, which represented 83% of the total cumulative sample signal. Features that could not be assigned a brutto level lipid identification included common contaminants or unknown ions that did not match with a known mass from the lipid databases or LipidMaps. These unknown features were all referred to as contaminants. Medio level identifications were made for 87 of the 130 brutto species after manual inspection of the MS/MS fragmentation spectra. Therefore, 75% of the total sample signal in positive mode was identified at the medio level. After removing the identified contaminants and unknowns from the top 85% of total abundance, lipids were found to represent 84.5% of the cumulative signal in the positive mode. The relative abundance of a feature outside of the top 85% of signal was no more than 0.084% in positive mode.

In the negative mode, 236 features were in the top 85% of the total abundance within the sample (**Figure 4**). Within this top 85%, the feature with the smallest abundance contributed 0.037% to the total signal. Of the 236 features, 135 were manually inspected at the brutto level, which represented 73% of the total cumulative sample signal. Medio level identifications were made for 76 of the 135 brutto species after manual inspection of the MS/MS fragmentation spectra. Therefore, 65% of the total sample signal in negative mode was identified at the medio level. After removing the identified contaminants and unknowns from the top 85%, lipids were found to represent 82.4% of the cumulative signal in the negative mode. The relative abundance of a feature outside the top 85% of signal was no more than 0.045% in negative mode.

Within the top 85%, PC lipids contributed the most and accounted for 38% of the total sample abundance in positive mode (**Figure 5**). TG lipids represented just under 30% of the overall sample abundance and the remaining lipid subclass groups contributed less than 5% each to the total abundance. This included 2.7 % of the abundance as SM followed by 1.8% as LPC and then 1.4% as CE. Forty-two features were identified as TGs species and 27 as PC despite the PC lipid subclass contributing the most to the cumulative abundance. Sixty features were identified as contaminants and contributed under 10% to the cumulative abundance. Other lipids included 7 SM species, 4 LPC species and 3 CE species at the lower end of the top 85% abundance. Four ISTD were identified within the top 85% of abundance.

PC was also the major lipid subclass identified in negative mode accounting for almost 45% by abundance (**Figure 6**). SM had a cumulative abundance just over 10% in negative mode followed by LPC (4.4%), PI (1.2%), PE (1.2%), Ceramides (Cer) (0.4%), PS (0.3%) and then phosphatidylglycerol (PG) (0.1%). Contaminants represented just under 20% of the total abundance but were identified the most (n=160). Thirty features were manually identified as PC, 11 as SM, 7 as LPC, 6 as PI, 7 as PE, 4 as Ceramides, 1 as PS and 2 as PG. Eight ISTD were identified within the top 85% of abundance.

5.4.4 Quantitation of the top 20 most highly abundant lipids

Similar PC lipids were identified within the top 20 lipids in both the positive and negative polarities (**Table 5 & 6**) of SRM 1950. The top feature in both the positive and negative ESI-mode was identified as a lipid at the medio level. Upon manual inspection the first feature was identified as PC 16:0_18:2. PC 16:0_18:2 was present in SRM 1950 at concentrations of 726.0 nmol/mL in positive mode and 694.8 nmol/mL in negative mode. The next lipid identified at the

medio level in order of high to low abundance was PC 18:0_18:2 which was present at 437.5 nmol/mL in positive mode and 412.0 nmol/mL in negative mode. Seven other PC species, 1 SM and 1 LPC were also identified in both positive and negative modes.

In positive mode, nonpolar TG and CE were included in the top 20 most abundant lipids identified and quantitated. The third ranked lipid in order of descending abundance included the co-eluting TG species of TG 16:0_18:1_18:2 | TG 16:1_18:0_18:2 (**Table 5**). The | symbol denotes co-elution, and the order of the ID depicts decreasing intensity of the fragment ions. This means that the abundance, and therefore the concentration, of TG 16:0_18:1_18:2 and TG 16:1_18:0_18:2 cannot be differentiated and both species contribute to the overall abundance produced by the 874.7902 ion. These two lipid species were found at a combined concentration of 408.1 nmol/mL within the sample. The next lipid of highest abundance was PC 16:0_20:4 which had a concentration of 349.3 nmol/mL followed by PC 16:0_18:1 at 405.1 nmol/mL. The next three TG species of highest abundance included TG 16:0_18:1_18:1 | TG 16:1_18:0_18:1 (TG 52:2), TG 18:1_18:1_18:2 | TG 16:0_18:2_20:2 | TG 18:0_18:2_18:2 (TG 54:4), and TG 16:0_16:0_18:2 | TG 16:1_16:0_18:1 | TG 14:0_18:1_18:1 (TG 50:2). Individual medio lipids could not be quantitated but the overall concentration of TG 52:2 was 354.7 nmol/mL, TG 54:4 was 145.1 nmol/mL and TG 50:2 was 186.6 nmol/mL. A single SM species was identified within the top 20 lipids of highest abundance in positive mode. SM d18:1_16:0 was found at 325.6 nmol/mL. CE 18:2 had the lowest abundance of the quantified lipids but was calculated to be present within the sample at 2068 nmol/mL which was the most highly concentrated compound identified in SRM 1950.

In negative mode, additional polar lipids were in the top 20 as nonpolar lipids do not ionize and were not detected. Most lipids quantified in negative mode belonged to the PC lipid

subclass. After PC 16:0_18:2 (694.8 nmol/mL) and PC 18:0_18:2 (412.0 nmol/mL), PC 16:0_18:1 at 413.5 nmol/mL and PC 16:0_20:4 at 330.1 nmol/mL were the third and fourth ranked lipids by abundance (**Table 6**). The medio level identification and quantification of the top four SM species, in order of their abundance, were SM d18:1_16:0 at 257.4 nmol/mL, SM d18:2_24:1 at 101.5 nmol/mL, SM d18:1_22:0 at 77.3 nmol/mL and SM d18:1_24:0 at 53.2 nmol/mL. The lipid of lowest abundance in negative mode was PI 18:0_20:4 at a quantity of 33.1 nmol/mL.

Table 3. Fully Automated Identifications of features in the top 85% of positive mode cumulative abundance by Progenesis QI software with follow up manual lipid inspection results in the Quadrupole-Orbitrap platform.

Retention time (min)	m/z	Highest Ranked Automated ID[1]	Corresponding Manual ID	Correct Automated ID
32.07	846.7580	TG 16:0_16:1_18:2	TG 16:1_16:1_18:1 | TG 16:0_16:1_18:2 | TG 14:0_18:1_18:2	Partial[3]
32.88	690.6181	Cholesterol derivative_20:3[2]	CE 20:4	No
31.32	870.7563	TG 16:0_18:2_18:3	TG 16:0_18:2_18:3 | TG 16:1_18:1_18:3	Partial[3]
32.94	834.7553	TG 16:0_16:1_17:1	TG 16:0_16:1_17:1 | TG 16:1_16:1_17:0 | TG 15:0_16:0_18:2 | TG 15:0_16:1_18:1 | TG 15:1_16:0_18:1 | TG 14:0_17:1_18:1 | TG 14:0_17:0_18:2 | TG 15:0_17:1_17:1 | TG 15:1_17:0_17:1	Partial[3]

TG, triacylglycerol; CE, cholesterol ester.

[1]Progenesis provides a list of possible raw identifications (ID) based on matching m/z and fragmentation patterns to ChemSpider and LipidBlast databases and accepts a raw ID when only one fragmentation score >50.

[2]The cholesterol ester derivative was identified as *(3beta,22E)-Stigmasta-5,22-dien-3-yl (9Z,12Z,15Z)-9,12,15-octadecatrienoate.*

[3]Manual inspection revealed more than one TG isomers coeluting at the retention time.

Table 4. Fully Automated Identifications of features in the top 85% of negative mode cumulative abundance by Progenesis QI software with follow up manual lipid inspection results in the Quadrupole-Orbitrap platform.

Retention time (min)	m/z	Highest Ranked Automated ID[1]	Corresponding Manual ID	Correct Automated ID
18.30	797.6011	Contaminant	ISTD, PC 15:0_18:1(d7)	No
22.85	855.6561	SM 18:2_24:1	SM 18:2_24:1	Yes
25.41	637.5868	Contaminant[2]	Contaminant	Not confirmed[3]

ISTD, internal standard; PC, phosphatidylcholine; SM, sphingomyelin.
[1]Progenesis provides a list of possible raw identifications (ID) based on matching m/z and fragmentation patterns to ChemSpider and LipidBlast databases and accepts a raw ID when only one fragmentation score >50.
[2]Contaminant was automatically identified from Progenesis as *N,N'-Ethylenebis(stearamide)*.
[3]Manual inspection did not identify the structure of the contaminant.

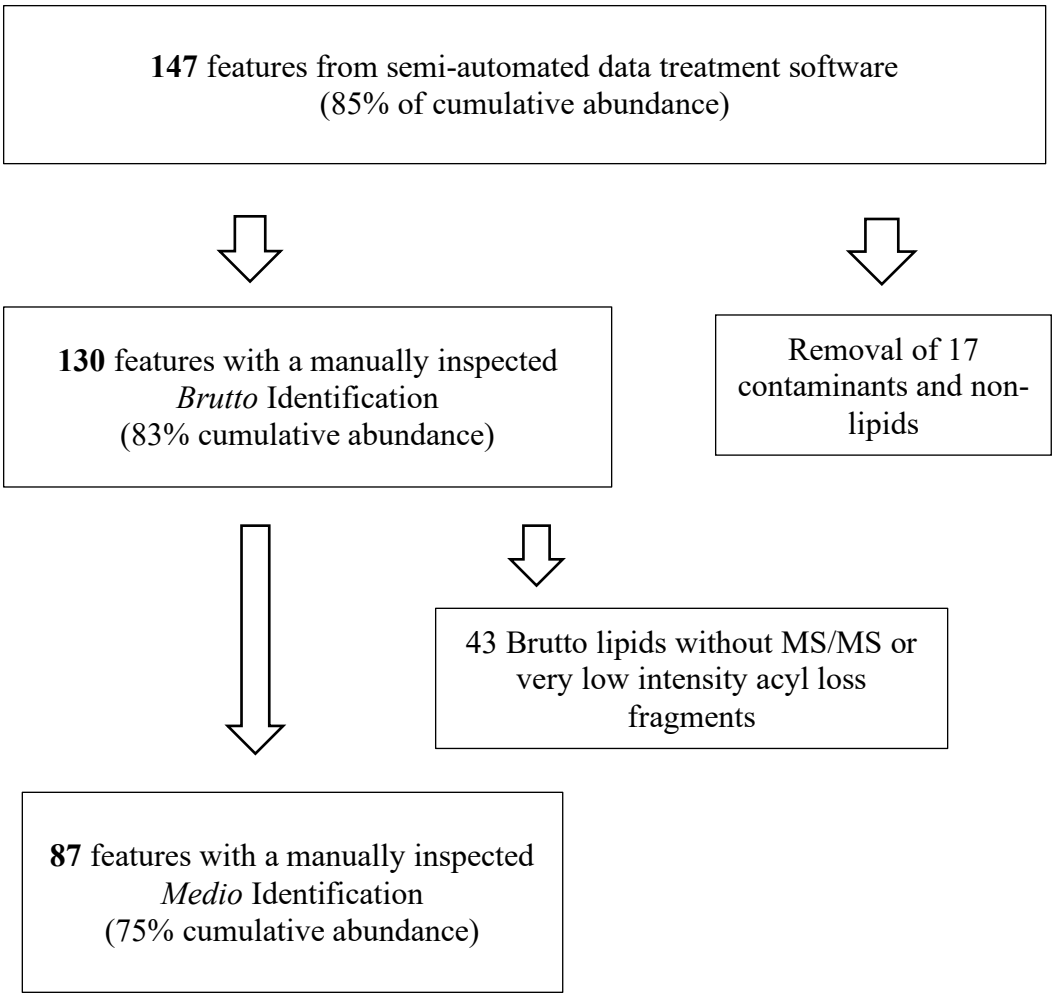

Fig 3. Process of identifying lipids from features to medio level in positive mode of the Quadrupole-Orbitrap platform. Features in Standard Reference Material 1950 at the top 85% of cumulative abundance were collected semi-automatically by Progenesis and manually inspected to confirm lipid identifications at the brutto and medio level.

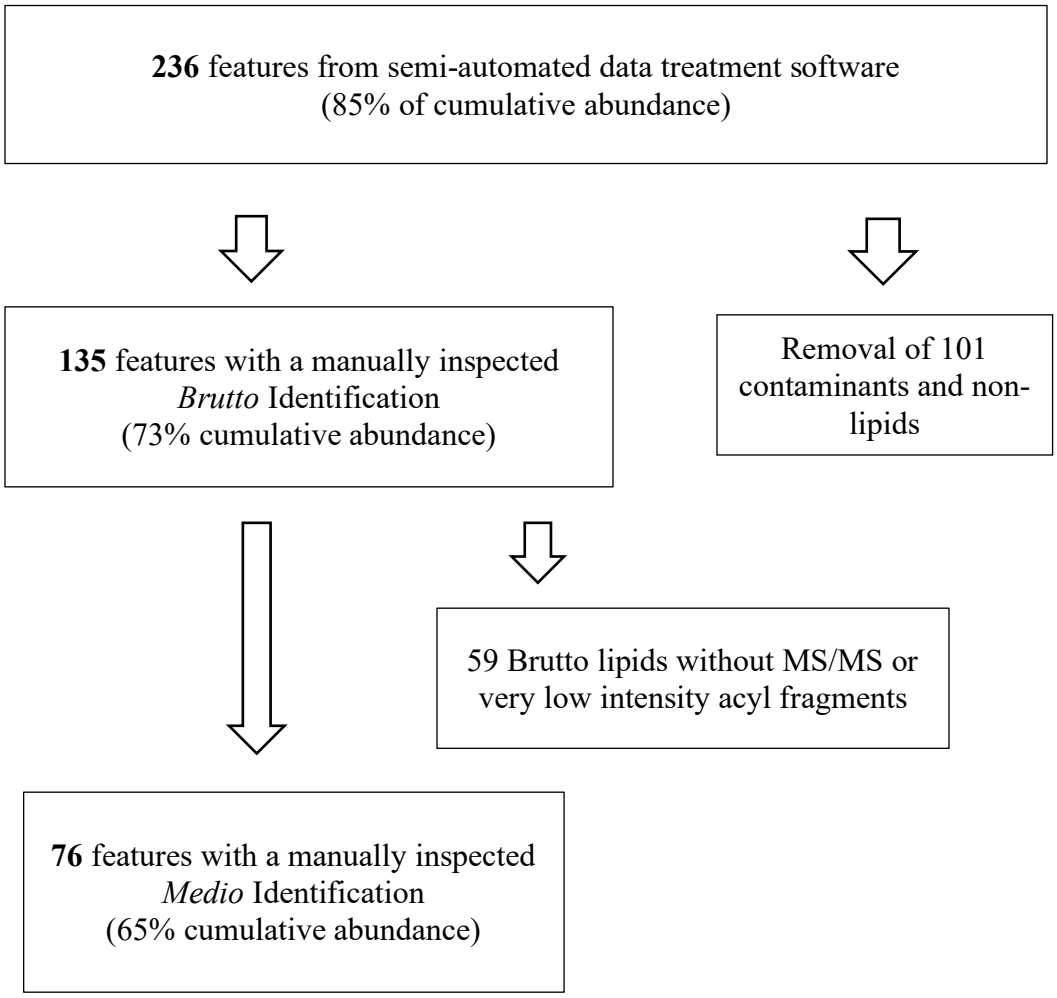

Fig 4. Process of identifying lipids from features to medio level in negative mode of the Quadrupole-Orbitrap platform. Features in Standard Reference Material 1950 at the top 85% of cumulative abundance were collected semi-automatically by Progenesis and manually inspected to confirm lipid identifications at the brutto and medio level.

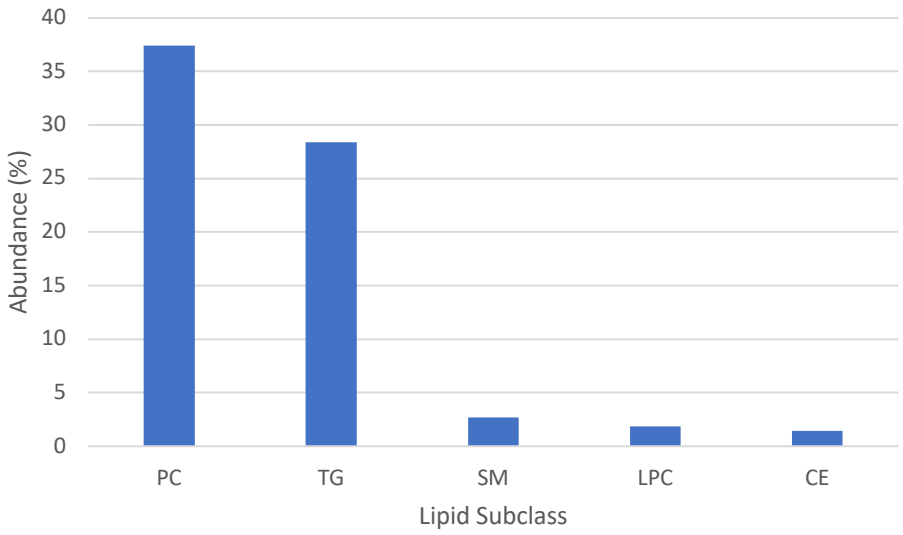

Fig 5. The Abundance by Lipid Subclass within Standard Reference Material 1950 via the Quadrupole-Orbitrap platform in positive polarity.
PC, phosphatidylcholine (n=27); TG, triacylglycerol (n=42); SM, sphingomyelin (n=7); LPC, lysophosphatidylcholine (n=4); CE, cholesterol ester (n=3).

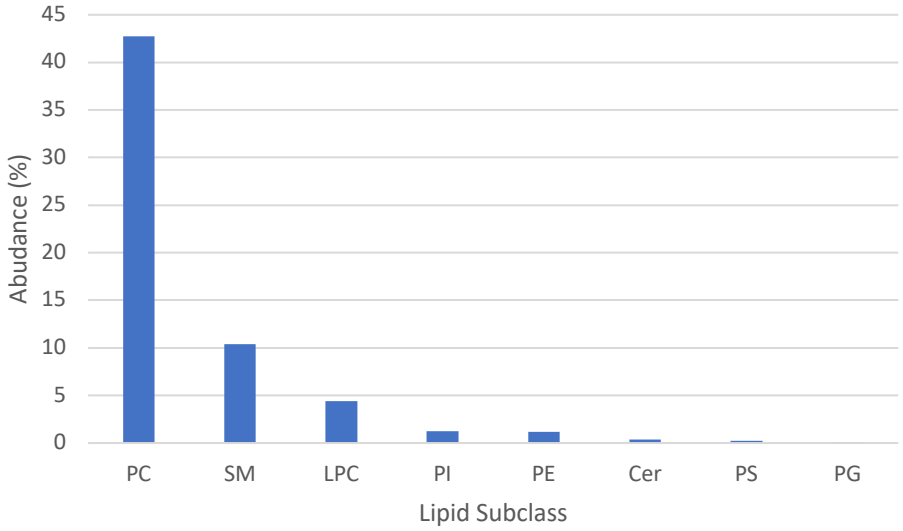

Fig 6. The Abundance by Lipid Subclass within Standard Reference Material 1950 via the Quadrupole-Orbitrap platform in negative polarity.
PC, phosphatidylcholine (n=30); SM, sphingomyelin (n=11);
LPC, lysophosphatidylcholine (n=7); PI, phosphatidylinositol (n=6);
PE, phosphatidylethanolamine (n=7); Cer, ceramide (n=4); PS, phosphatidylserine (n=1);
PG, phosphatidylglycerol (n=2).

Table 5. Quantitation of the top 20 lipids of highest abundance using positive polarity in the Quadrupole-Orbitrap.

m/z	Brutto ID	Medio ID	Plasma concentration (nmol/mL)
758.5718	PC 34:2	PC 16:0_18:2	726.0 ± 5.9
786.6032	PC 36:2	PC 18:0_18:2	437.5 ± 1.7
874.7902	TG 52:3	TG 16:0_18:1_18:2 | TG 16:1_18:0_18:2	408.1 ± 1.6
782.5714	PC 36:4	PC 16:0_20:4	349.3 ± 2.6
760.5871	PC 34:1	PC 16:0_18:1	405.1 ± 2.2
876.8070	TG 52:2	TG 16:0_18:1_18:1 | TG 16:1_18:0_18:1	354.7 ± 1.4
810.6032	PC 38:4	PC 18:0_20:4	211.8 ± 1.8
806.5714	PC 38:6	PC 16:0_22:6	152.3 ± 1.7
900.8066	TG 54:4	TG 18:1_18:1_18:2 | TG 16:0_18:2_20:2 | TG 18:0_18:2_18:2	145.1 ± 3.4
848.7746	TG 50:2	TG 16:0_16:0_18:2 | TG 16:1_16:0_18:1 | TG 14:0_18:1_18:1	186.6 ± 7.4
902.8225	TG 54:3	TG 18:0_18:1_18:2	133.6 ± 7.8
850.7901	TG 50:1	TG 16:0_16:0_18:1	123.5 ± 4.6
898.7893	TG 54:5	TG 18:1_18:2_18:2 | TG 18:1_18:1_18:3	83.9 ± 2.8
784.5870	PC 36:3	PC 18:1_18:2	94.7 ± 0.3
846.7580	TG 50:3	TG 16:0_16:1_18:2	90.0 ± 3.2
703.5748	SM 34:1	SM d18:1_16:0	325.6 ± 2.3
496.3404	LPC 16:0	LPC 16:0	270.3 ± 10.5
788.6179	PC 36:1	PC 18:0_18:1	76.9 ± 0.7
812.6184	PC 38:3	PC 18:0_20:3	71.6 ± 0.7
666.6175	CE 18:2	CE 18:2	2068 ± 43

Values are mean ± S.D. of n=4 technical replicates. PC, phosphatidylcholine; TG, triacylglycerol; SM, sphingomyelin; LPC, lysophosphatidylcholine; CE, cholesterol ester.

Table 6. Quantitation of the top 20 lipids of highest abundance using negative polarity in the Quadrupole-Orbitrap.

m/z	Brutto ID	Medio ID	Plasma concentration (nmol/mL)
802.5564	PC 34:2	PC 16:0_18:2	694.8 ± 13.7
830.5875	PC 36:2	PC 18:0_18:2	412.0 ± 2.1
804.5723	PC 34:1	PC 16:0 _18:1	413.5 ± 10.4
826.5566	PC 36:4	PC 16:0 _20:4	330.1 ± 7.8
747.5628	SM 34:1	SM d18:1_16:0	257.4 ± 5.4
828.5724	PC 36:3	PC 16:0 _20:3	191.5 ± 4.0
854.5876	PC 38:4	PC 18:0_20:4	164.2 ± 4.6
540.3288	LPC 16:0	LPC 16:0	203.7 ± 3.4
857.6715	SM 42:3	SM d18:2_24:1	101.5 ± 2.9
828.5725	PC 36:3	PC 18:1_18:2	99.5 ± 2.1
856.6037	PC 38:3	PC 18:0 _20:3	84.5 ± 3.5
831.6561	SM 40:1	SM d18:1_22:0	77.3 ± 1.8
832.6031	PC 36:1	PC 18:0_18:1	84.9 ± 2.8
859.6872	SM 42:1	SM d18:1_24:0	53.2 ± 3.2
826.5564	PC 36:4	PC 18:2_18:2	61.9 ± 7.0
850.5569	PC 38:6	PC 16:0_22:6	63.2 ± 2.6
568.3598	LPC 18:0	LPC 18:0	92.5 ± 2.6
852.5726	PC 38:5	PC 18:1_20:4 | PC 16:0_22:5	61.8 ± 1.5
855.6561	SM 42:3	SM d18:2_24:1	54.4 ± 1.4
885.5456	PI 38:4	PI 18:0_20:4	33.1 ± 1.3

Values are mean ± S.D. of n=3 technical replicates. PC, phosphatidylcholine; SM, sphingomyelin; LPC, lysophosphatidylcholine; PI, phosphatidylinositol.

5.5 Discussion

The qOrbi was able to characterize the macrolipidome of SRM 1950 at the medio level through an untargeted approach. Automated annotation using the Progenesis QI software was attempted but was largely unsuccessful. However, the raw MS/MS fragment ions spectra produced by the qOrbi tended to be highly resolved allowing relatively straightforward manual medio identifications. Using a macrolipidomic approach that focuses on highly abundant lipids, the number of features examined manually decreased from over 11,000 to 147 features in positive mode and from over 25,000 to 236 features in negative mode. The first 20 features within SRM 1950 contributed 58% of the total abundance in positive mode (+) and 52% in negative mode (-) (**Appendix A.1 & A.2**). These 20 lipids of highest abundance were also quantified using internal standards.

Difficulties in automated software annotation included a low number of automatic identifications with several being incorrect after manual inspection (**Table 3 & 4**). More species could have been automatically identified by lowering the required fragmentation score of >50 to >40, but this also reduced the quality of the automated ID which was already poor at >50. The automated ID process was also not able to recognize when other lipids were co-eluting as it matches spectra patterns preferentially to the high intensity signals and can disregard lower intensity signals that can be informative. For example, Progenesis identified the 834.7553 m/z ion as TG 16:0_16:1_17:1 when there were nine other co-eluting compounds present. Although Progenesis was capable of partially annotating the lipid, essential medio level information is missed through this process and manual inspection of each automated ID is required. It was hypothesized that the qOrbi would produce **a low number of false positives during the identification process, as the orbitrap requires longer scan times to oscillate ions to achieve**

high resolution and sensitivity. Based on the present results this hypothesis must be rejected. However, the low number of identifications and the relatively high % of false identifications is more of a reflection of the data treatment software and possibly the inability to fully isolate individual lipid species by the upfront UHPLC separation and not the qOrbi mass spectrometer.

When determining the macrolipidome, features that fell within the top 85% of the total abundance were examined and the relative % contributions were examined. The smallest feature in the top 85% contributed 0.08% in positive mode and 0.04% in negative mode. After removal of contaminants within the top 85% of signal abundance, the relative abundance of the smallest feature was 0.08% (+) and 0.05% (-) therefore any lipid with a relative abundance greater than 1% was identified when a top 85% approach was used. As a result, in addition to examining features that fall within the top 85% of the total abundance, any feature that contributes 1% relative abundance should also be examined and considered part of the macrolipidome. After manually inspecting features in the top 85% of the total abundance, medio level identifications were made for 75% of the total abundance in positive mode and 65% in the negative mode (**Figures 3 & 4**). GP, GL and CE were the three major lipid classes in SRM 1950 which agrees with previous reports on human plasma.[14,15] All three ionize in the positive ESI-mode[87,88] but GL and CE will not ionize in negative mode and go undetected. The inability of negative mode to detect these high abundant lipids is the main reason that only 65% of the total abundance were assigned medio levels in negative mode as the features in top 85% included many with smaller relative % contributions.

Manual medio level identification was laborious. The process would start by examining the possible raw ID using the data treatment software (Progenesis) where there could be multiple suggestions for a single feature. Manual inspection of the fragmentation in Progenesis was

completed that often-required consultation with the Lipid Maps online tools (www.lipidmaps.org) to confirm common fragmentation patterns of a specific lipid. Overall, the data from the qOrbi imported well into Progenesis and the fragmentation spectra could be viewed. When the data importation is poor and MS/MS fragmentation data is not available in the data treatment software (Progenesis), the raw spectra on the data acquisition software (XCalibur for the qOrbi) would need to be consulted. Examining raw spectra using XCalibur was not required very often. Medio level identifications of TG species was particularly difficult. With three fatty acyls, the number of possible TG isomers is high which also increase the chances for co-elution. Co-elution results in overlapping mass spectra at a single retention time. The brutto ID is known, so the different fatty acyl combinations can eventually be discriminated but teasing apart multiple isomers is particularly tedious. The fact that TG only ionize in positive mode further complicates the identification process. Fatty acyl chains can only hold a negative charge, so in positive mode, acyl chain patterns are determined by comparing fragments to the parent ion and determining the fatty acyl that was lost. Calculating the neutral loss of potential fatty acyl species while determining all the potential different fatty acyl combinations present for the detected mass of co-eluting isomeric TG was a significant manual burden that needs to be addressed before macrolipidomic profiling of plasma can be used routinely.

PC was the most abundant lipid subclass in the SRM 1950 macrolipidome (**Figures 5 and 6**) which is consistent with literature. PC is an important component of plasma lipoproteins and is abundant in other biological tissues as a major component of cell membranes and is the most common dietary phospholipid which can be found in egg yolk and soybeans.[14,15, 89] TG species were found in high abundance in the positive mode as expected as they are carried within lipoproteins (**Figure 5**).[88] The abundance of CE determined in positive mode was lower than

anticipated based on quantitation reports in the literature.[15] This reflects an important difference between abundance and quantification and will be discussed in more detail below when examining the quantitation of CE 18:2 (**Table 5**). More GP lipid subclass compounds such as PI, PE, PS and PG were identified in negative polarity which was expected as they ionize well in negative mode (**Figure 6**). The hypothesis that **the qOrbi platform will produce fragmentation for identification of lipids of high abundance at the medio level due to operation and functionality of DDA** can be accepted. Operating the qOrbi in DDA combines the high resolution obtained from the orbitrap mass spectrometer with the top five most abundant ions present at the time of the full MS scan. Therefore, the most abundant lipids at any chromatographic time point are most likely to be fragmented and have corresponding MS/MS data resulting in the ability to describe the macrolipidome at the medio level.

The deuterated ISTD (SPLASH Lipidomix) contains a deuterated internal standard for each lipid class and was used for quantitation to account for differences in instrument response and ionization efficiency between lipid classes.[90] SPLASH Lipidomix accounts for the variation in the concentrations of each native lipid class physiologically by mimicking the concentrations with the concentrations of each of the deuterated lipids.[84] For lipids that were ionizable in both positive and negative polarities, it was supportive to observe the lipids with the same medio ID in both polarities have concentrations in the same range (**Tables 5 & 6**). For example, PC 16:0_18:2 and SM d18:1_16:0 were the PC and SM lipids with the highest concentration across both polarities. In positive mode, the concentration of PC 16:0_18:2 was 726.0 nmol/mL and 694.8 nmol/mL in negative mode, while SM d18:1_16:0 was found at 325.6 nmol/mL and 257.4 nmol/mL. There was a pattern for positive mode to generate higher concentrations than negative mode for the same lipids. This is likely due to higher ionization efficiency in positive mode.[91]

The quantitation of CE 18:2 was problematic. By abundance, CE 18:2 (666.6175 m/z) was ranked 20th yet it had the highest concentration after quantitation. CE ionizes much less efficiently than TG and the cholesterol structure readily fragments and loses water molecule ([M-H_2O]$^+$) resulting in a diagnostic 369.3515 m/z ion even at the MS level. The intensity of this fragment is higher than that of the parent ion resulting in matrix effects and ion suppression of the parent due to competition and interference from the more intense fragment ion.[38,92] The ISTD of CE 18:1(d7) is meant to control for this but to do so requires additional calculations. The deuterated component of the ISTD does not get included in the 369.3515 m/z diagnostic ion and the 369.3515 m/z fragment from native CE 18:1 in SRM 1950 co-elutes with that of the ISTD. However, a ratio of the AUC from the CE 18:1/CE 18:1(d7) parent ions that co-elute can be separated by mass which was calculated and then applied to the AUC of the co-eluting 369.3515 m/z ion to identify the amount of 369.3515 m/z from CE 18:1 and CE 18:1(d7) for quantitation. The resulting concentration of 2068 ± 43 nmol/mL for CE 18:2 was the most abundant lipid species in SRM 1950 which is similar to a previous report of 1820 ± 147 nmol/mL in SRM 1950.[15] For future working defining the macrolipidome, the abundance and quantitation of CE should be examined at the CE class level to identify CE species of high abundance and concentrations. CE 18:2 has been estimated to make up 62% of the CE pool, but CE 18:1, CE 20:4 and CE 16:0 may be found in high concentrations in plasma as well but were not at high abundance due to the behaviour of CE in the mass spectrometer.

5.6 Conclusion

In this chapter, the medio level ID of highly abundant lipids in SRM 1950 were characterized using the qOrbi. Although Progenesis QI software was used to aid in lipid annotation, the

identification of co-eluting and isomeric species still required manual identification using XCalibur software. This was specifically an obstacle in TG species where challenges in chromatographic separation of isomeric species are present. Utilizing the top 85% of total abundance proved to be a useful tool in identifying the macrolipidome, since every feature with >0.1% relative abundance was reviewed in this approach. Overall, the qOrbi platform was successful in fragmenting lipid compounds of high abundance which resulted in medio level ID for the top 20 most highly abundant lipids. Quantitation of the most abundant lipids was also successful and showed similar trends between both polarities. The most abundant lipid at the medio level was identified by raw abundance as PC 16:0_18:2 at concentrations of 726 nmol/mL by positive and 695 nmol/mL by negative chromatograms respectively. CE 18:2 had low raw abundance but was the lipid with the highest concentration after adjusting with the ISTD. The instrument raw acquisition data was compatible with the data treatment software which also aided in identification and efficiency of the qOrbi platform for a manual approach. The automatic lipid annotation through Progenesis was not useful and clearly is an area that requires additional development at the software level, but could also be aided by technological advancements in analyte separation to eliminate co-elution.

Chapter 6
SRM 1950 Macrolipidomics using Quadrupole-Time of Flight MS/MS

6.1 Rational and Objectives

Human plasma provides a valuable source of physiological insight from the impacts of chronic disease and dietary intake. Despite attempts of brutto lipid species identification in SRM 1950 to gain insight on the human plasma lipidome, it is evident that the use of different lipidomic workflows, which includes the use of different mass spectrometer platforms, produces variation in lipid profiling.[14, 15, 58] Time of flight mass spectrometers have become more popular due to improved mass resolution through ion beam focusing, reflectron designs and infused lock mass correction. The Waters QToF (described in more detail in **Section 2.5.2**) can provide high resolution scans without compromising scanning speeds, which should detect features for the most abundant lipids in human plasma SRM 1950. This MS UHPLC-MS/MS platform has also been used successfully by our laboratory for lipidomic profiling of various biological samples.[49] The same SRM 1950 lipid extract was examined on this QToF platform using a similar UHPLC separation and untargeted macrolipidomic approach as used in Chapter 5 for the qOrbi. The present Chapter will focus on the analytical results within this instrument, while cross-platform comparisons is the focus of Chapter 8.

6.2 Hypothesis

- The QToF will identify a high number of features in SRM 1950 but there will be a high false positive rate and many features will be low abundant, non-lipids, due to the fast scan times the QToF.

6.3 Methods, Materials and Study Design

6.3.1 Sample Collection and Lipid Extraction

SRM 1950 was obtained from NIST (as previously described in **Section 4.3**). Lipids were extracted via a modified Folch procedure and stored in chloroform at -80°C until analysis (as previously described in **Section 4.4**). For analysis, the SRM 1950 lipid extract was dried under nitrogen gas and reconstituted to 1500 µL using 65:30:5 acetonitrile:isopropanol:water +0.1% formic acid.

6.3.2 Macrolipidomic Profiling

A Waters Acquity UHPLC system coupled to a Waters Synapt G2Si QToF mass spectrometer (Waters Corporation, Milford, MA, USA) was operated in quadruplicate for both positive and a negative ESI-polarity method. More information can be found in **Chapter 4** on the LC gradient, column, and other general methods used.

The mass spectrometer was operated in positive ESI mode with a spray voltage of 2.5 kV, in high-resolution mode (approximately 42,000 resolution), scan range m/z from 50 to 1000, scan time 0.2s/scan, cone voltage 40V. The cone gas flow rate was 100 L/hr, the desolvation gas flow rate 600 L/hr, the nebulizer gas flow rate 7.0 bar, source temperature 140 °C, and the desolvation temperature 400 °C. Lock mass correction was performed using constant infusion of leucine enkephalin (m/z 556.2771 for $[M+H]^+$). Tandem mass spectrometry was used in DDA conditions for top-5 ions with an interval of ±1.0 Da scanning window. Scan frequency was 0.1 s/scan, transfer cell collision energy ramp of 20 V to 30 V at low mass (m/z 50) and 30 V to 50 V at high mass (m/z 100).

Negative ESI mode was operated using a spray voltage of -2.5 kV. High-resolution mode (approximately 42,000 resolution) with scan range m/z 100 to 1200, scan time 0.2 s/scan, cone voltage 40 V, cone gas flow 100 L/hr, desolvation gas flow 600 L/hr, nebulizer gas flow 7.0 bar, source temperature 140 °C, and desolvation temperature 400 °C was used. Lock mass correction was performed using constant infusion of leucine enkephalin (m/z 554.2615 for $[M-H]^-$). Collision energies in the transfer cell were ramped from 30 C to 45V at low mass (m/z 100) and 35 V to 60 V at high mass (m/z 1200) for negative-ESI.

All data was analyzed using Progenesis QI software (v2.3, Nonlinear Dynamics, UK) as described earlier in more detail in **Chapter 4.5**. This included raw data for three replicates in positive mode and four replicates in negative mode. A list of features in descending abundance was created through Progenesis QI software and the data was automatically processed to accept lipid annotations where only one of the possible raw ID has a fragmentation score >50. The automated ID lipid annotations were compared with the manual lipid annotation approach. The features were then manual inspected to identify lipids within Progenesis data treatment software and raw chromatograms using MassLynx (version 4.1; Waters, Milford, MA, USA) data acquisition software were viewed for confirmation when necessary. Brutto lipid identifications were made based off the mass and retention time of a feature, and medio identifications were made if corresponding MS/MS spectra was available. Features were manually inspected until 85% of the cumulative abundance within the sample, or the top 85% most abundant compounds, were reviewed. MassLynx was also utilized for manual peak integrations to obtain area under the curve (AUC) values for quantitation of the 20 lipids of highest abundance.

6.4 Results

6.4.1 Number of Features using Progenesis

In the positive (+) and negative (-) methods, Progenesis obtained 3042 (+) and 5785 (-) features and 2299 (+) and 3918 (-) of these features had at the minimum one possible raw ID. Of these, 164 (+) and 213 (-) features were fragmented and have corresponding MS/MS data and 120 (+) and 187 (-) of these were assigned a possible raw ID at the medio level.

6.4.2 Fully Automated Lipid Annotation process via Progenesis QI software

The automated lipid annotation process in positive mode using Progenesis generated one automated ID within the top 85% of most abundant compounds (257 features) when accepting a raw ID that had only one possible fragmentation score >50 (**Table 7**). The highest ranked automated ID was a contaminant. This was not correct according to manual inspection which identified the feature as LPC 18:0. In negative mode, three automated IDs were made within the top 85% of abundance (420 features) (**Table 8**). This included two contaminants and SM d18:2_24:1. Both automatically identified contaminants were identified as PC O-18:0_20:4 and PC P-16:0_18:2 upon manual inspection.

6.4.3 Lipid contribution to the Top 85% of Cumulative Abundance

Features from each run (positive and negative) were ordered by decreasing abundance and the MS mass spectra of features that were in the top 85% of the total cumulative abundance were examined manually (**Appendix A.3 & A.4**).

In the positive mode, the most abundant 257 features made up the top 85% (**Figure 7**). Within the top 85%, the feature with the smallest abundance contributed 0.050% to the total

signal. Of these 257 features, 161 were manually inspected at the brutto level, which represented 60% of the total cumulative sample signal. Features that could not be assigned a brutto level lipid identification included common contaminants or unknown ions that did not match with a known mass from the lipid databases or LipidMaps. These features were all referred to as contaminants. Medio level identifications were made for 86 of the 161 brutto species after manual inspection of the MS/MS fragmentation spectra. Therefore, 43% of the total sample signal in positive mode was identified at the medio level. After removing the identified contaminants and unknowns from the top 85% of total abundance, lipids were found to represent 80.4% of the cumulative signal in the positive mode. The relative abundance of a feature after the top 85% of signal was no more than 0.068% in positive mode.

In the negative mode, the most abundant 420 features made up 85% of the total abundance within the sample (**Figure 8**). Within the top 85%, the feature with the smallest abundance contributed 0.022% to the total signal. Of the 420 features, 122 were manually inspected at the brutto level, which represented 36% of the total cumulative sample signal. Medio level identifications were made for 99 of the 122 brutto species after manual inspection of the MS/MS fragmentation spectra. Therefore, 35% of the total sample signal in negative mode was identified at the medio level. After removing the identified contaminants and unknowns from the top 85% of signal abundance, lipids were found to represent 69.6% of the cumulative signal in the negative mode. The relative abundance of a feature after the top 85% of signal was no more than 0.045% in negative mode.

Within the top 85% of most abundant compounds, PC lipids contributed the most and made up just over half of the identified medio lipid abundance in positive mode (**Figure 9**). PC contributed 22% to the total abundance. The next most abundant lipid class was TG which

represented almost 15% of the total abundance. The remaining groups contributed less than 5% each to the total abundance. SM lipids had an abundance of 1.5% followed by LPC and CE lipids which had an abundance around 1.3%, followed by cholesterol with less than 1%. The greatest number of features were identified as TG despite the PC lipid subclass contributing the most to the cumulative abundance. One-hundred-and-seventy features were identified as contaminants and contributed 42.6% to the cumulative abundance. The number of features manually identified as lipids included 35 TG, and 31 PC. The lipids at the lower end of the top 85% abundance included 6 SM species, 4 LPC species, and 5 CE. Six ISTD were identified within the top 85% of abundance.

By abundance, PC was also the major lipid subclass identified in negative mode (**Figure 10**). PC accounted for 21.4% of the total cumulative abundance which was over half of the abundance that was identified at the medio level in negative mode. SM had a cumulative abundance of 7%. The remaining subclasses each had a cumulative abundance less than 3%. This included LPC (2.5%), followed by PI (0.7%), PE (0.5%), Cer (0.3%), FFA (0.2%), Hexosylceramide (HexCer) (0.1%) and then LPE (0.03%). Contaminants represented 50.3% of the total abundance and were identified the most (n=322). Thirty-seven features were manually identified as PC, 24 as SM, 9 as LPC, 6 as PI, 6 as PE, 3 as Cer, 4 as FFA, 2 as HexCer and 1 as LPE. Six ISTD were identified within the top 85% of abundance.

6.4.4 Quantitation of the top 20 most highly abundant lipids

Similar PC lipids were identified within the top 20 lipids in both the positive and negative polarities (**Table 9 & 10**) of SRM 1950. The top lipid in both the positive and negative ESI- mode was identified at the medio level through manual inspection as PC 16:0_18:2. PC

16:0_18:2 was present in SRM 1950 at concentrations of 498.1 nmol/mL in positive mode and 825.9 nmol/mL in negative mode. The first four lipids identified at the medio level in order of high to low abundance were all PC lipids and had consistent rankings between polarities. The next most abundant lipid was PC 18:0_18:2 which was present at 369.7 nmol/mL in positive mode and 485.6 nmol/mL in negative mode. PC 16:0_18:1was present at 360.7 nmol/mL in positive mode and 425.5 nmol/mL in negative mode. PC 16:0_20:4 was present at 298.1 nmol/mL and 356.4 nmol/mL in negative mode.

In positive mode, the 5th greatest lipid identified was TG 16:0_18:1_18:2 with a concentration of 256.6 nmol/mL which was the greatest GL identified. The next greatest medio level lipid identified was TG 16:0_18:1_18:1 at 306.6 nmol/mL. The next two greatest GL species could not be identified at the medio level due to poor intensity of the loss of acyl chain fragment ions. These GL were both TG species and included TG 58:3 with a concentration of 164.2 nmol/mL and TG 58:2 at 165.8 nmol/mL. CE 18:2 was the next most abundant lipid that did not belong to the GL or GP lipid class and was found at a concentration of 2179 nmol/mL in SRM 1950. One SP lipid was identified within the top 20 most abundant ions in positive mode which was SM d18:1_16:0 at 313.1 nmol/mL.

In negative mode, the top 20 most abundant lipid species were all PC, LPC or SM lipids. After the first four PC lipids the next two most abundant lipids were also PC lipids: PC 16:0_20:3 with a concentration of 193.1 nmol/mL and PC 18:0_20:4 207.3 nmol/mL. The seventh most abundant lipid was LPC 16:0 with a concentration of 248.8 nmol/mL within the plasma sample. LPC 18:0 at 88.1 nmol/mL and LPC 18:2 at 72.3 nmol/mL were other LPC species quantified within the first 20 lipids. The medio level identification and quantification of the top four SM species, in order of their abundance, were SM d18:1_24:1 at 169.7 nmol/mL,

SM d18:1_16:0 at 248.9 nmol/mL, SM d18:1_24:0 at 67.5 nmol/mL, and SM d18:1_22:0 at 91.5 nmol/mL.

Table 7. Fully Automated Identifications of features in the top 85% of positive mode cumulative abundance by Progenesis QI software with follow up manual lipid inspection results in the Quadrupole-Time-of-Flight platform.

Retention time (min)	m/z	Highest Ranked Automated ID[1]	Corresponding Manual ID	Correct Automated ID
5.01	524.3711	Contaminant	LPC 18:0	No

LPC, lysophosphatidylcholine.
[1]Progenesis provides a list of possible raw identifications (ID) based on matching m/z and fragmentation patterns to ChemSpider and LipidBlast databases and accepts a raw ID when only one fragmentation score >50.

Table 8. Fully Automated Identifications of features in the top 85% of negative mode cumulative abundance by Progenesis QI software with follow up manual lipid inspection results in the Quadrupole-Time-of-Flight platform.

Retention time (min)	m/z	Highest Ranked Automated ID[1]	Corresponding Manual ID	Correct Automated ID
21.63	855.6592	SM d18:2_24:1	SM d18:2_24:1	Yes
20.86	840.6112	Contaminant	PC O-18:0_20:4	No
17.17	786.5643	Contaminant	PC P-16:0_18:2	No

SM, sphingomyelin; PC, phosphatidylcholine; PC O, plasmanyl species; PC P, plasmenyl species.
[1]Progenesis provides a list of possible raw identifications (ID) based on matching m/z and fragmentation patterns to ChemSpider and LipidBlast databases and accepts a raw ID when only one fragmentation score >50.

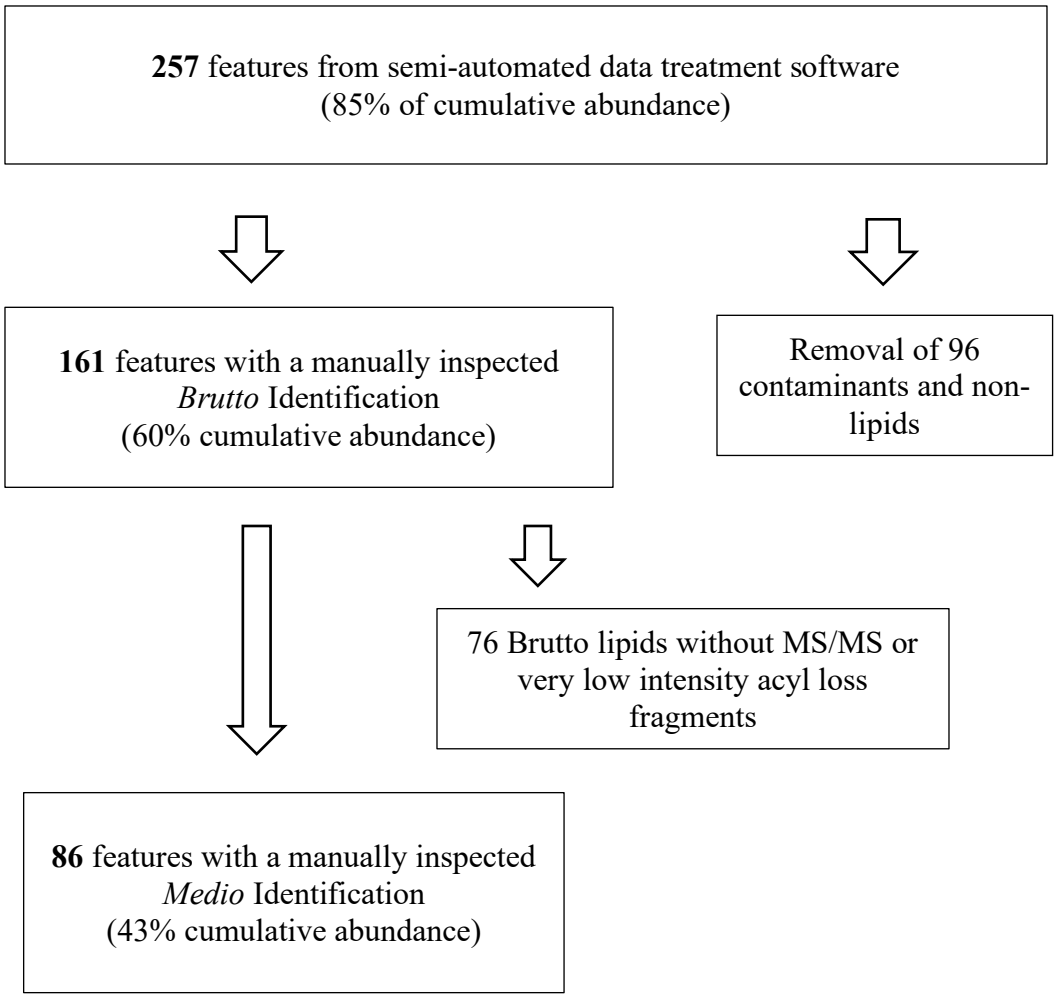

Fig 7. Process of identifying lipids from features to medio level in positive mode of the Quadrupole-Time-of-Flight platform. Features in Standard Reference Material 1950 at the top 85% of cumulative abundance were collected semi-automatically by Progenesis and manually inspected to confirm lipid identifications at the brutto and medio level.

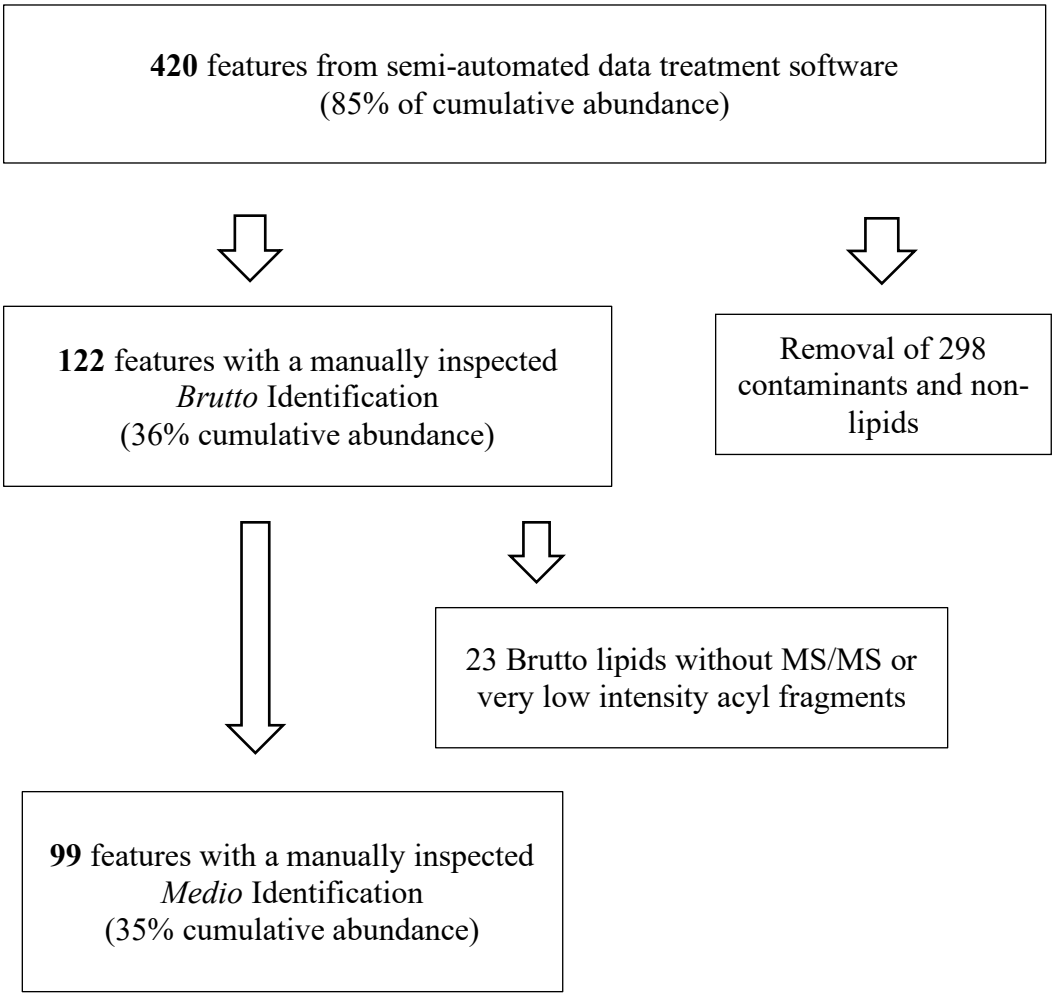

Fig 8. Process of identifying lipids from features to medio level in negative mode of the Quadrupole-Time-of-Flight platform. Features in Standard Reference Material 1950 at the top 85% of cumulative abundance were collected semi-automatically by Progenesis and manually inspected to confirm lipid identifications at the brutto and medio level.

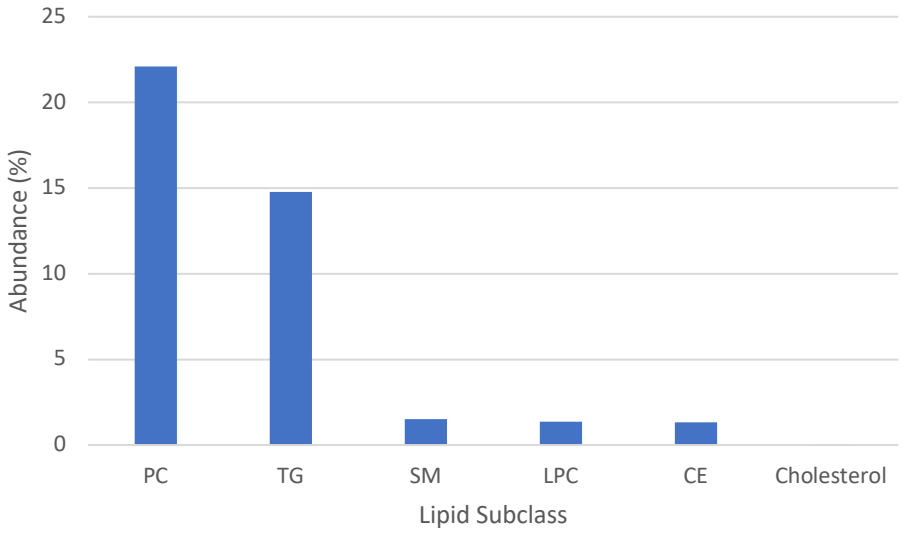

Fig 9. The Abundance by Lipid Subclass within Standard Reference Material 1950 via the Quadrupole-Time-of-Flight platform in positive polarity.
PC, phosphatidylcholine (n=31); TG, triacylglycerol (n=35); SM, sphingomyelin (n=6); LPC, lysophosphatidylcholine (n=4); CE, cholesterol ester (n=5);
Cholesterol, Free Cholesterol (n=1).

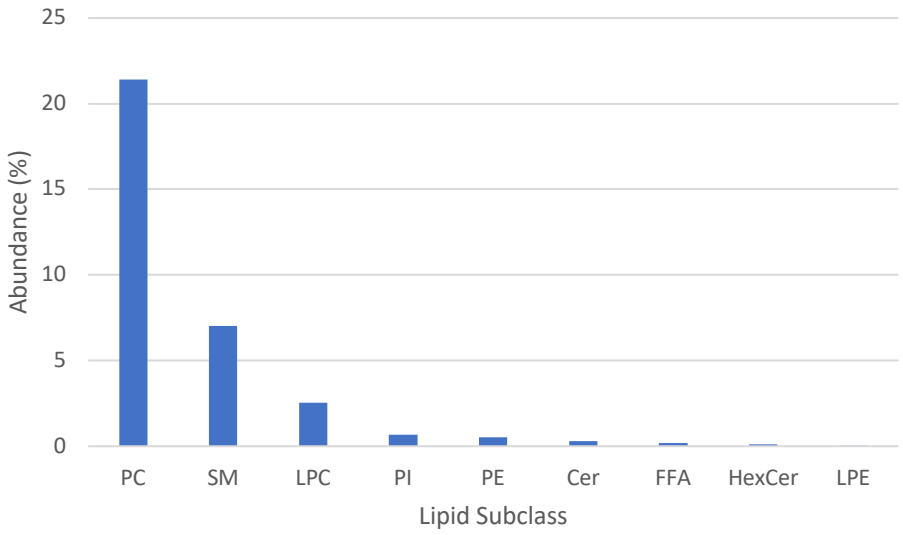

Fig 10. The Abundance by Lipid Subclass within Standard Reference Material 1950 via the Quadrupole-Time-of-Flight platform in negative polarity.
PC, phosphatidylcholine (n=37); SM, sphingomyelin (n=24);
LPC, lysophosphatidylcholine (n=9); PI, phosphatidylinositol (n=6);
PE, phosphatidylethanolamine (n=6); Cer, ceramide (n=3); FFA, free fatty acid (n=4);
HexCer, Hexosylceramide (n=2); LPE, lysophosphatidylethanolamine (n=1).

Table 9. Quantitation of the top 20 lipids of high abundance using positive polarity in the Quadrupole-Time of Flight.

m/z	Brutto ID	Medio ID	Plasma concentration (nmol/mL)		
758.5757	PC 34:2	PC 16:0_18:2	498.1	±	5.7
786.6028	PC 36:2	PC 18:0_18:2	369.7	±	1.8
760.5868	PC 34:1	PC 16:0_18:1	360.7	±	4.2
782.5712	PC 36:4	PC 16:0_20:4	298.1	±	1.5
874.7896	TG 52:3	TG 16:0_18:1_18:2	256.6	±	9.0
876.8053	TG 52:2	TG 16:0_18:1_18:1	306.6	±	21.3
810.6013	PC 38:4	PC 18:0_20:4	215.4	±	4.9
958.8792	TG 58:3		164.2	±	7.8
784.5850	PC 36:3	PC 16:0_20:3	196.4	±	6.6
960.8945	TG 58:2		165.8	±	8.1
806.5702	PC 38:6	PC 16:0_22:6	176.8	±	1.1
848.7698	TG 50:2	TG 16:0_16:1_18:1 | TG 14:0_18:1_18:1	190.4	±	3.9
900.8006	TG 54:4	TG 18:1_18:1_18:2 | TG 18:0_18:2_18:2 | TG 16:0_18:1_20:3	160.2	±	4.0
902.8165	TG 54:3	TG 18:0_18:1_18:2	144.0	±	5.4
850.7859	TG 50:1	TG 16:0_16:0_18:1	154.6	±	9.7
872.7697	TG 52:4	TG 16:0_18:2_18:2 | TG 16:1_18:1_18:2	175.8	±	6.8
956.8631	TG 58:4		133.5	±	6.3
666.6190	CE 18:2	CE 18:2	2179	±	114
703.5750	SM 34:1	SM d18:1_16:0	313.1	±	6.6
944.8629	TG 57:3		80.5	±	2.3

Values are mean ± S.D. of n=3 technical replicates. PC, phosphatidylcholine;
TG, triacylglycerol; SM, sphingomyelin; LPC, lysophosphatidylcholine; CE, cholesterol ester.

Table 10. Quantitation of the top 20 lipids of high abundance using negative polarity in the Quadrupole-Time of Flight.

m/z	Brutto ID	Medio ID	Plasma concentration (nmol/mL)		
802.5602	PC 34:2	PC 16:0_18:2	825.9	±	22.6
830.5915	PC 36:2	PC 18:0_18:2	485.6	±	12.7
804.5759	PC 34:1	PC 16:0_18:1	425.5	±	8.3
826.5604	PC 36:4	PC 16:0_20:4	356.4	±	6.0
828.5757	PC 36:3	PC 16:0_20:3	193.1	±	3.6
854.5921	PC 38:4	PC 18:0_20:4	207.3	±	3.0
540.3305	LPC 16:0	LPC 16:0	248.8	±	27.4
857.6753	SM 42:2	SM d18:1_24:1	169.7	±	7.9
747.5650	SM 34:1	SM d18:1_16:0	248.9	±	5.3
856.6072	PC 38:3	PC 18:0_20:3	76.4	±	2.3
828.5758	PC 36:3	PC 18:1_18:2	94.6	±	0.8
859.6912	SM 42:1	SM d18:1_24:0	67.5	±	1.7
850.5601	PC 38:6	PC 16:0_22:6	73.9	±	0.9
568.3614	LPC 18:0	LPC 18:0	88.1	±	3.1
826.5598	PC 36:4	PC 18:2_18:2	35.7	±	2.0
852.5752	PC 38:5	PC 18:1_20:4 | PC 16:0_22:5	59.9	±	1.0
832.6072	PC 36:1	PC 18:0_18:1	94.7	±	1.6
564.3299	LPC 18:2	LPC 18:2	72.3	±	5.2
831.6591	SM 40:1	SM d18:1_22:0	91.5	±	4.3
855.6592	SM 42:3	SM d18:2_24:1	77.0	±	1.9

Values are mean ± S.D. of n=4 technical replicates. PC, phosphatidylcholine; LPC, lysophosphatidylcholine; SM, sphingomyelin.

6.5 Discussion

The SRM 1950 macrolipidome was characterized at the medio level using the QToF through an untargeted approach. An automated lipid annotation approach using the Progenesis QI software was also attempted. Challenges between the compatibility of the Waters raw data and the data treatment software (Progenesis) led to difficulties in medio level identifications. The QToF instrument has quicker scan times which lead to a large number of features contributing to the top 85% of total abundance. The 20 most abundant lipids were also quantified.

When the raw acquisition data was imported into Progenesis, it was evident that the QToF DDA data is not fully compatible with Progenesis QI software. This is likely because the Waters Synapt G2Si QToF instrument was developed primarily for DIA based proteomic analyses. When DDA is used in these experiments, the Waters instrument software appears to fail to correctly associate the MS/MS data with the corresponding precursor ion for the importation into the Progenesis software. This was particularly problematic with the positive ESI raw data and the Progenesis software was unable to associate MS/MS fragmentation with a feature. Progenesis therefore used only the precursor m/z to predict ID without any fragmentation ion data. The raw data in MassLynx (version 4.1; Waters, Milford, MA, USA) had fragmentation data for many of the features that Progenesis labeled as having no fragmentation. With these compatibility issues, it is not surprising that the fully automated ID process using Progenesis data treatment software was not successful in the QToF (**Table 7 & 8**). The lipids in positive mode therefore required comprehensive manual analysis which includes searching for the ion in the raw data and manually solving for the fatty acyl chains depending on the ion fragments present. In addition, the features of the top 5 MS/MS scans need to be examined to confirm which features were fragmented versus ions that were not selected for fragmentation. This was a large obstacle and

made the lipid annotation process extremely time consuming. The number of features generated by Progenesis was also low, which led to more features contributing to the top 85% of abundance and ultimately required even more manual identifications through the raw data. It is unclear of the exact effect the compatibility issues would have on the number of generated features within Progenesis.

It was hypothesized that **the QToF will identify a high number of features in SRM 1950 but there will be a high false positive rate and many features will be low abundant, non-lipids, due to the fast scan times the QToF**. Unfortunately, the fully automated lipid ID process through Progenesis was not functional and the false positive metric could not be confirmed. There were however a large number of features observed in the top 85% of lipid abundance, many of which were contaminants due to quick the scanning speed of the QToF which is in agreement with the hypothesis. This ultimately led to a low percentage of lipids being identified in the macrolipidome. This approach still proved to be viable as after the non-lipids and contaminants were removed, as the percentage of lipids identified was much closer to 80% in positive mode and 70% in negative mode which is a significant increase from the 60% and 36% identified abundance prior to removal of contaminants.

The importance of a macrolipidomic approach is highlighted when observing the number of features that were identified as part of the SRM 1950 lipidome in the QToF. A high number of features were detected in positive mode (257 features) with even more features identified in negative mode (420 features) which contributed to the top 85% of abundance. This was interesting because a low number of overall features were generated in both the positive (3042 features) and negative (5785 features) mode. However, a lot of contaminants, which included background ions and unknown ions with a mass that did not have a match with a known lipid

mass from the databases were identified within this 'top 85%'. The high number of contaminants was anticipated due to the quick scan times of the MS instrument, but it does not entirely explain why the total number of features generated by Progenesis is lower. This could be caused by the lack of compatibility between the data acquisition software and data treatment software. The high detection rate of non-lipid species was observed in the percentage of features that were able to be identified since only 43% of the signal abundance was identified at the medio level in positive mode and 35% in negative mode. The higher cumulative % of lipid abundance identified in positive mode at the medio level is due to more lipids within the macrolipidome ionizing in the positive mode which was explained in more detail earlier in **Chapter 5.5**. A better understanding of the abundance contribution from the identified lipids was observed after removing these unknown and contaminant features. The cumulative abundance of features that were identified as a lipid increased from 42% to 80% (+) and 35% to 70% (-). The relative abundance of a feature after the 'top 85%' remained similar after removal of the contaminants as well only increasing slightly from 0.050% to 0.068% (+) and from 0.022% to 0.045% (-). This means any lipid that contributed more than 0.1% to the overall sample signal was being identified within SRM 1950 and confirms that the macrolipidome was characterized.

Examination of the lipid class of identified medio level lipids by abundance determined PC was the lipid subclass with the highest abundance in SRM 1950 in both positive and negative polarities (**Figure 9 & 10**). This was expected within the human plasma lipidome which was explained in more detail previously in **Chapter 5.5**. TG species outnumbered PC, which is attributed to more fatty acyl combinations available with three possible fatty acyl chains compared to the GP lipid class which only contains two fatty acyl chains. The top PC lipid was also found at a higher concentration than that of the highest TG lipid species which demonstrated

a similar response between abundance and concentration in the platform. For lipid species that were present in both polarities, specifically PC lipids, there was some discrepancy between the concentration of the lipid within the plasma sample. The most abundant PC lipid PC 16:0_18:2 for example was found at 498.1 nmol/mL in positive mode and 825.9 nmol/mL in negative mode (**Table 9 & 10**). Calculations of the concentration in negative mode appear to be inversely exaggerated across the concentration range compared to the positive mode so that lipids of higher abundance have an inflated concentration and the concentration is depressed when in the lower abundance range. PC 16:0_22:6 for example, was the least concentrated PC lipid quantified that appeared in both polarities. PC 16:0_22:6 was found at higher concentrations in positive mode, 176.8 nmol/mL, compared to negative mode, 73.9 nmol/mL. This was also observed in the other cross-polarity lipid species SM d18:1_16:0 which was quantified at higher concentrations in the positive polarity compared to the negative and was the second lowest lipid by abundance in positive mode. This could be caused by the linear range of the instrument. The response factor of the analytes will differ between lipid classes, chain lengths, and degree of unsaturation along with the adduct which could explain differences between polarities.[90] The response factors of the lipid classes between polarities could differ due to the signal intensity of the different adducts and thus possibly alter this relationship. This means that two lipids from different lipid classes of equal concentrations could produce different signal intensities within the instrument. This effect between polarities, however, should be accounted for through internal standards so it is interesting that these differences were still observed.

The abundance of CE was low (**Figure 9**) and did not reflect its concentration. Complications of measuring CE was addressed in more detail in **Chapter 5.5**. The instrument response of the CE lipid class was low but was accounted for through the use of a deuterated

ISTD. After normalizing the AUC of CE 18:2 to that of the CE ISTD, including the use of the ratio of the breakdown 369 m/z ion between that of CE 18:1 and CE 18:1(d7), the concentration of CE 18:2 was 2179 ± 114 nmol/mL. A high concentration of CE 18:2 in SRM 1950 as CE has been found previously.[14]

TG species of high carbon numbers were also observed within the QToF but were not able to be identified at the medio level (**Table 9**). Within the top 20 most abundant lipids, TG 58:3, TG 58:2, TG 58:4 and TG 57:3 species matched the accurate mass of the brutto TG identification according to LipidMaps. Upon inspection of the raw chromatograms in the MassLynx acquisition software, these ions had a high signal intensity and were selected for MS/MS fragmentation through DDA top-5. The fragmentation spectra however were confusing, as the parent ion would be clearly visible, however the rest of the spectrum consisted of extremely low intensity noise. This meant that no fragments for the loss of an acyl chain could be observed and no medio level identifications could be made. The retention times of these ions however could also be considered when confirming the brutto ID. The use of reverse-phase chromatography and the C18 column establishes that non-polar lipids will elute later in the chromatogram. All these ions eluted ~30 min in the chromatogram which is consistent with other TG that were identified in this platform and thus this was another confirmation that the ions were actual TG species.

6.6 Conclusion

In this chapter, a macrolipidomic approach was utilized to characterize and quantify the most abundant lipids in SRM 1950 using the QToF platform. Many contaminants and other non-lipid species were also identified within the top 85% of abundance due to the fast-scanning times of the QToF. This made it appear as if less lipids had been identified but after removal of

contaminants, 80% of the abundance in positive mode and 70% in negative mode were identified as lipids. The most abundant lipids were not all fully characterized at the medio level. The fatty acyl composition of high carbon TG species could not be identified despite being selected for fragmentation. Another complication in this platform was the incompatibility between the raw data and the data treatment software. Progenesis could not import majority of the MS/MS spectra, which is likely due to the functionality of DDA in the QToF platform. This created a labour-intensive process for lipid annotation. The automated ID function within Progenesis could also not operate due to this obstacle.

. Quantitation of the most abundant lipids was successful but lipids that were present in both polarities did not show consensus. Concentrations of lipids deviated when approaching either extreme of high or low signal abundance. The most abundant lipid at the medio level was identified as PC 16:0_18:2 at concentrations of 498.1 nmol/mL and 825.9 nmol/mL when calculated using the positive and negative chromatograms respectively.

Chapter 7
SRM 1950 Macrolipidomics using Trapped Ion Mobility-Quadrupole-Time of Flight MS/MS

7.1 Rational and Objectives

The human plasma lipidome contains a variety of structurally complex lipid species that includes a large amount of TG species.[15,14] This creates an analytical challenge as a single TG with a set number of carbon and double bonds can represent multiple combinations of fatty acyl chains. These TG isomers present a challenge as they have similar structural properties and thus similar retention times when trying to separate them chromatographically. This can lead to poor separation and ultimately co-elution of unique lipid species. The Bruker timsToF Pro (described in more detail in **Section 2.5.3**) utilizes trapping ion mobility spectroscopy (TIMS) technology for the additional separation of ions.[93,94,95] The incorporation of ion mobility as a prior method of ion separation could potentially counter the overlap often encountered within the TG lipid subclass. Isomeric lipids that would not be distinguishable by mass (m/z) might be separated by their IM. This additional separation could allow for more lipids to be selected for fragmentation in comparison to analysis after chromatography alone without a loss in sensitivity.[93,94,95] In the present study, an untargeted macrolipidomic approach was used to characterize SRM 1950 at the medio level using UHPLC coupled to a Bruker timsToF mass spectrometer which includes a hybrid quadrupole, time-of-flight instrument.

7.2 Hypothesis

- Due to the incorporation of ion mobility separation, the Bruker timsToF will identify a high number of features and fragment a high percentage of these ions to provide MS/MS

scans for majority of lipids in the macrolipidome of SRM 1950. This will lead to a high number of unique lipid specie identifications.

7.3 Methods, Materials and Study Design

7.3.1 Sample Collection and Lipid Extraction

SRM 1950 was obtained from NIST (as previously described in **Section 4.3**). Lipids were extracted via a modified Folch procedure (as previously described in **Section 4.4**). The dried sample was reconstituted in 500 µL hexane for shipping on dry ice to Bruker Daltonics (MA, USA) for analysis. After receiving the SRM 1950 lipid extract, it was evaporated by Vacufuge to dryness and then reconstituted to 500 µL using 65:30:5 acetonitrile:isopropanol:water +0.1% formic acid which was then diluted 10-fold.

7.3.2 Macrolipidomic Profiling

A Bruker Elute UHPLC coupled to a Bruker timsToF Pro (timsToF; Bruker Scientific, MA, USA) was operated in positive and negative mode. The sample was measured in triplicate in positive mode and duplicate in negative mode. More information can be found in **Chapter 4** on the LC gradient, column, and other general methods used but they were similar to those used with the qOrbi and QToF in Chapters 5 and 6. The Bruker Elute LC system was operated with an autosampler temperature of 4 °C.

The mass spectrometer was operated using a positive and negative polarity ESI method. The nebulizer gas was set to 2.5 bar, dry gas 11 L/min, source temperature 230 °C and ESI 4200 V (+/-). In positive mode the TIMS scan time was set to 100 ms, and the ion mobility was scanned

from 0.5 to 1.9 1/K0 (or Vs/cm^2). In negative mode the TIMS scan time was set to 300 ms, and the ion mobility was scanned from 0.6 to 1.8 1/K0. The mass range was set to 100 – 1350 m/z. An external calibration on sodium formate clusters was used. Analyses were performed by a Bruker Applications Specialists (Dr. Heino Heyman and Dr. Xuejun Peng).

The raw data was acquired by Compass DataAnalysis (version 5.3; Bruker Scientific, MA, USA) and converted to an open-source data file format (mzXML) at Bruker which was then shared, imported and analyzed using Progenesis QI software (v2.3, Nonlinear Dynamics, UK) at the University of Waterloo Mass Spectrometry Facility. This included raw data for three replicates in positive mode and two replicates in negative mode. A list of features in descending abundance was created through Progenesis QI software and the data was automatically processed to accept lipid annotations where only one of the possible raw ID has a fragmentation score >50. The automated ID lipid annotations were compared with the manual lipid annotation approach. The features were then manually inspected to identify lipids within Progenesis data treatment software and raw chromatograms were viewed for confirmation when necessary, using a trial copy of the Compass DataAnalysis data acquisition software. Brutto lipid identifications were made based off the mass and retention time of a feature, and medio identifications were made if the corresponding MS/MS spectra was available. Features were manually inspected until 85% of the cumulative abundance within the sample (top 85% most abundant compounds) were reviewed. Compass DataAnalysis was also utilized for manual peak integrations to obtain area under the curve (AUC) values for quantitation of the 20 lipids of highest abundance.

7.4 Results

7.4.1 Number of Features using Progenesis

Progenesis obtained 10675 (+) and 3091 (-) features and 8429 (+) and 2575 (-) of these features had at the minimum one possible raw ID. Of these, 732 (+) and 588 (-) ions were fragmented and had corresponding MS/MS data, of which 643 (+) and 541 (-) also had a possible raw ID at the medio level.

7.4.2 Fully Automated Lipid Annotation process via Progenesis QI software

The automated lipid annotation process in positive mode using Progenesis generated seven automated ID within the top 85% of most abundant compounds (130 features) when accepting a raw ID that had only one possible fragmentation score >50 (**Table 11**). Five of these automated ID were correct according to manual inspection. In order from high to low abundance these automated ID were LPC 16:0, TG 16:0_18:1_18:1, TG 16:0_16:1_18:1, LPC 18:0 and TG 16:0_16:0_18:1. An in-source fragmentation ion was incorrectly identified automatically as a cholesterol derivative and an ISTD was incorrectly identified as a contaminant. In negative mode, seven automated IDs within the top 85% of abundance (142 features) were generated (**Table 12**). This included four contaminants, PE 19:1_22:6, SM 18:2_24:1, and PE O-18:0_19:1. All the automated ID were incorrect except for SM 18:2_24:1 which was partially correct since upon manual inspection the medio level could not be confirmed. The four contaminants were all identified as GP upon manual inspection.

7.4.3 Lipid contribution to the Top 85% of Cumulative Abundance

Features from each run (positive and negative) were ordered by decreasing abundance and the MS mass spectra of features that were in the top 85% of the total cumulative abundance were examined manually (**Appendix A.5 & A.6**).

In the positive mode, the most abundant 130 features made up the top 85% (**Figure 11**). Within the top 85%, the feature with the smallest abundance contributed 0.090% to the total signal. Of the 130 features, 70 were manually inspected at the brutto level, which represented 45% of the total cumulative sample signal. Features that could not be assigned a brutto level lipid identification included common contaminants or unknown ions that did not match with a known mass from the lipid databases or LipidMaps. These features were all referred to as contaminants. Medio level identifications were made for 65 of the 70 brutto species after manual inspection of the MS/MS fragmentation spectra. Therefore, 45% of the total sample signal in positive mode was identified at the medio level. After removing the identified contaminants and unknowns from the top 85% of total abundance, lipids were found to represent 76.0% of the cumulative signal in the positive mode. The relative abundance of a feature after the top 85% of signal was no more than 0.125% in positive mode.

In the negative mode, the most abundant 142 features made up 85% of the total abundance within the sample (**Figure 12**). Within the top 85%, the feature with the smallest abundance contributed 0.074% to the total signal. Of the 142 features, 92 were manually inspected at the brutto level, which represented 58% of the total cumulative sample signal. Medio level identifications were made for 86 of the 92 brutto species after manual inspection of the MS/MS fragmentation spectra. Therefore, 57% of the total sample signal in negative mode was identified at the medio level. After removing the identified contaminants and unknowns

from the top 85% of signal abundance, lipids were found to represent 78.4% of the cumulative signal in the negative mode. The relative abundance of a feature after the top 85% of signal was no more than 0.108% in negative mode without contaminants.

Within the top 85% of most abundant compounds, PC lipids contributed the most and accounted for just over half of the medio identified abundance in positive mode (**Figure 13**). PC lipids contributed 23% to the total sample abundance. The next most abundant lipid subclass was CE, which had an abundance of 8.4%. TG species represented 7.4% of the total abundance. The remaining lipid subclass groups contributed less than 3% each to the total abundance. This included LPC (2.2%), SM (1.2%), Cholesterol (0.3%) and FFA (0.1%). Sixty-five features were identified as contaminants and had an abundance of 40%. The number of features identified as lipids in order of descending abundance contribution were 24 as PC, 7 as CE, 19 as TG, 4 as LPC, 4 as SM, 1 as cholesterol and 1 as FFA. Five ISTD were identified within the top 85% of abundance.

In negative mode, majority of the abundance constituted of the PC and LPC lipid subclass within the top 85% (**Figure 14**). PC accounted for 26% of the identified abundance, and LPC lipids had an abundance of 13%. SM had an abundance of 7.0% and FFA had an abundance of 6.2%. The remaining lipid subclasses contributed less than 1% to the total abundance and included PE (0.8%), PI (0.4%) and PG (0.1%). Contaminants represented just under 30% of the total identified abundance which constituted of 56 features. Thirty-seven features were manually identified as PC, 10 as LPC, 17 as SM, 8 as FFA, 5 as PE, 3 as PI, and 1 as PG. Six ISTD were identified within the top 85% of abundance.

7.4.4 Quantitation of the top 20 most highly abundant lipids

Quantitation of the top 20 lipids of highest abundance in SRM 1950 was completed in both positive (**Table 13**) and negative (**Table 14**) modes which identified similar PC lipids between both polarities. The most highly abundant PC lipid was identified at the medio level as PC 16:0_18:2 which was present in SRM 1950 at concentrations of 881.6 nmol/mL in positive mode and 545.5 nmol/mL in negative mode. PC 16:0_18:2 was also the lipid of highest abundance in positive mode however in negative mode LPC 16:0 had a higher abundance but was quantified to have a lower concentration of 173.9 nmol/mL. The third, fourth and fifth most abundant lipids in SRM 1950 were consistent between platforms and were identified as PC 18:0_18:2 at 429.2 nmol/mL in positive mode and at 384.8 nmol/mL in negative mode, PC 16:0_18:1 at 408.3 nmol/mL in positive mode and at 411.6 nmol/mL in negative mode, and PC 16:0_20:4 at 348.8 nmol/mL in positive mode and at 336.4 nmol/mL in negative mode. SM d18:1_16:0 was also identified as the most abundant SP between platforms with a concentration in the plasma sample of 239.3 nmol/mL in positive mode and 157.3 nmol/mL in negative mode. LPC 16:0 was also identified at 210.8 nmol/mL in positive mode and 173.9 nmol/mL in negative mode.

In positive mode, the next lipid of highest abundance after PC 16:0_18:2 was identified as CE 18:2 (**Table 13**). This was found in SRM 1950 at a concentration of 2454 nmol/mL. In the timsToF, CE 20:4 and CE 18:1 were also identified within the top 20 lipids of highest abundance and CE 20:4 had a concentration of 384 nmol/mL while CE 18:1 had a concentration of 1002 nmol/mL. TG lipid species were also found to be highly concentrated in SRM 1950. The top four TG lipid species included TG 16:0_18:1_18:2 at 424.8 nmol/mL, TG 16:0_18:1_18:1 at 346.2 nmol/mL, TG 16:1_18:1_18:2 at 187.6 nmol/mL and TG 16:0_16:1_18:1 at 199.3 nmol/mL. The

lipid specie with the lowest quantified concentration is SRM 1950 was PC 18:0_20:3 at 58.5 nmol/mL in positive mode.

Only PC, LPC and SM lipid subclasses were quantified within the top 20 lipids of highest abundance in SRM 1950 in negative mode (**Table 14**). Following LPC 16:0, three other LPC lipid species were identified. This included LPC 18:0 at 65.7 nmol/mL, LPC 18:2 at a concentration of 55.4 nmol/mL and LPC 18:1 at 53.5 nmol/mL. Following SM d18:1_16:0 the three other SM species quantified were SM d18:2_16:0 at 40.0 nmol/mL, SM d18:1_24:1 at 34.1 nmol/mL and SM d18:2_24:1 at 21.5 nmol/mL. SM d18:2_24:1 was the lipid of lowest abundance and also lowest concentration in the plasma sample in negative mode. After the four most abundant PC lipids, seven more PC lipids were quantified. The next most concentrated PC lipids were the tenth and eleventh lipids of highest abundance and were identified as PC 18:0_20:4 at 182.4 nmol/mL and PC 16:0_20:3 at 115.6 nmol/mL.

Table 11. Fully Automated Identifications of features in the top 85% of positive mode cumulative abundance by Progenesis QI software with follow up manual lipid inspection results in the Trapped Ions Mobility Spectrometry-Quadrupole-Time-of-Flight platform.

Retention time (min)	m/z	Highest Ranked Automated ID[1]	Corresponding Manual ID	Correct Automated ID
4.57	496.3392	LPC 16:0	LPC 16:0	Yes
42.18	876.8023	TG 16:0_18:1_18:1	TG 16:0_18:1_18:1	Yes
42.54	369.3515	Cholesterol derivative	Cholesterol (in-source)	No
41.82	848.7707	TG 16:0_16:1_18:1	TG 16:0_16:1_18:1	Yes
6.30	524.3709	LPC 18:0	LPC 18:0	Yes
42.18	850.7865	TG 16:0_16:0_18:1	TG 16:0_16:0_18:1	Yes
41.78	829.7987	Contaminant	ISTD, TG 15:0_18:1(d7)_15:0	No

LPC, lysophosphatidylcholine; TG, triacylglycerol; ISTD, internal standard.
[1]Progenesis provides a list of possible raw identifications (ID) based on matching m/z and fragmentation patterns to ChemSpider and LipidBlast databases and accepts a raw ID when only one fragmentation score >50.

Table 12. Fully Automated Identifications of features in the top 85% of negative mode cumulative abundance by Progenesis QI software with follow up manual lipid inspection results in the Trapped Ions Mobility Spectrometry-Quadrupole-Time-of-Flight platform.

Retention time (min)	m/z	Highest Ranked Automated ID[1]	Corresponding Manual ID	Correct Automated ID
4.80	566.3448	Contaminant	LPC 18:1	No
20.50	852.5732	PE 19:1_22:6	PC 16:0_22:5	No
27.62	855.6568	SM 18:2_24:1	SM 42:3	Partial[2]
22.53	812.5782	Contaminant	PC O-16:0_20:4	No
22.55	786.5629	Contaminant	PC P-16:0_18:2	No
26.19	840.6098	Contaminant	PC O-18:0_20:4	No
25.83	790.5941	PE O-18:0_19:1	PC O-16:0_18:1	No

LPC, lysophosphatidylcholine; PE, phosphatidylethanolamine; SM, sphingomyelin; PC, phosphatidylcholine; PC/PE O, plasmanyl species; PC P, plasmenyl species.
[1]Progenesis provides a list of possible raw identifications (ID) based on matching m/z and fragmentation patterns to ChemSpider and LipidBlast databases and accepts a raw ID when only one fragmentation score >50.
[2]Manual inspection could not determine the acyl fragments.

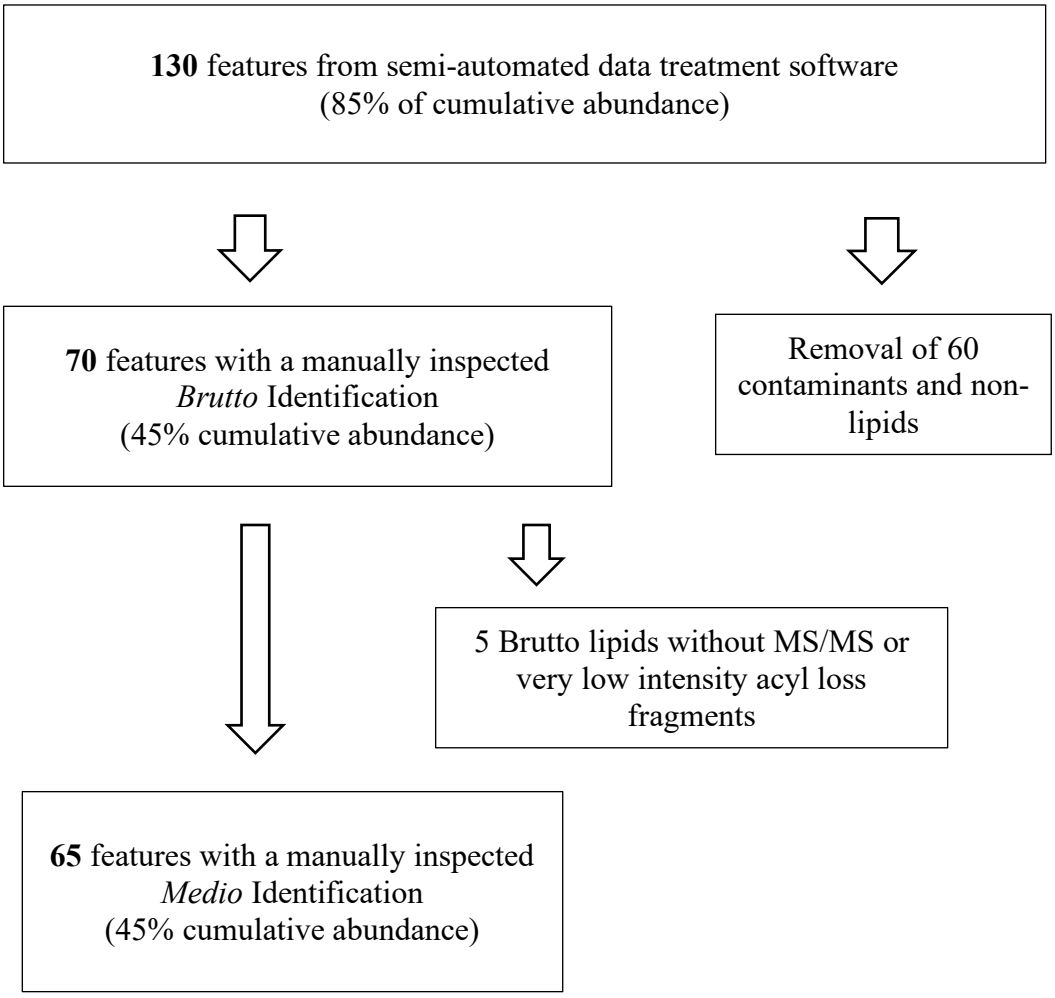

Fig 11. Process of identifying lipids from features to medio level in positive mode of the Trapped Ions Mobility Spectrometry-Quadrupole-Time-of-Flight platform. Features in Standard Reference Material 1950 at the top 85% of cumulative abundance were collected semi-automatically by Progenesis and manually inspected to confirm lipid identifications at the brutto and medio level.

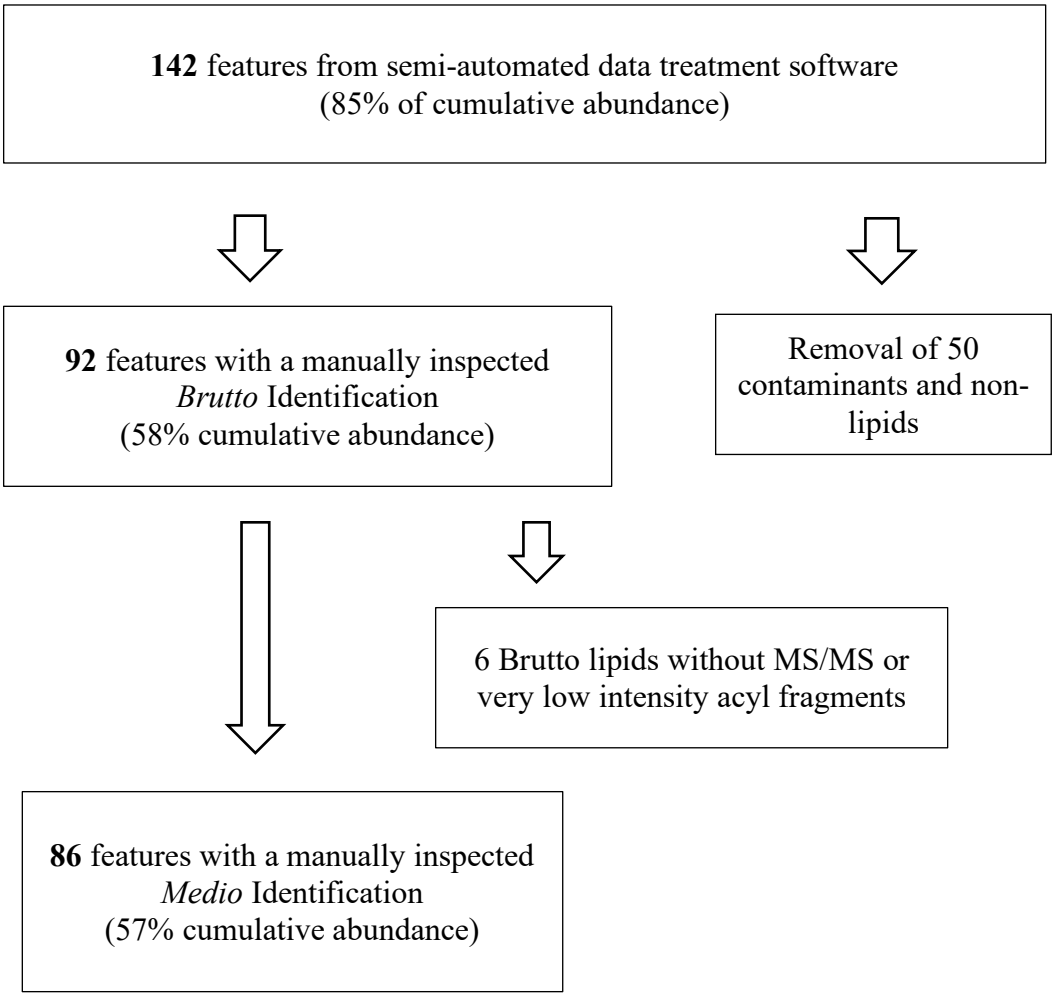

Fig 12. Process of identifying lipids from features to medio level in negative mode of the Trapped Ions Mobility Spectrometry-Quadrupole-Time-of-Flight platform. Features in Standard Reference Material 1950 at the top 85% of cumulative abundance were collected semi-automatically by Progenesis and manually inspected to confirm lipid identifications at the brutto and medio level.

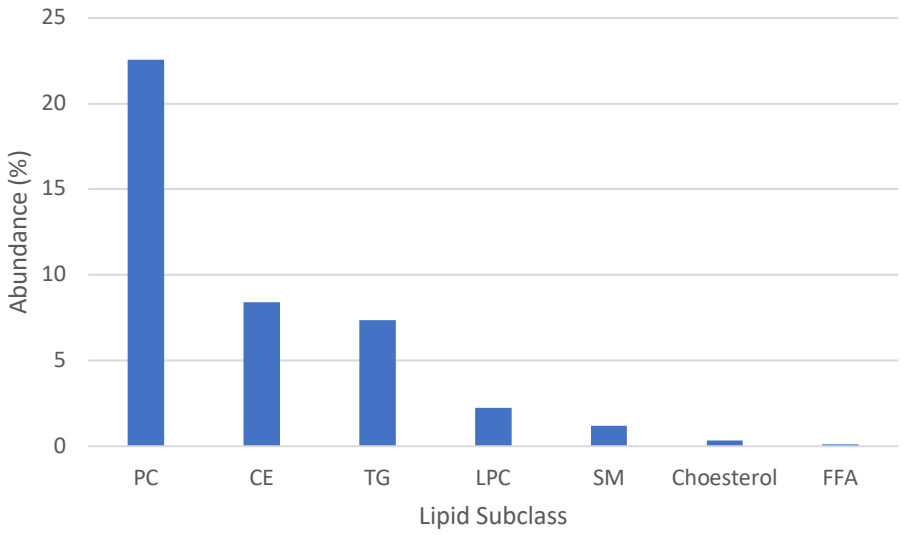

Fig 13. The Abundance by Lipid Subclass within Standard Reference Material 1950 via the Trapped Ions Mobility Spectrometry-Quadrupole-Time-of-Flight platform in positive polarity. PC, phosphatidylcholine (n=24); CE, cholesterol ester (n=7); TG, triacylglycerol (n=19); LPC, lysophosphatidylcholine (n=4); SM, sphingomyelin (n=4); Cholesterol, Free Cholesterol (n=1); FFA, free fatty acid (n=1).

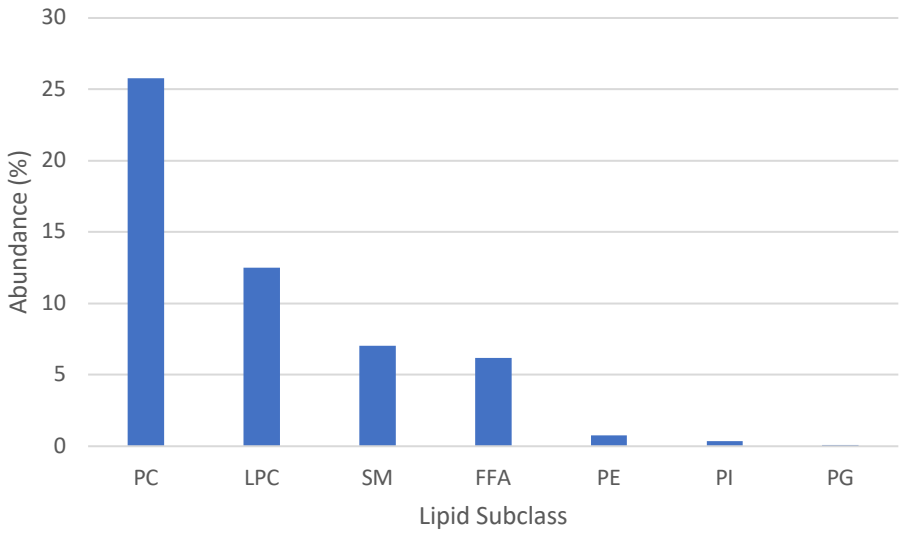

Fig 14. The Abundance by Lipid Subclass within Standard Reference Material 1950 via the Trapped Ions Mobility Spectrometry-Quadrupole-Time-of-Flight platform in negative polarity. PC, phosphatidylcholine (n=37); LPC, lysophosphatidylcholine (n=10);
SM, sphingomyelin (n=17); FFA, free fatty acid (n=8), PE, phosphatidylethanolamine (n=5); PI, phosphatidylinositol (n=3); PG, phosphatidylglycerol (n=1).

Table 13. Quantitation of the top 20 lipids of high abundance using positive polarity in the TIMS-Time of Flight

m/z	Brutto ID	Medio ID	Plasma concentration (nmol/mL)
758.5707	PC 34:2	PC 16:0_18:2	881.6 ± 18.1
666.6196	CE 18:2	CE 18:2	2454 ± 160
786.6017	PC 36:2	PC 18:0_18:2	429.2 ± 1.1
760.5858	PC 34:1	PC 16:0_18:1	408.3 ± 1.1
782.5701	PC 36:4	PC 16:0_20:4	348.8 ± 1.1
874.7852	TG 52:3	TG 16:0_18:1_18:2	424.8 ± 7.5
784.5851	PC 36:3	PC 16:0_20:3	155.5 ± 0.7
810.6012	PC 38:4	PC 18:0_20:4	181.6 ± 1.1
496.3392	LPC 16:0	LPC 16:0	210.8 ± 3.4
690.6187	CE 20:4	CE 20:4	553 ± 28.7
876.8023	TG 52:2	TG 16:0_18:1_18:1	346.2 ± 3.0
668.6342	CE 18:1	CE 18:1	1002 ± 18
872.7698	TG 52:4	TG 16:1_18:1_18:2	187.6 ± 3.4
784.5851	PC 36:3	PC 18:1_18:2	102.7 ± 1.6
703.5753	SM 34:1	SM d18:1_16:0	239.3 ± 3.2
848.7707	TG 50:2	TG 16:0_16:1_18:1	199.3 ± 4.5
806.5700	PC 38:6	PC 16:0_22:6	83.0 ± 1.3
900.8016	TG 54:4	TG 18:1_18:1_18:2 | TG 18:0_18:2_18:2 | TG 16:0_18:1_20:3	117.8 ± 0.4
788.6168	PC 36:1	PC 18:0_18:1	65.5 ± 1.0
846.7538	TG 50:3	TG 16:0_16:1_18:2 | TG 16:1_16:1_18:1	88.1 ± 2.6

Values are mean ± S.D. of n=3 technical replicates. PC, phosphatidylcholine; TG, triacylglycerol; LPC, lysophosphatidylcholine; CE, cholesterol ester.

Table 14. Quantitation of the top 20 lipids of high abundance using negative polarity in the TIMS-Time of Flight

m/z	Brutto ID	Medio ID	Plasma concentration (nmol/mL)		
540.3294	LPC 16:0	LPC 16:0	173.9	±	0.1
802.5591	PC 34:2	PC 16:0_18:2	545.5	±	16.3
830.5897	PC 36:2	PC 18:0_18:2	384.8	±	0.3
804.5744	PC 34:1	PC 16:0_18:1	411.6	±	1.7
826.5584	PC 36:4	PC 16:0_20:4	336.4	±	1.9
747.5642	SM 34:1	SM d18:1_16:0	157.3	±	4.7
568.3598	LPC 18:0	LPC 18:0	65.7	±	1.4
564.3286	LPC 18:2	LPC 18:2	55.4	±	1.2
566.3448	LPC 18:1	LPC 18:1	53.5	±	0.0
854.5893	PC 38:4	PC 18:0_20:4	182.4	±	0.5
828.5728	PC 36:3	PC 16:0_20:3	115.6	±	4.8
828.5733	PC 36:3	PC 18:1_18:2	122.5	±	2.8
850.5585	PC 38:6	PC 16:0_22:6	161.7	±	3.1
832.6050	PC 36:1	PC 18:0_18:1	105.8	±	0.2
745.5480	SM 34:2	SM d18:2_16:0	40.0	±	0.9
826.5575	PC 36:4	PC 18:2_18:2	72.6	±	0.6
856.6050	PC 38:3	PC 18:0_20:3	77.7	±	1.8
857.6725	SM 42:2	SM d18:1_24:1	34.1	±	0.1
852.5732	PC 38:5	PC 16:0_22:5 | PC 18:1_20:4	73.3	±	1.4
855.6568	SM 42:3	SM d18:2_24:1	21.5	±	0.6

Values are mean ± S.D. of n=2 technical replicates. PC, phosphatidylcholine; LPC, lysophosphatidylcholine; SM, sphingomyelin.

7.5 Discussion

The SRM 1950 macrolipidome was characterized at the medio level using the timsToF through an untargeted approach. An automated annotation approach using the Progenesis QI software was also examined. The largest obstacle was accessibility to the Bruker acquisition software to view the raw data, which was limited to a 60-day trial from Bruker. The timsToF instrument has quicker scan times with additional separation using trapped ion mobility which aided in identification of fatty acyl chain composition. The 20 most abundant lipids were also quantified.

A large obstacle in the analysis of the timsTOF data was the accessibility to the raw acquisition data. Originally, the converted Bruker raw files were imported into Progenesis for manual lipid inspection and the top 85% of lipid abundance was inspected fully within the preview of the data treatment software. The majority of the spectra, especially in positive mode, looked extremely noisy and contained repeating fragments with a difference of 68 mass units. These fragments were problematic as they occurred throughout the mass range and could easily be mistaken for acyl loss fragments. It was difficult to determine what the actual acyl, or acyl loss fragments were versus the background in the data treatment software as access to the raw acquisition data was necessary. Manual inspection was first attempted fully within Progenesis and ID with less abundant acyl fragments or odd chain fatty acyls were reviewed in the acquisition data software once the DataAnalysis software was made available from Bruker. This was an additional challenge since access to the data acquisition software was only provided from Bruker for 60 days. Ultimately, 29 medio ID were changed from their original manual ID made in Progenesis after review of the raw spectra within DataAnalysis. In negative mode, 20 medio ID were changed after viewing the raw acquisition spectra. Upon further inspection of the raw

data in DataAnalysis, it was determined that Progenesis often imported and combined both the full MS scan and MS/MS scans of a single feature. This explained why the MS/MS spectra within Progenesis were often noisy and it became clear from the full MS scans that the repeating units belonged to background contaminants. These background fragments included: 226.9513, 294.9388, 362.9258, 430.9133, 498.90006, 566.882, 634.8755, 702.8626 and so on with additional 68u until the upper mass range 1246.7648 in positive mode. A spectrum containing a pattern of repeating units is representative of a polymer contaminant. The poor import of the data into Progenesis meant that the raw data needed to be heavily referenced to confirm the medio level of information to ensure the full MS scan was not also contributing to the spectrum. Progenesis often suggested incorrect possible raw ID since it would try to match these repeating fragments.

Based on some of the observed m/z values, it appeared that $[M+Na]^+$ ions exist in the Bruker timsTOF analysis. Sodium (Na) is a common contaminant in mass spectrometry instruments, and typically can present itself in instruments overtime after frequent use such that lipids in positive mode include $[M+H]^+$ (where M is the compound of interest) as well as a sodium adduct $[M+Na]^+$. At the University of Waterloo Mass Spectrometry Facility, $[M+Na]^+$ ions are not regularly detected and if they are they are very low in abundance as the type of analyses and the frequency of them are relatively low compared with industrial applications. Typically for the University of Waterloo Mass Spectrometry Facility, protonated (H^+) and ammoniated (NH_4^+) adducts are selected for positive experiments because they are most common. The timsTOF instrument at Bruker does frequent analysis of external samples including proteomic based analyses that would likely increase the risk sodium contamination of their instruments or sample preparation equipment. For this reason, another Progenesis experiment was created which

included sodium adducts during the pre-selection of potential adducts settings in the Progenesis software to properly de-convolute and process the data. This helped to confirm lipids especially if they were ionized with multiple different adducts. Viewing the raw spectra through DataAnalysis was able to confirm the presence of sodium adducts as the sodiated lipid would appear at the same retention time as the ammoniated or protonated adduct. As mentioned previously, a lower abundance of lipids in positive mode could be caused by more contaminants ionizing in positive mode which are not typically observed otherwise.

The fully automated lipid annotation process was successful at correctly identifying lipids in positive mode (**Table 11**) but not as successful in negative mode (**Table 12**). Considering the difficulties in incorporating the raw data into Progenesis and difficulties in observing a single possible raw ID with a fragmentation score >50 (described in **Section 5.5** and **6.5**), this was surprising. The platform did provide good fragmentation spectra of abundant lipids but often the preview within Progenesis included ions from both the full MS scan and the fragmentation scan. When matching reference database spectra with the experimental data, Progenesis appears to match m/z fragments even if they are of low intensity, which would explain why the software was still able to generate automated ID. With a manual approach, identification of these fragment ions would not occur as less intense ions are typically caused by less common fragmentation patterns or background noise. Without knowledge of the efficiency of the data import, a manual inspection approach would falsely identify these lipids since the background peaks would be mistaken for belonging to the structure of the compound which was experienced during the initial identification of lipids using Progenesis alone.

The distribution of the lipid class abundance in human plasma was similar to the literature.[15,14] This was mostly observed in positive mode (**Figure 13**) since the major lipid

classes of PC, TG and CE are ionized in positive mode. Glycerophospholipids, mainly PC are expected to be the most abundant. Levels of other glycerophospholipids such as PE, PI and PG were observed in negative polarity (**Figure 14**) which were anticipated to be slightly more abundant. This, however, could be caused by using the abundance value provided by Progenesis and not the actual area under the curve from the raw acquisition data. Progenesis uses signal intensity of the ion to create the abundance value and abundance quantities do not adjust for different ionization potentials of the different classes, whereas this is corrected for with internal standards when calculating concentrations.

A high number of contaminants were observed, which was anticipated due to functionality of the QToF instrument. This was reflected in the 45% in positive mode and 57% in negative mode of cumulative abundance that was characterized at the medio level (**Figure 11 & 12**) and through the number of contaminants that were observed with high abundance (Appendix A.5 & A.6). Most of the contaminants that appeared at high abundance eluted within the ~0.1 minute of the chromatograms. This included 9 out of 10 of the most abundant contaminants in positive mode and 8 out of 10 in negative mode (Appendix A.5 & A.6). Utilizing the retention time helps to confirm the presence of these contaminants as they were likely part of the mobile phase that does not interact with the column stationary phase and thus elutes immediately. It was hypothesized that **incorporation of ion mobility would aid in fragmentation of highly abundant lipids** which was confirmed as the percentage of lipids identified at the brutto level was very similar to that at the medio level. In positive mode (**Figure 11**) 45% of the cumulative abundance was identified at the brutto level and the medio, whereas in negative mode (**Figure 12**) 58% of the abundance was characterized at the brutto level and 57% at the medio. This meant that if a lipid was identified based on its accurate mass for the brutto level, a clear fragmentation spectrum was

also produced for the ion that allowed for characterization of the fatty acyl chains. Interestingly, more lipids were characterized at the medio level in negative than positive mode. Typically, because TG and CE only ionize in the positive mode, the positive mode has higher coverage of lipids in the macrolipidome (explained in more detail in **Section 5.5**). A possible explanation for the lower characterization of the lipid abundance in positive mode was due to poor incorporation of the raw data into the Progenesis data treatment software and the presence of positive sodium adducts that was unique to the timsToF instrument which could be a source of ionization in positive mode for contaminants.

The top 20 lipids of highest abundance were quantified in the timsToF using DataAnalysis (**Table 13 & 14**). Interestingly, many LPC species were found at levels of high abundance in negative mode. Although LPC is also anticipated to be abundant in human plasma,[15] it was interesting that LPC 16:0 was the lipid of highest abundance in negative mode and only quantitated to be 173.9 nmol/mL. In positive mode LPC 16:0 had a concentration of 210.8 nmol/mL.[90] However, the concentration of LPC species by the timsToF was similar or slightly lower than the concentrations determined by the qOrbi and QToF platforms (**Tables 17 & 18**). The high abundance of LPC lipid species observed relative to their concentration in the timsToF is likely due to the response of the instrument and a potential impact of the ion mobility separation that was unique to this platform. Without direct access to the instrument this is difficult to access but with ion mobility differences of abundances between lipid classes from ion "cooling" effects has been observed.[96] The cooling effect is believed to be caused by the absorption of collisional energy by the gas used for ion mobility that can result in less fragmentation and an increase in the relative abundance of the parent ion that then reflects greater total abundance. In addition, the concentrations of LPC 16:0 observed across the

platforms herein was relatively high to a previous report of 29.9 nmol/mL in SRM 1950[15] although the consensus location was 73 nmol/mL with considerable deviation across 20 laboratories in the harmonization analysis exercise that used SRM 1950.[14] As such, interpreting the concentration of LPC 16:0 in this study is difficult, but some hydrolysis of PC to generate LPC may have occurred during sample handling and preparation.

PC 16:0_18:2 was found at 545.5 nmol/mL in negative mode and 881.6 nmol/mL in positive mode. In general, lipid species were calculated to have a higher concentration in positive mode which was also the case for SM d18:1_16:0 which was the only SM identified within the top 20 in both polarities. In positive mode, SM d18:1_16:0 had a concentration of 239.3 nmol/mL and 157.3 nmol/mL in negative mode. Overall, quantities of the lipid species showed similar trends between polarities.

A limitation in quantitation was the lack of an ISTD for the FFA lipid class. The timsToF platform identified three FFA species, FFA 18:1, FFA 18:2 and FFA 16:0 within the top 20 lipids of highest abundance in negative mode (**Appendix A.6**). The SPLASH Lipidomix[84] was the internal standard used which contains a deuterated standard for each major lipid class however it does not have a deuterated FFA equivalent. This meant that lipids of possible significance could not be quantified in the macrolipidome. FFA concentrations in plasma are low and have been reported to be low in SRM 1950[14,15] so it was interesting to detect FFA with high abundance (**Appendix A.6**). However, considering the observations made between the abundance and concentration values within the LPC lipid class, the high abundance of FFA lipids is likely due to the response of the instrument in combination with the use of TIMS. This could again be related to the previously mentioned ion cooling effect which would not directly correlate to higher concentrations of FFA within the platform.

Co-eluting glycerolipids were observed within the top 20 lipids of highest abundance (**Table 13**). This was also observed in both polarities for glycerophospholipids specifically PC (**Table 13 & 14**). It was anticipated that the additional ion mobility separation would aid in separating isomeric species and help to identify individual lipid species. The first four TG species were identified without any co-elution from additional isomers however there were still two ions, 900.8016 and 846.7538 that represented multiple different TG species. This means that the concentration attributed to these ions cannot be recognised for each specific medio ID and thus the concentration seen is representative of the cumulative concentration of the co-eluting lipid species. Separation of TG species is a challenge in lipidomics, and benefits from prior chromatographic separation based on the interaction of the acyl chains with the stationary phase however the high number of TG isomers still proves challenging with a untargeted approach.[55] Although ion mobility separates based on the morphology of the compounds, which would differ between isomers, separation is still difficult for isomers with similar elemental composition and global morphology as observed within lipid classes which was observed in the timsToF.[97] The hypothesis that **due to the incorporation of ion mobility separation, the Bruker timsToF will identify a high number of features and fragment a high percentage of these ions to provide MS/MS scans for majority of lipids in the macrolipidome of SRM 1950 and lead to a high number of unique lipid specie identifications** can be partially accepted. A high percentage of lipid features identified were fragmented for characterization at the medio level as discussed earlier. Most of the lipids within the macrolipidome were also able to be characterized at the medio level however, co-elution of TG and PC lipids still occurred.

7.6 Conclusion

In this chapter, a macrolipidomic approach was utilized to characterize and quantify the most abundant lipids in SRM 1950 using the timsToF platform. Many contaminants and other non-lipid species were also identified within the top 85% of abundance due to the fast-scanning times of the QToF. This made it appear as if less lipids had been identified, but after removal of contaminants, 76% of the abundance in positive mode and 79% in negative mode were identified as lipids. The incorporation of ion mobility separation seemed to aid in fragmentation of highly abundant lipids as majority of identified lipids were able to be characterized at the medio level upon manual inspection.

A complication of this study was the lack of access to the platform and the software. A temporary trial was granted by Bruker for the data acquisition software (DataAnalaysis). This meant that lipids needed to be reviewed quickly to ensure lipid quantitation could be completed. More lipids than expected needed to be reviewed within the raw acquisition data due to improper importation of the raw data. Additional experiments may have also provided insights into the effects of ion cooling effects in IM and the potential impact on the abundance of LPC and FFA lipids observed. However, quantitation of the most abundant lipids was successful and showed similar trends in concentration between polarities.

Chapter 8
SRM 1950 Lipidomics – A Literature and Cross-platform Integrative Comparison

8.1 Rational and Objectives

Characterizing the lipid profile of SRM 1950 can improve the understanding of the lipids in human plasma. This will assist goals to identify potential clinical biomarkers and help define and establish an inclusion list for routine targeted MS/MS analyses. SRM 1950 is an ideal sample as it is a composed of multiple samples (n=100) selected to represent the adult population of the United States of America and there is a large enough sample volume available for multiple replicate analyses. This allows methodology to be established and verified as the sample remains consistent across laboratories and analytical platforms.

Although SRM 1950 was originally intended for metabolite analysis, attempts at characterizing the lipidome have been made (more details in **Section 3.3**). Quehenberger et al.,[15] in collaboration with the LIPID MAPS consortium (www.lipidmaps.org) were the first to identify the diversity of lipids found within human plasma using SRM 1950. Their work, however also highlighted how precise and accurate quantitation of these structurally diverse lipids requires targeted lipidomic workflows and platforms. The study also exhibited how the bias and interest of an analyst can influence the lipids detected as there was an extensive effort to identify eicosanoids as compared with the identification of glycerolipids. This was highlighted further in an interlaboratory exercise by Bowden et al.,[14] where various lipidomic workflows produced variable outcomes in the profiles of SRM 1950 and there was considerable variation in amounts of lipids when the same lipids species were identified across laboratories. The data presented in both of these studies was reported mainly at the brutto level, creating difficulties in comparison of individual lipid species. Other studies have also analyzed SRM 1950 through

mass spectrometry, but attempted to establish methods or software for lipidomics and their focus was not on the characterization of the plasma lipidome itself.[41,58,77–80,80–83]

Current studies have confirmed the lack of consensus in the lipidome of SRM 1950 and the variation present between workflows.[14,35] Some of this variation exists because of a lack of definition and/or variation in the term lipidomics itself. The basic definition implies the characterization of all lipids in the sample, but in practice, lipidomics is used to indicate a UHPLC-MS/MS approach was used even when examining only a single class of lipids. The term macrolipidomics can be used to indicate attempts to characterize the high abundant lipids that make up most of the lipids in a sample. Defining the macrolipidome of biological samples highlights GP that provide insight on cellular membrane composition and GL that provide insight on storage lipids, both which are important in linking nutrition and health. In addition, knowing the fatty acyl species of lipids is critical for the application of lipidomics to nutritional research, therefore identification of SRM 1950 lipids at the medio level is necessary. Completing untargeted UHPLC-MS/MS analyses of SRM 1950 using similar workflows on three different platforms and identifying the macrolipidome at the medio level is unique to the lipidomic field. The macrolipidomes obtained from the studies in **chapters 5, 6** and **7** were compared with each other to attempt to establish a consensus. These results were also compared to the data that is currently available in the literature. Establishing a preliminary list of lipid species in the macrolipidome of SRM 1950 at the medio level can be used for future studies and accelerate the use of lipidomics in nutritional applications.

8.2 Hypotheses

- The number of lipid species identified in the macrolipidome at the medio level may differ slightly but will be relatively similar across platforms due to the focus on highly abundant lipids.
- The qOrbi instrument will have the lowest false positive rate but will have a lower number of initial features as compared with the QToF and timsToF.
- The timsToF will select and provide fragmentation for a greater number of species due to an increased ToF scan speed combined with the additional TIMS separation.
- The additional MS/MS ion fragments detected by the timsTof instrument will correspond to lipid species belonging to the microlipidome.
- Manual inspection of the macrolipidome at the medio level will identify a higher number of GL species in comparison to previous reports on GL species in SRM 1950.
- The integrative cross-platform and cross-study comparison will identify a mean consensus of the overall lipid class composition of SRM 1950 that can be used for an inclusion list for the analysis of human plasma samples in the future.

8.3 Methods, Materials and Study Design

8.3.1 Sample Collection

Data collected from chapters 5, 6 and 7 were compared for a cross-platform analysis of the SRM 1950 macrolipidome. The focus was on the types of lipids identified and the quantitation of the 20 most highly abundant lipids. A one-way ANOVA with the Bonferroni correction ($p<0.05$) was utilized to determine significant differences in concentrations between platforms.

8.3.2 Literature Comparison

The Quehenberger et al., 2010[15] and Bowden et al., 2017[14] studies focused on characterizing the lipidome of SRM 1950 and were used for primary comparisons. The term "SRM 1950 lipid" was also entered into PubMed and yielded 25 results as of February 2021 to identify other potential papers with comparable data to be considered. These studies were summarized in **Table 1** of **Section 3.3**.

8.4 Results

8.4.1 Features generated through Progenesis across Platforms

Progenesis QI data treatment software was used with the same parameters across all three platforms to import the raw data and generate a list of features for further inspection which was then compared across platforms (**Table 15**). The highest number of features was generated in the qOrbi which included 13039 features in positive mode and 25647 features in negative mode. The lowest number of features were generated in the QToF. Specifically, the QToF positive mode generated only 3042 features while 5785 were generated in negative mode. Interestingly, the timsToF platform had 10675 features in positive mode, but only 3091of features in negative mode. The timsToF platform fragmentated the most features in both polarities: 732 in positive mode and 588 in negative mode. The QToF had the lowest number of fragmentated features (164) in positive mode while the qOrbi had the lowest (157) in negative mode. The number of features with fragmentation and a raw ID followed similar trends. For example, the timsToF also had the highest number of features that were fragmented but also had a raw ID with 643 features in positive mode and 541 in negative mode. Interestingly, after manual inspection the number of medio identifications made were relatively similar across the platforms. The timsToF had the

lowest number of medio ID which was interesting considering it was the platform with the highest number of fragmented features.

8.4.2 Number of unique Medio level lipid identifications across platforms

Manually inspected medio level identifications were compared across platforms (**Figure 15**) and across polarities within platforms (**Figure 16**) to observe the number of unique and overlapping lipids present from each analysis of SRM 1950. In positive polarity, the qOrbi identified the highest number of unique lipids (**Figure 15.A**). The qOrbi identified 37 unique lipids, the QToF 34, and the timsToF 18. The highest overlap between two platforms was observed between the qOrbi and the QToF. There were 27 identical medio lipids across all three UHPLC-MS/MS platforms. In negative polarity, the highest number of unique medio level characterized lipids was also identified within the qOrbi platform (**Figure 15.B**). The qOrbi identified 22 unique lipids, the QToF 16, and the timsToF 22. More consensus was found in negative mode as demonstrated by the 37 medio level ID found consistently across all three platforms. Not including the 37 overlapping ID found across all three platforms, the QToF and timsToF identified 21overlapping ID which is significantly more compared to the qOrbi and QToF which had five overlapping ID or the qOrbi and the timsToF which only had two.

Interestingly, the number of unique medio level ID was not consistently higher in one polarity for the SRM 1950 analyses. Within the qOrbi, more unqiue ID were identified in positive polarity (**Figure 16.A**). This included 54 medio ID in positive mode, 40 in negative and 26 which overlapped between polarities. In the QToF platform, an equal number of unique lipids were identified in the positive and negative polarities (**Figure 16.B**) with 51 unique medio lipid ID that were annotated in both positive and negative mode and an additional 28 lipids that

overlapped between the polarities. Lastly, in the timsToF platform, 53 unique lipids were identified in the negative polarity, 28 in the positive polarity, and 27 lipid species overlapped between the two polarities (**Figure 16.C**).

8.4.3 Number of Lipids identified within SRM 1950 by Lipid Class

The number of unique lipids by lipid class was summed for comparison across the three UHPLC-MS/MS platforms and literature (**Table 16**). The lipids reported by Bowden et al.,[14] were identified only at the brutto level, whereas Quehenberger et al.,[15] identified some medio level lipids in the SP lipid class. Within the three MS platforms, unique brutto identifications were also included for comparison to the literature. The total number of lipids identified by Bowden et al.,[14] was 1527 unique lipids which was the highest total reported. This value however decreased significantly to 339 when viewing only unique lipids that were identified by at least 5 laboratories. This was still higher than the total lipids identified within all three UHPLC-MS/MS platforms which detected 206 unique lipids in the qOrbi, 196 in the QToF and 119 in the timsToF. Quehenberger at al.,[15] had identified 107 fatty acyls which included eicosonaids while the 5-lab consensus in Bowden et al., reported 14 fatty acyls. Fatty acyl lipids constituted of the lowest number of unique lipids within the macrolipidome of SRM 1950 in the qOrbi, QToF and timsToF platforms. Glycerolipid identification was 78 in the QToF, 67 in the qOrbi and only 20 in the timsToF platform. The lipid class with the highest number of identified lipids was glycerophospholipids with 101 in the qOrbi, 75 in the QToF and 58 in the timsToF. Quehenberger and Bowden also identified a high number of GP lipids however the Quehenberger study identified 204 unique sphingolipid species which was the highest number of lipids within a lipid class. SP lipids were the only lipid class with more than one fatty acyl chain

reported at the medio level by Quehenberger et al.[15] The number of SP were more consistent but lower with 33 in the qOrbi , 33 in the QToF and 22 in the timsToF. Lastly, a small number of unique sterol lipids were identified with 4 in the qOrbi, 5 in the QToF and 10 in the timsToF in comparison to the 36 and 34 sterol lipids reported between the two literature studies. Quehenberger at al., also reported prenol lipids however this lipid class is outside of the macrolipidome and was not a main area of focus in the cross-platform analysis. This highlights that both Quehenberger at al.,[15] and the Bowden et al.,[14] exercise were attempts to characterize the full lipidome and not just the macrolipidome in the present cross platform assessment.

8.4.4 Cross-platform comparison of the 20 most highly abundant lipids

Lipid concentrations for the top 20 lipids in SRM 1950 of highest abundance that were quantified in the previous chapters were compared across the qOrbi, QToF, and timsToF platforms (**Table 17 and 18**). Comparison of the coefficient of variation (CV) between platforms is provided in **Appendix B.1** for the positive quantitation and **Appendix B.2** for the negative. The percent CV was lowest for lipids quantified using the timsToF platform. Data from studies by Quehenberger et al., 2010[15], and Bowden et al.,2017[14] were also included with the corresponding quantified brutto lipid and the few fatty acyl characterized (medio) lipids when available.

Lipids from five different lipid subclasses were quantified between the three platforms in the positive polarity (**Table 17**). The most highly concentrated lipid across all platforms was consistently CE 18:2 which ranged in plasma concentration from 1700 nmol/mL reported in Bowden et al.[14], to 2454 nol/mL reported in the timsToF platform. PC lipids were identified quite consistently across the three platforms. The concentrations however were consistently

higher compared to the concentrations of the two literature studies. The qOrbi and timsToF instrument also produced similar concentration values throughout. For example, the most abundant PC lipid was quantified as PC 16:0_18:2 with a concentration of 726 nmol/mL (qOrbi), 498 nmol/mL (QToF) and 881 nmol/mL (timsToF) compared to the corresponding brutto identification of 220 nmol/mL by Quehenber and 240 nmol/mL by the Bowden consensus. The differences observed in the concentration of PC 16:0_18:1 with the QToF platform were significantly different compared to the other two platforms. Similar trends were also observed in other lipids identified across the platforms such as PC 16:0_18:1 and PC 18:0_18:2. As the number of carbon and double bonds increase however, the qOrbi and QToF platform appear to provide more consistent results. PC 18:0_20:4 for example has a concentration of 211 nmol/mL in the qOrbi, 215 nmol/mL in the QToF and 181 nmol/mL in the timsToF. A similar trend is observed for PC 16:0_22:6. Not all lipids were within the top 20 across all platforms such as LPC 16:0. LPC 16:0 was similar between the qOrbi (270 nmol/mL) and timsToF (211 nmol/mL) but were significantly higher than the Quehenberger et al. (39 nmol/mL) and the Bowden consensus (73 nmol/mL) studies. Thirteen different TG species were identified between the three platforms within the top 20 lipids of highest abundance. TG species of high concentration also appeared to be more consistent between the qOrbi and timsToF platforms. TG 52:3, which was the most concentrated triacylglycerol in the plasma sample, had a concentration of 408 nmol/mL (qOrbi), 256 nmol/mL (QToF) and 424 nmol/mL (timsToF). This was significantly higher than the 255 nmol/mL (Quehenberger et al.) and 100 nmol/mL (Bowden et al.) reported in the other studies. TG with co-eluting isomers were compared based off of the brutto ID. One SM species was identified in positive mode across all platforms. SM d18:1_16:0 had a similar concentration between the qOrbi (326 nmol/mL) and QToF (313 nmol/mL) platforms. The timsToF produced a

slightly lower concentration of 239 nmol/mL however all three platforms were significantly higher than the Quehenberger et al. (78 nmol/mL) and Bowden et al. studies (100 nmol/mL).

In negative polarity, four different lipid subclasses were quantified across the three UHPLC-MS/MS platforms (**Table 18**). The most highly concentrated lipid was identified as PC 16:0_18:2 which was also the most concentrated glycerophospholipid in positive polarity. PC 16:0_18:2 was found at concentrations of 695 nmol/mL (qOrbi), 826 nmol/mL (QToF) and 546 nmol/mL (timsToF). These values were much higher than the 220 nmol/mL (Quehenberger et al.) and 240 nmol/mL (Bowden et al.) found in literature. The QToF appears to inflate the concentration of lipids of higher abundance. This trend was also observed with PC 18:0_18:2 for example where the concentrations in the qOrbi and timsToF were 412 nmol/mL and 385 nmol/mL respectively and 486 nmol/mL in the QToF. LPC lipids were consistently quantified more highly in the platforms compared to the literature. Identification of LPC compounds were less consistent across platforms. LPC 16:0 and LPC 18:0 were found across all three platforms, LPC 18:2 was found in the QToF and timsToF, and LPC 18:1 was only found within the top 20 most abundant lipids in the timsToF. LPC 16:0 was the most abundant LPC species and was quantitated at a concentration of 204 nmol/mL (qOrbi) and 249 nmol/mL (QToF) and 174 nmol/mL (timsToF) which was consistently higher than 39.9 nmol/mL (Quehenberger et al.) and 73 nmol/mL (Bowden et al.) reported in literature. PI 18:0_22:4 was the only lipid of its subclass that was quantitated and it only appeared in the top 20 of the qOrbi instrument. The concentration was found to be 33 nmol/mL which was more than the corresponding brutto ID found in literature of 12.5 nmol/mL (Quehenberger et al.) and 19 nmol/mL (Bowden et al.). Seven different SM species were quantified within the three platforms. Quantitation of SM produced more similar concentrations between the qOrbi and QToF platform compared to the

timsToF, however the three instruments all produced higher values compared to what is reported in literature. The most highly concentrated SM for example, SM d18:1_16:0, was found at concentrations of 257 nmol/mL (qOrbi), 249 nmol/mL (QToF), and 157 nmol/mL (timsToF). SM d18:1_16:0 was reported at 78 nmol/mL in the Quehenberger et al., study whereas Bowden et al., reported only the overall number of carbons and double bonds with a concentration of 100 nmol/mL.

Table 15. Summary of Feature and Possible Raw Identifications generated by Progenesis in the qOrbi vs QToF vs timsToF

Polarity	Instrument	Features	Features with a raw IDs	Features with fragmentation	Features with a raw ID and fragmentation	Features with a manual medio ID
Positive	qOrbi	13039	11428	467	419	87
	QToF	3042	2299	164	120	86
	timsToF	10675	8429	732	643	65
Negative	qOrbi	25647	22178	157	117	76
	QToF	5785	3918	213	187	99
	timsToF	3091	2575	588	541	86

A Feature is an ion with a unique mass and retention time that is generated by Progenesis QI software. A raw ID is a possible identification (ID) based off m/z and fragmentation patterns with the databases.

qOrbi, Quadrupole-Orbitrap; QToF, Quadrupole-Time of Flight; timsToF, Trapped Ion Mobility Spectrometry-Quadrupole-Time of Flight

A. Positive polarity

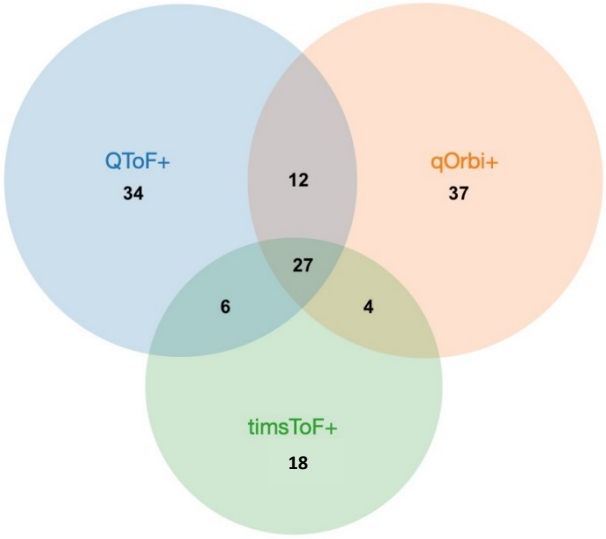

B. Negative polarity

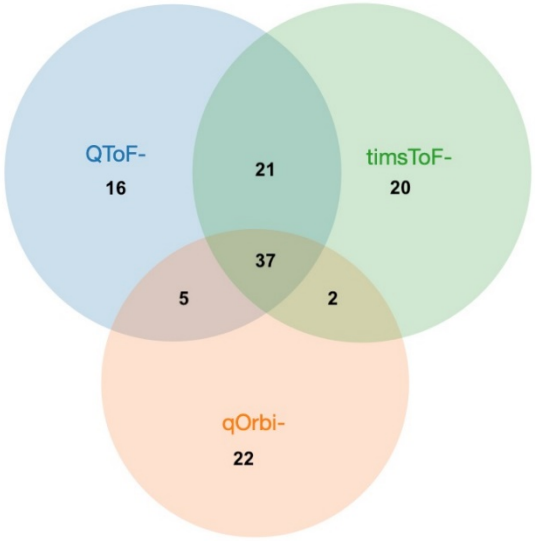

Fig 15. Number of unique and overlapping lipid Medio Identifications in SRM 1950 across the qOrbi, QToF, and timsToF platforms in **A)** positive polarity and **B)** negative polarity.
qOrbi, Quadrupole-Orbitrap; QToF, Quadrupole-Time of Flight; timsToF, Trapped Ion Mobility Spectrometry-Quadrupole-Time of Flight

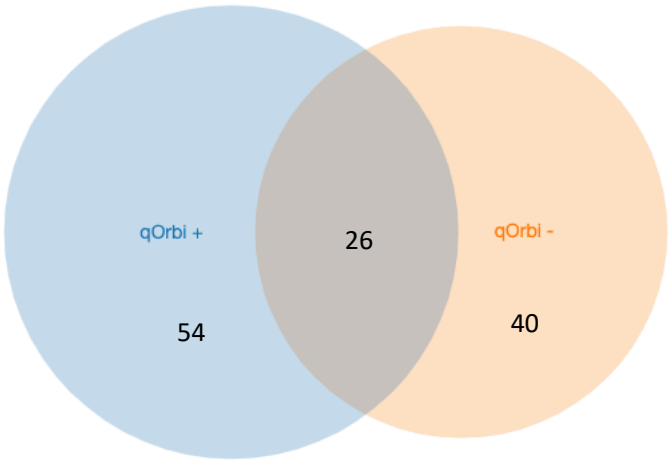

A. qOrbi

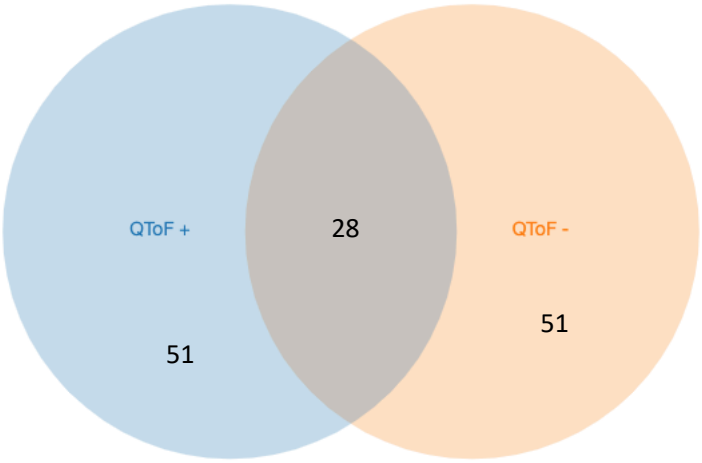

B. QToF

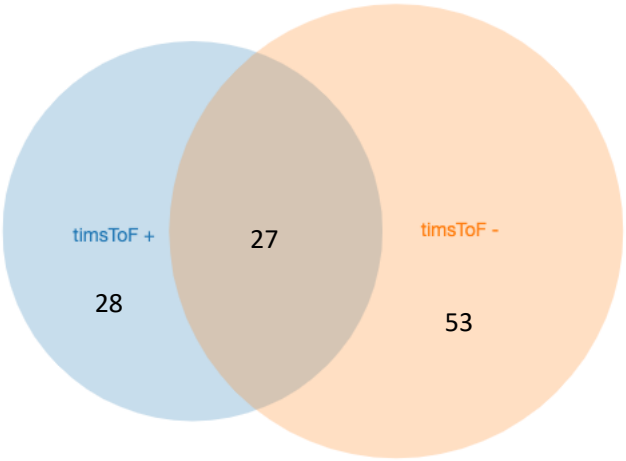

C. timsToF

Fig 16. Number of unique and overlapping lipid Medio Identifications in SRM 1950 across the electrospray ionization polarities in **A)** qOrbi (n=120) and **B)** QToF (n=130) and **C)** timsToF (n=108) where *n* represents the number of unique medio lipids identified with the platform. qOrbi, Quadrupole-Orbitrap; QToF, Quadrupole-Time of Flight; timsToF, Trapped Ion Mobility Spectrometry-Quadrupole-Time of Flight

Table 16. Number of unique lipids identified at the Brutto level in Standard Reference Material 1950 within three mass spectrometry platforms and literature.

Lipid Category	Number of Species					
	qOrbi	QToF	timsToF	Quehenberger et al.	Bowden et al. Reported by 5+ labs	Bowden et al. Reported by <5 labs
Fatty acyls	1	5	9	107	14	177
Glycerolipids	67	78	20	73	83	317
Glycerophospholipids	101	75	58	160	150	679
Sphingolipids	33	33	22	204	58	236
Sterol lipids	4	5	10	36	34	118
Prenol lipids				8		
Total	206	196	119	588	339	1527

Unique lipid species found in Quehenberger et al.[15], using multiple analyses and Bowden et al.[14], by multiple laboratories by number of identifications.
qOrbi, Quadrupole-Orbitrap; QToF, Quadrupole-Time of Flight; timsToF, Trapped Ion Mobility Spectrometry-Quadrupole-Time of Flight

Table 17. Cross-platform quantitation of lipids with the highest abundance in positive mode compared to literature quantitation.

Brutto ID	Medio ID	qOrbi (n=4)	QToF (n=3)	timsToF (n=3)	Quehenberger et al.	Bowden et al.
			Plasma concentration (nmol/mL)			
PC 34:1	PC 16:0_18:1	405.1±2.2	360.7±4.2*	408.3±1.1	89.3	120
PC 34:2	PC 16:0_18:2	726±5.9*	498.1±5.7*	881.6±18.1*	188	240
PC 36:1	PC 18:0_18:1	76.9±0.7	-	65.5±1	99.8	26
PC 36:2	PC 18:0_18:2	437.5±1.7*	369.7±1.8*	429.2±1.1*	254	140
PC 36:3	PC 16:0_20:3	-	196.4±6.6	155.5±0.7	165	100
	PC 18:1_18:2	94.7±0.3	-	102.7±1.6		
PC 36:4	PC 16:0_20:4	349.3±2.6	298.1±1.5*	348.8±1.1	172	150
PC 38:3	PC 18:0_20:3	71.6±0.7	-	-		26
PC 38:4	PC 18:0_20:4	211.8±1.8	215.4±4.9	181.6±1.1*	254	84
PC 38:6	PC 16:0_22:6	152.3±1.7*	176.8±1.1*	83±1.3*	62.9	41
LPC 16:0	LPC 16:0	270.3±10.5		210.8±3.4	29.8	73
TG 50:1	TG 16:0_16:0_18:1	123.5±4.6	154.6±9.7	-	63.6	38
TG 50:2	TG 14:0_18:1_18:1	186.6±7.4	190.4±3.9	-	79.8	47
	TG 16:0_16:1_18:1			199.3±4.5		
	TG 16:0_16:0_18:2		-	-		
TG 50:3	TG 16:0_16:1_18:2	90±3.2	-	88.1±2.6	57.1	23
	TG 16:1_16:1_18:1	-	-			
TG 52:2	TG 16:0_18:1_18:1	354.7±1.4	306.6±21.3*	346.2±3	139.5	44
	TG 16:1_18:0_18:1		-	-		
TG 52:3	TG 16:0_18:1_18:2	408.1±1.6*	256.6±9*	424.8±7.5*	214.8	100
	TG 16:1_18:0_18:2		-	-		
TG 52:4	TG 16:0_18:2_18:2	-	175.8±6.8	-	90.9	48
	TG 16:1_18:1_18:2	-		187.6±3.4		
TG 54:3	TG 18:0_18:1_18:2	133.6±7.8	144±5.4	-	69.1	26
TG 54:4	TG 16:0_18:2_20:2	145.1±3.4*	-	-	68.5	36
	TG 18:0_18:2_18:2					
	TG 18:1_18:1_18:2		160.2±4*	117.8±0.4*		
	TG 16:0_18:1_20:3	-				
TG 54:5	TG 18:1_18:1_18:3	83.9±2.8	-	-	53.6	27
	TG 18:1_18:2_18:2		-	-		
TG 57:3	-	-	80.5±2.3	-	-	-
TG 58:2	-	-	165.8±8.1	-	-	-
TG 58:3	-	-	164.2±7.8	-	-	-
TG 58:4	-	-	133.5±6.3	-	-	-
CE 18:1	CE 18:1	-	-	1002.6±17.8	533	440
CE 18:2	CE 18:2	2068±43$^{\Psi}$	2179±114	2454±160	1820	1700
CE 20:4	CE 20:4	-	-	553.4±28.7	237	350
SM 34:1	SM d18:1_16:0	325.6±2.3	313.1±6.6	239.3±3.2	81.0	100

A dash indicates that the lipid specie was not identified within the top 20 lipids of highest abundance and thus were not quantitated. The (*) denotes a significant difference between the indicated platform(s), (Ψ) denotes a significant difference between the qOrbi and timsToF platforms according to ANOVA with the Bonferroni correction, p-value<0.05.PC, phosphatidylcholine; LPC, lysophosphatidylcholine; TG, triacylglycerol; CE, cholesterol ester; SM, sphingomyelin.

Table 18. Cross-platform quantitation of the 20 lipids with the highest abundance in negative mode and compared to literature quantitation.

Brutto ID	Medio ID	qOrbi (n=3)	QToF (n=4)	timsToF (n=2)	Quehenberger et al.	Bowden et al.
		Plasma concentration (nmol/mL)				
PC 34:1	PC 16:0 _18:1	413.5±10.4	425.5±8.3	411.6±1.7	89.3	120
PC 34:2	PC 16:0_18:2	694.8±13.7*	825.9±22.6*	545.5±16.3*	188	240
PC 36:1	PC 18:0_18:1	84.9±2.8*	94.7±1.6*	105.8±0.2*	99.8	26
PC 36:2	PC 18:0_18:2	412±2.1	485.6±12.7*	384.8±0.3	254	140
PC 36:3	PC 16:0 _20:3	191.5±4	193.1±3.6	115.6±4.8*	165	100
	PC 18:1_18:2	99.5±2.1*	94.6±0.8*	122.5±2.8*		
PC 36:4	PC 16:0 _20:4	330.1±7.8	356.4±6.0*	336.4±1.9	172	150
	PC 18:2_18:2	61.9±7.0	35.7±2.0*	72.6±0.6		
PC 38:3	PC 18:0 _20:3	84.5±3.5#	76.4±2.3	77.7±1.8	-	26
PC 38:4	PC 18:0_20:4	164.2±4.6*	207.3±3.0*	182.4±0.5*	254	84
PC 38:5	PC 16:0_22:5 | PC 18:1_20:4	61.8±1.5	59.9±1.0	73.3±1.4*	86.3	42
PC 38:6	PC 16:0_22:6	63.2±2.6*	73.9±0.9*	161.7±3.1*	62.9	41
LPC 16:0	LPC 16:0	203.7±3.4	248.8±27.4^	173.9±0.1	29.8	73
LPC 18:0	LPC 18:0	92.5±2.6	88.1±3.1	65.7±1.4*	23.3	27
LPC 18:1	LPC 18:1	-	-	53.5±0	14.8	18
LPC 18:2	LPC 18:2	-	72.3±5.1	55.4±1.2	16.9	22
PI 38:4	PI 18:0_20:4	33.1±1.3	-	-	11.0	19
SM 34:1	SM d18:1_16:0	257.4±5.4	248.9±5.3	157.3±4.7*	81.0	100
SM 34:2	-	-	-	40±0.9	0.7	16
SM 40:1	SM d18:1_22:0	77.3±1.8	91.5±4.3	-	15.0	20
SM 42:1	SM d18:1_24:0	53.2±3.2	67.5±1.7	-	5.9	20
SM 42:2	SM d18:1_24:1	101.5±2.9*	169.7±7.9*	34.1±0.1*	12.5	44
SM 42:3	SM d18:2_24:1	54.4±1.4*	77.0±1.9*	21.5±0.6*	33.0	17

A dash indicates that the lipid specie was not identified within the top 20 lipids of highest abundance and thus was not quantitated. The (*) denotes a significant difference between the indicated platform(s), (#) denotes a significant difference between the qOrbi and QToF platforms, (^) denotes a significant difference between the QToF and timsToF platforms according to ANOVA with the Bonferroni correction, p-value<0.05.

PC, phosphatidylcholine; LPC, lysophosphatidylcholine; PI, phosphatidylinositol; SM, sphingomyelin.

8.5 Discussion

In this chapter, the SRM 1950 macrolipidome was analyzed through a comparison of identified lipids between a qOrbi, QToF, and timsToF UHPLC-MS/MS instruments analyzed in the previous chapters (**Chapter 5, 6 & 7**). Previous studies completed by Quehenberger et al., 2010[15] and Bowden et al., 2017[14] were also included for a comparison as they had a similar goal of profiling complex lipids within SRM 1950 although these studies were not restricted to characterizing the macrolipidome. Due to the large analytical output of mass spectrometric data, only the top 20 lipids of highest abundance were quantitated and compared across platforms.

It was hypothesized that **the qOrbi instrument would have the lowest false positive rate but would have a lower number of initial features as compared with the QToF and timsToF**. An in-depth analysis of the number of false positives was not completed in this study due to the incompatibilities and lack of functionality of the fully automated lipid annotation process within Progenesis, which was described in more detail in the previous chapters (**Chapter 5.5, 6.5, 7.5**). Interestingly, Progenesis generated the highest number of features in the qOrbi platform (**Table 15**). The lowest number of combined features between polarities was generated in the QToF platform by Progenesis. This was not as anticipated, since the qOrbi has slower scanning frequencies compared to the QToF instruments. The timsToF also had 10675 initial features generated which was closer to the 13039 features in the qOrbi in positive mode, but the timsToF also generated less features (3091) in negative mode which was similar to the QToF (5785). The significant decrease in features generated for the QToF in positive mode could be contributed to the poor functionality of Progenesis to process the QToF raw data. The association of an MS/MS scan to the parent ion is affected in the QToF but it is not established to what extent the data is handled by Progenesis. Progenesis QI customer service has been contacted in

the past however they were unable to establish the cause of incompatibility between the data treatment software and the raw Waters acquisition software. Overall, it cannot be concluded as to why Progenesis generates a high number of features within the qOrbi platform. However, the number of features that contributed to the top 85% of abundance was lower in the qOrbi compared to the QToF. Fewer known contaminants or unknowns were also found within the top 85% of the qOrbi which indicates that the slower scanning speeds favour ions of higher abundance.

Ion mobility mass spectrometry is an additional form of separation that can be utilized in lipidomics to potentially combat the issue of co-eluting isomeric species and it has been reported to chromatographically favour the fragmentation of more ions.[95] It was hypothesized that **the timsToF will select and provide fragmentation for a greater number of species due to an increased ToF scan speed combined with the additional TIMS separation.** Analysis of the features with fragmentation in **Table 15** confirmed that the number of features with fragmentation was significantly higher in the timsToF platform compared to the qOrbi or QToF. The timsToF fragmented 732 features in positive mode and 588 in negative mode while the qOrbi fragmented 467 in positive mode and 157 in negative mode which was the next largest number of fragmented features. However, only 130 of the total features in positive mode and 142 in negative mode contributed to the top 85% of abundance in the timsToF. There was a high number of fragmented features that did not contribute to the top 85% which agrees with the hypothesis that **the additional MS/MS ion fragments detected by the timsTof instrument will correspond to lipid species belonging to the microlipidome.**

Despite differences in the number of overall features generated by Progenesis within platforms, and the number of features that contributed to the top 85%, the number of medio level

identifications made for unique lipid species was similar in the qOrbi and QToF (**Figures 15 & 16**). It was hypothesized that **the number of lipid species identified in the macrolipidome at the medio level may differ slightly but will be relatively similar across platforms due to the focus on highly abundant lipids.** Comparison of the number of unique medio level lipids found across the platforms mostly agrees with this hypothesis, but a lower number of unique medio lipids were observed in the timsToF platform (**Figure 15**). Within the individual platforms, 120 unique medio ID were made with the qOrbi, 130 with the QToF and 108 with the timsToF (**Figure 16**). The decrease in unique medio identifications was caused from the lack of identifications in the positive timsToF polarity. Almost half the number of unique lipids were identified in the positive polarity with the timsToF (**Figure 15.A**) and the timsToF was the only platform to identify less unique lipids in the positive mode compared to the negative mode (**Figure 16.C**). This is likely caused by the response factor of the instrument. The CE lipid class was observed in previous chapters to be the lipid class of highest concentration despite the instrument producing a relatively lower signal for CE ions. The timsToF instrument however produced higher ion intensities for the CE lipids, which contributed to more of the cumulative abundance. In the qOrbi instrument 1.4% of the abundance was attributed to CE, in the QToF 1.3% of the abundance was CE and in the timsToF CE had an abundance of 8.4% (**Appendix A.1, A.3 & A.5**). The high detection and thus contribution of CE to the top 85% led to less unique medio ID in the platform.

Isomeric species are problematic in lipidomics and are highly observed in glycerolipid species. The structure of TG results in species with a similar overall number of carbons and double bonds which creates difficulty in their separation and identification. A single brutto TG species can be representative of multiple different TG at the medio level. For this reason, it was

hypothesized that **manual inspection of the macrolipidome at the medio level will identify a higher number of GL species in comparison to previous reports on GL species in SRM 1950.** Both Quehenberger et al.,[15] and the more recent initiative by Bowden et al.,[14] reported GL at the brutto level and lacked identification of the unique lipids at the medio level. Surprisingly, the number of unique GL reported in these studies was like that of the QToF but surpassed identifications in the qOrbi and timsToF. Review of the GL lipid species identified in these literature studies revealed many DAG species. In the current study, DAG species were not reported due to low concentrations in human plasma and thus they were not within the top 85% of features examined as the macrolipidome. In Quehenberger et al., 56 of the 73 unique GL lipid species were DAG and Bowden et al., reported 24 of the 83 GL as DAG species. This is a significant portion of the GL species identified within the studies and it reflects an interest in microlipidomic bioactive signalling molecules. Considering unique TG species alone, the manual approach with medio level identifications did identify a higher number of unique TG species in the qOrbi and QToF. The timsToF likely identified less TG species due to the high abundance of CE detected which was discussed previously. The highest number of TG were identified with the QToF, which also detected TG species with a high number of carbons with three to four double bonds that was not observed in the other platforms (**Table 17**). These species were highly abundant and selected for fragmentation but had no fragmentation spectra in the instrument. Bowden et al., also reported TG with high carbon numbers such as 58:7, 58:8 and 58:9 which had more double bonds compared to the species found in the QToF.[14] The concentration of these TG species in the Bowden study were calculated to be no greater than 2 nmol/mL in plasma. However, the TG species detected in the QToF were quantified at concentrations between 80.5 and 165.8 nmol/mL which is higher and indicates these species contribute to the macrolipidome.

Due to the lack of consensus within the other platforms and a lack of loss of acyl chain fragments, it is difficult to confirm whether these TG species are real.

The number of GP species identified by Quehenberger et al.,[15] and Bowden et al.,[14] compared to those found across the platforms revealed that more unique GP were identified in the literature studies (**Table 16**). For similar reasons as the GL lipid class, more unique GP lipids would be anticipated to be identified in a manual approach. The medio level defines the two fatty acyl chains that constitute the overall GP lipid and thus a brutto identification is representative of multiple GP lipids at the medio level. However, the supplementary data from these studies prove that majority of the GP lipids identified belong to the microlipidome and explain why there was such a high number of unique GP lipids identified. Quehenberger et al., identified 160 GP lipids, of which 53 were PC and 25 were LPC. Only six of these PC or LPC lipids had a concentration over 50 nmol/mL. In Bowden et al., 150 GP lipids were reported, however only 31 of these were PC and 12 were LPC. Eleven of these lipids had concentrations over 50 nmol/mL. A high number of PE, PS, PG, PA and PI lipids were reported in these studies but are typically found in the microlipidome and explains why they were not reported in the cross-platform methods. Therefore, the manual approach proved to benefit the number of unique lipids identified for the GP lipid class as well.

Although similar trends were observed in the concentrations of highly abundant lipids across the platforms, significant differences were still observed between platforms (**Tables 17 & 18**). The final hypothesis was that **the integrative cross-platform and cross-study comparison will identify a mean consensus of the overall lipid class composition of SRM 1950 that can be used for an inclusion list for the analysis of human plasma samples in the future.** The overall number of lipids in the platform analyses contributing to each lipid class (**Table 16**)

provides a reference for lipid identifications to anticipate in the SRM 1950 macrolipidome. The concentration of these lipids (**Tables 17 & 18**) provide insight into the average physiological quantities that can be anticipated to be found in human plasma. The quantification of these lipids can be improved significantly through more targeted approaches and implementing inclusion lists during future analyses. This will depend on the analyte of interest but can be applied to both research and clinical settings.

The concentrations of quantified lipids were consistently higher in the qOrbi, QToF and timsToF compared to what has been previously reported in literature.[14,15] The differences in concentrations can be attributed to the differences between the workflows of the platforms in this study versus the literature studies. The platforms in this study utilized DDA to acquire the five most highly abundant lipids at the specified time of the scan. The instrument parameters in the literature studies were not specified, especially in the Bowden et al.,[14] study where over 31 laboratories participated and few high resolution mass spectrometers were utilized.[98] Quehenberger[15] also utilized eight different targeted approaches to favour the different lipid classes however a clear focus on low abundant eicosanoid and other fatty acyl species was taken, which could contribute to lower quality quantitation of other lipid classes. Lower resolution instruments such as the triple quadrupole mass spectrometer were also used in this study.

Similar medio level lipids were reported across the platforms except for instances of co-elution, specifically in the QToF TG species, which was discussed previously. Although significant differences were statistically computed across platforms for some lipids, the relative order of lipids from highest to lowest concentration within a platform remained consistent within lipid class and was almost consistent overall. For example, CE 18:2 was consistently the highest lipid identified across all platforms and literature, with a concentration of 2068 nmol/mL in the

qOrbi, 2179 nmol/mL in the QToF, 2454 nmol/mL in the timsToF, 1820 nmol/mL by Quehenberger et al., and 1700 nmol/mL by Bowden et al. The lowest concentrated lipid however differed across platforms and literature but the lowest lipid within a lipid class across platforms was consistent.

The timsToF platform highlighted how different instrument detectors can influence the lipids that are observed with high abundance. CE was found to be highly concentrated in SRM 1950 despite not having the highest abundance. CE 18:2 specifically was anticipated to be highly abundant due to the specificity of lecithin-cholesterol acyltransferase (LCAT) enzyme for 18:2n-6.[99] The timsTof platform detected three CE species within the top 20 lipids compared to only CE 18:2 that was detected in the qOrbi and QToF platforms (**Table 17**). Therefore, there is not a direct correlation between abundance and concentration of a lipid, which is a specific issue in the CE lipid class. The differences observed between abundance and concentration would have a large impact on the generation of inclusion lists. This is problematic when applying a discovery approach since a lipid may appear to be less concentrated if it has a lower signal abundance and may cause researchers to overlook potentially significant lipids of interest. More research needs to be completed in understanding the potential mechanism of CE detection in mass spectrometers.

8.6 Conclusion

A cross-platform analysis revealed no major benefits from the addition of TIMS, because although there was an increase in fragmentation, majority of the fragmented lipids contributed to the microlipidome which was not the focus of this study. Specifically, the use of the Bruker timsToF platform in the Bruker facility was a challenge for accessibility to both the instrument

and acquisition software however this platform was useful in providing additional insight into sources of variation from another platform, another separation technique (TIMS), and operator influences on the characterization of lipids. The major drawbacks of the Waters QToF platform were the compatibility issues between the raw acquisition data and the data treatment software. A high number of contaminants were also detected by the instrument which ultimately created a very labour-intensive process. Quantitation of lipids in the QToF also had the highest number of significantly different concentration values. The qOrbi platform was more user friendly, was compatible with the data treatment software and enabled identification of the highest overall number of unique lipids with contribution from every lipid class. It is therefore recommended that future macrolipidomic untargeted approaches utilize the qOrbi QE platform for similar studies within the lab.

Chapter 9
General Discussion

9.1 Overview

The characterization of SRM 1950 has been completed across three UHPLC-MS/MS platforms. Manual identification of fatty acyl chains using tandem mass spectrometry is a very beneficial methodology within lipidomics. Data treatment software has provided for more rapid and less labour-intensive work. However, it is difficult to confirm how well lipid annotation and data processing is being completed with an automated approach. Manual inspection proved to be extremely beneficial to the identification of lipids. Current software struggles to understand co-elution, isomers and in-source fragmentation which are prevalent within a lipidomic analysis. Manual lipid annotation has the major benefit of applying prior knowledge of the field, since lipids cannot always be simply identified through viewing the spectra alone. In this Chapter, the general hypotheses stated in Chapter 4 will be addressed.

It was hypothesized that a **manual inspection of mass spectra will improve the quality of identifications as compared with software-based identifications**. Unfortunately, this could not be fully determined since the fully automated lipid annotation through Progenesis data treatment software was not functional when two databases were used. However, during the manual inspection approach, it was evident that the possible raw ID with the highest rank was not always correct. This process is based strictly off the overall mass and fragment matching to the databases. The software listed possible raw ID in numerical or alphabetical order when fragment matching scores were identical. Viewing the raw spectra manually and applying knowledge of common fragmentation patterns allowed for identification of the lipid and consideration of the retention time also benefitted identifications, which data treatment software is not capable of doing automatically. Obstacles such as co-elution of isomers or in-source fragmentation could

typically be observed within messy spectra. Brutto identifications were not as problematic due to the accurate mass of the instruments and capabilities of the software to match the parent ion to the databases. A manual approach however greatly benefitted in annotating lipids at the medio level.

It was hypothesized that **TG, GP and CE would constitute the majority of the SRM 1950 macrolipidome.** This was confirmed from the abundance of the lipid subclasses observed in each platform where PC lipids consistently were the most abundant lipids (Section 5.4, Figures 5 & 6. Section 6.4, Figures 9 & 10. Section 7.4, Figures 13 & 14). Utilizing abundance values alone does not provide a full understanding of the characterization of the lipidome of SRM 1950. Instrument response was a significant factor in quantitation of lipids, specifically CE. Originally CE was observed to have a very low abundance, especially in the qOrbi and QToF platforms. After quantitation with the ISTD, CE was the most concentrated lipid class in SRM 1950. The number of lipid species is also misleading as CE was one of the lowest lipid classes identified with unique identifications. TG also often outnumbered PC but after normalization to the ISTD, TG lipids were found at ~1/2 of the concentration of the most abundant PC lipid. This also agreed with the hypothesis that **positive ESI-polarity will provide the greatest overview of the macrolipidome since majority of the lipidome consists of positive ionizing lipids** as all three of these lipid classes ionize in the positive polarity.

Manual identification was more efficient in the negative ESI-mode for medio level identifications. This is because fatty acyl fragments can be detected directly. Although diagnostic fragments that indicate the lipid class of the ion exist in both polarities, calculating the mass for loss of fatty acyl fragments can require considerable amounts of time. This is especially true for TG species that have three fatty acyl chains and only ionize in the positive polarity. These

observations agree with the hypothesis that **negative ESI-polarity will produce more confident identification of lipids species at the medio level since acyl fragments can be detected directly in this mode**.

The biggest obstacle when confirming the medio level of information is a lack of fragment ions of high intensity within the spectrum. In order to identify lipids at the medio level, the parent ion needs to have been fragmented by the instrument and produce fatty acyl chains. Lipids of high signal intensity are typically very abundant within the sample, and thus the fragment ions also produce a strong signal. This helps to differentiate noise within the spectra and fragment ions of importance. Instrument settings such as top-5 DDA also favour lipids of greater abundance since they create more ions to be detected by the instrument. This was observed across all platforms (**Appendix A.1-6)** since less medio level identifications were generally made as the abundance of the features decreased. This agrees with the hypothesis that **medio level identifications of SRM 1950 will be made for the most abundant lipids.**

Through the efforts of this study, the macrolipidome of human plasma is better understood. Previous reports had placed high emphasis on fatty acyl species, however by number the glycerophospholipids appear to have the highest number of unique lipids in human plasma. Specifically, PC makes up majority of these lipids. PC 16:0_18:1, PC 16:0_18:2, PC 18:0_18:2 and PC 16:0_20:4 are the major PC lipids within the plasma macrolipidome and were found to contribute anywhere from 12 to 25% of the signal abundance across three platforms and two polarities (**Appendix A.1-6**). PE has been reported previously in higher concentrations and would be anticipated to contribute to the macrolipidome. However, PE lipids that were observed in the macrolipidome were often due to in-source fragmentation of PC. It is anticipated that PE contributes less to the macrolipidome than previously reported.[14,15] By concentration,

glycerolipids are the next largest lipid class. Within the macrolipidome, this is entirely TG species. TG 16:0_18:1_18:2 is the most abundant with contribution from a TG 16:1_18:0_18:2 isomer. TG 16:0_18:1_18:1 and TG 16:1_18:0_18:2 are also significant. TG species with 50 to 54 with one to four double bonds are the major contributors. Fatty acyl chain composition frequently consists of lower carbon chain and unsaturation such as 16:0, 16:1, 18:0, 18:1, 18:2 and 18:3. Arachidonic acid is also frequently observed within both the GP and GL lipids. It was confirmed in this study that CE is the lipid class of highest concentration in the macrolipidome but also has the lowest unique lipid species. CE 18:2 is the mostly highly concentrated lipid. The abundance values alone are misleading to how large of a contribution CE has within the lipidome. The abundance, concentrations, and number of lipid species identified needs to be considered when characterizing the lipidome. The overall composition of the plasma macrolipidome could be estimated to be *~40% CE, ~30% PC, ~20% TG, 5% SM and 5% other lipids such as FFA and lower abundant GP such as PE, PI and PS.*

9.2 Addressing the Challenges and Limitations

The field of lipidomics still requires more standardized approaches and techniques to better understand what is already present in literature and expand the field. The field encompasses a variety of research focuses which require tailored techniques and can lead to biases in approaches and reporting. The field continues to grow from scientists who specialize in mass spectrometry and from those with a nutritional background which can lead to variation in approaches. However, lipidomic instruments and techniques have and continue to improve from the utilization of high-resolution instruments to continual efforts to improve ion mobility. The importance of standardization has also grown through initiatives and is recognized in more

recent publications.[12] A large obstacle remains in determining standardized practices within a large and still growing field.

The macrolipidome provides an area of focus when enabling a global approach, however utilizing the top 85% of abundance is still not a standardized method in plasma. The top 85% of abundance is efficient at identifying highly abundant lipids however the effectiveness of considering the relative abundance was also observed in this study. In this study, the relative abundance remained consistent even after removal of contaminants and the lowest identified feature did not surpass 0.1%. Even in platforms where the smallest reviewed feature had a low relative abundance (0.02%), the number of lipids that were identified decreased beyond a relative abundance of 0.1% (**Appendix A.4**). Until a concrete definition of the macrolipidome is created, it will remain difficult to compare lipidomic profiling data across studies specifically in human plasma. A potential obstacle when reviewing the macrolipidome by abundance is the relationship between abundance and concentration. In this thesis it was evident that CE species specifically have a much lower abundance than their corresponding concentration. The timsToF also demonstrated how the instrument will influence the detected abundance of different lipid classes. A misleading abundance value could lead to lipids of importance not being quantified or included in inclusion lists for future targeted analyses. An emphasis on improving quantitation in mass spectrometry in general must continue to allow lipidomics and metabolomics to move away from the use of relative and semi-quantified data as quantitation will be required for standardized methods to be developed.

A challenge of this study involved inclusion of the timsToF platform from Bruker at their facility in the U.S.A. Access to the software was challenging because the lipids had to be quantitated in a limited time but also figuring out how to use the software had to be learned

during a restricted period of time. The data was first processed using Progenesis to get a better understanding of the lipid composition of the sample before beginning the software trail, but more lipids than anticipated had to be reviewed manually through the raw chromatogram. However, this platform was useful in providing an additional insight into sources of variation from another platform, another separation technique (TIMS), and operator influences on the characterization of lipids.

Another large difficulty with defining human plasma is the quantitation of lipid species through an untargeted approach. Although a global approach ensures profiling of lipids from all lipid classes, the method can never benefit all lipid classes equally since the very first step of the workflow of lipid extraction already influences the lipids that will be observed. The identifications of TG were still a significant challenge in this thesis despite incorporating prior separation via UHPLC. Since TG species are highly abundant in both concentration and by number of unique species, it could be beneficial to aid in the coelution of isomers through additional UHPLC separation. The benefit of a dual column has been explored in seed oil and food analyses for identifying TG species in our lab.[49] Increasing separation time however will also decrease analytical throughput and separation of TG species could be better dealt with through development of instrumentation.

Harmonization within the field of lipidomics will require advances in software. While data treatment software is available and has improved upon as the field grows, it is still unreliable for annotation. The automated data processing and identification of lipids was dysfunctional in this study, and processing isomers which are abundant in lipidomics is a formidable task. This is concerning as automated identifications are commonly reported in literature due to the labour-intensive task of manual annotations.[58,100] Until automated software improves and is

demonstrated experimentally to correctly identify lipid species, the manner in which lipidomic data is acquired and processed must openly be disclosed and assessed. The lack of harmonization and software challenges are also amplified by constantly evolving instrumentation platforms.

9.3 Conclusion

This thesis explored the use of an untargeted macrolipidomic approach on the characterization of medio level lipids across three UHPLC-MS/MS platforms. Lipidomics remains a challenge due to the large analytical outputs from analyses. A macrolipidomic approach, where 85% of the signal abundance is reviewed proved to be an efficient and successful technique to identify unique lipids of high abundance in plasma SRM 1950. A high number of unique lipids were identified in the qOrbi and QToF platforms. The timsToF did not identify as many lipids due to high detection of CE species, which also highlighted potential obstacles when utilizing signal abundance to identify potential lipids of interest. Highly abundant lipids within this thesis were consistent across platforms at the medio level, which is promising for applications in routine clinical plasma analysis through the use of inclusion lists. However, manual inspection is still required to have confidence in annotated lipids and improvements in data treatment software are still needed as identifying unknown lipids will be required to capture the variations in lipidomic profiles of individuals within populations. Studies exploring this variation relative to the SRM 1950 will be needed to refine an SRM 1950 based inclusion list before standardized lipidomic protocols can be fully developed and embraced. Despite these challenges, the present study indicates that this will eventually be possible and when it is the medio level of lipidomic information will allow for enhanced insights into the impact of diet and the role of complex lipid metabolism in human health and disease.

References

(1) Lai, M.; Al Rijjal, D.; Röst, H. L.; Dai, F. F.; Gunderson, E. P.; Wheeler, M. B. Underlying Dyslipidemia Postpartum in Women with a Recent GDM Pregnancy Who Develop Type 2 Diabetes. *eLife* **2020**, *9*, e59153. https://doi.org/10.7554/eLife.59153.

(2) Feng, L.; Yang, J.; Liu, W.; Wang, Q.; Wang, H.; Shi, L.; Fu, L.; Xu, Q.; Wang, B.; Li, T. Lipid Biomarkers in Acute Myocardial Infarction Before and After Percutaneous Coronary Intervention by Lipidomics Analysis. *Med. Sci. Monit. Int. Med. J. Exp. Clin. Res.* **2018**, *24*, 4175–4182. https://doi.org/10.12659/MSM.908732.

(3) Wang, Y.; Jiang, C.-T.; Song, J.-Y.; Song, Q.-Y.; Ma, J.; Wang, H.-J. Lipidomic Profile Revealed the Association of Plasma Lysophosphatidylcholines with Adolescent Obesity. *BioMed Res. Int.* **2019**, *2019*, e1382418. https://doi.org/10.1155/2019/1382418.

(4) Wong, M. W.; Braidy, N.; Poljak, A.; Pickford, R.; Thambisetty, M.; Sachdev, P. S. Dysregulation of Lipids in Alzheimer's Disease and Their Role as Potential Biomarkers. *Alzheimers Dement.* **2017**, *13* (7), 810–827. https://doi.org/10.1016/j.jalz.2017.01.008.

(5) Agarwal, M.; Khan, S. Plasma Lipids as Biomarkers for Alzheimer's Disease: A Systematic Review. *Cureus 12* (12). https://doi.org/10.7759/cureus.12008.

(6) Whiley, L.; Sen, A.; Heaton, J.; Proitsi, P.; García-Gómez, D.; Leung, R.; Smith, N.; Thambisetty, M.; Kloszewska, I.; Mecocci, P.; Soininen, H.; Tsolaki, M.; Vellas, B.; Lovestone, S.; Legido-Quigley, C.; AddNeuroMed Consortium. Evidence of Altered Phosphatidylcholine Metabolism in Alzheimer's Disease. *Neurobiol. Aging* **2014**, *35* (2), 271–278. https://doi.org/10.1016/j.neurobiolaging.2013.08.001.

(7) Mapstone, M.; Cheema, A. K.; Fiandaca, M. S.; Zhong, X.; Mhyre, T. R.; MacArthur, L. H.; Hall, W. J.; Fisher, S. G.; Peterson, D. R.; Haley, J. M.; Nazar, M. D.; Rich, S. A.; Berlau, D. J.; Peltz, C. B.; Tan, M. T.; Kawas, C. H.; Federoff, H. J. Plasma Phospholipids Identify Antecedent Memory Impairment in Older Adults. *Nat. Med.* **2014**, *20* (4), 415–418. https://doi.org/10.1038/nm.3466.

(8) Bandu, R.; Mok, H. J.; Kim, K. P. Phospholipids as Cancer Biomarkers: Mass Spectrometry-Based Analysis. *Mass Spectrom. Rev.* **2018**, *37* (2), 107–138. https://doi.org/10.1002/mas.21510.

(9) Wenk, M. R. The Emerging Field of Lipidomics. *Nat. Rev. Drug Discov.* **2005**, *4* (7), 594–610. https://doi.org/10.1038/nrd1776.

(10) Řezanka, T.; Kolouchová, I.; Gharwalová, L.; Palyzová, A.; Sigler, K. Lipidomic Analysis: From Archaea to Mammals. *Lipids* **2018**, *53* (1), 5–25. https://doi.org/10.1002/lipd.12001.

(11) Sun, T.; Wang, X.; Cong, P.; Xu, J.; Xue, C. Mass Spectrometry-Based Lipidomics in Food Science and Nutritional Health: A Comprehensive Review. *Compr. Rev. Food Sci. Food Saf.* **2020**, *19* (5), 2530–2558. https://doi.org/10.1111/1541-4337.12603.

(12) Köfeler, H. C.; Ahrends, R.; Baker, E. S.; Ekroos, K.; Han, X.; Hoffmann, N.; Holčapek, M.; Wenk, M. R.; Liebisch, G. Recommendations for Good Practice in Mass Spectrometry-Based Lipidomics. *J. Lipid Res.* **2021**, 100138. https://doi.org/10.1016/j.jlr.2021.100138.

(13) Guo, J.; Huan, T. Comparison of Full-Scan, Data-Dependent, and Data-Independent Acquisition Modes in Liquid Chromatography–Mass Spectrometry Based Untargeted Metabolomics. *Anal. Chem.* **2020**, *92* (12), 8072–8080. https://doi.org/10.1021/acs.analchem.9b05135.

(14) Bowden, J. A.; Heckert, A.; Ulmer, C. Z.; Jones, C. M.; Koelmel, J. P.; Abdullah, L.; Ahonen, L.; Alnouti, Y.; Armando, A. M.; Asara, J. M.; Bamba, T.; Barr, J. R.; Bergquist,

J.; Borchers, C. H.; Brandsma, J.; Breitkopf, S. B.; Cajka, T.; Cazenave-Gassiot, A.; Checa, A.; Cinel, M. A.; Colas, R. A.; Cremers, S.; Dennis, E. A.; Evans, J. E.; Fauland, A.; Fiehn, O.; Gardner, M. S.; Garrett, T. J.; Gotlinger, K. H.; Han, J.; Huang, Y.; Neo, A. H.; Hyötyläinen, T.; Izumi, Y.; Jiang, H.; Jiang, H.; Jiang, J.; Kachman, M.; Kiyonami, R.; Klavins, K.; Klose, C.; Köfeler, H. C.; Kolmert, J.; Koal, T.; Koster, G.; Kuklenyik, Z.; Kurland, I. J.; Leadley, M.; Lin, K.; Maddipati, K. R.; McDougall, D.; Meikle, P. J.; Mellett, N. A.; Monnin, C.; Moseley, M. A.; Nandakumar, R.; Oresic, M.; Patterson, R.; Peake, D.; Pierce, J. S.; Post, M.; Postle, A. D.; Pugh, R.; Qiu, Y.; Quehenberger, O.; Ramrup, P.; Rees, J.; Rembiesa, B.; Reynaud, D.; Roth, M. R.; Sales, S.; Schuhmann, K.; Schwartzman, M. L.; Serhan, C. N.; Shevchenko, A.; Somerville, S. E.; St John-Williams, L.; Surma, M. A.; Takeda, H.; Thakare, R.; Thompson, J. W.; Torta, F.; Triebl, A.; Trötzmüller, M.; Ubhayasekera, S. J. K.; Vuckovic, D.; Weir, J. M.; Welti, R.; Wenk, M. R.; Wheelock, C. E.; Yao, L.; Yuan, M.; Zhao, X. H.; Zhou, S. Harmonizing Lipidomics: NIST Interlaboratory Comparison Exercise for Lipidomics Using SRM 1950-Metabolites in Frozen Human Plasma. *J. Lipid Res.* **2017**, *58* (12), 2275–2288. https://doi.org/10.1194/jlr.M079012.

(15) Quehenberger, O.; Armando, A. M.; Brown, A. H.; Milne, S. B.; Myers, D. S.; Merrill, A. H.; Bandyopadhyay, S.; Jones, K. N.; Kelly, S.; Shaner, R. L.; Sullards, C. M.; Wang, E.; Murphy, R. C.; Barkley, R. M.; Leiker, T. J.; Raetz, C. R. H.; Guan, Z.; Laird, G. M.; Six, D. A.; Russell, D. W.; McDonald, J. G.; Subramaniam, S.; Fahy, E.; Dennis, E. A. Lipidomics Reveals a Remarkable Diversity of Lipids in Human Plasma. *J. Lipid Res.* **2010**, *51* (11), 3299–3305. https://doi.org/10.1194/jlr.M009449.

(16) Aristizabal Henao, J. J.; Bradley, R. M.; Duncan, R. E.; Stark, K. D. Categorizing and Qualifying Nutritional Lipidomic Data: Defining Brutto, Medio, Genio, and Infinio Lipid Species within Macrolipidomics and Microlipidomics. *Curr. Opin. Clin. Nutr. Metab. Care* **2018**, *21* (5), 352–359. https://doi.org/10.1097/MCO.0000000000000495.

(17) Panuwet, P.; Hunter, R. E.; D'Souza, P. E.; Chen, X.; Radford, S. A.; Cohen, J. R.; Marder, M. E.; Kartavenka, K.; Ryan, P. B.; Barr, D. B. Biological Matrix Effects in Quantitative Tandem Mass Spectrometry-Based Analytical Methods: Advancing Biomonitoring. *Crit. Rev. Anal. Chem.* **2016**, *46* (2), 93–105. https://doi.org/10.1080/10408347.2014.980775.

(18) Lísa, M.; Cífková, E.; Holčapek, M. Lipidomic Profiling of Biological Tissues Using Off-Line Two-Dimensional High-Performance Liquid Chromatography-Mass Spectrometry. *J. Chromatogr. A* **2011**, *1218* (31), 5146–5156. https://doi.org/10.1016/j.chroma.2011.05.081.

(19) Hansen, A. E.; Wiese, H. F. Essential Fatty Acids and Human Nutrition. II. Serum Level for Unsaturated Fatty Acids in Poorly-Nourished Infants and Children. *J. Nutr.* **1954**, *52* (3), 367–374. https://doi.org/10.1093/jn/52.3.367.

(20) The Effect of Dose Level of Essential Fatty Acids upon Fatty Acid Composition of the Rat Liver. *J. Lipid Res.* **1963**, *4* (2), 151–159. https://doi.org/10.1016/S0022-2275(20)40341-4.

(21) Koulman, A.; Prentice, P.; Wong, M. C. Y.; Matthews, L.; Bond, N. J.; Eiden, M.; Griffin, J. L.; Dunger, D. B. The Development and Validation of a Fast and Robust Dried Blood Spot Based Lipid Profiling Method to Study Infant Metabolism. *Metabolomics* **2014**, *10* (5), 1018–1025. https://doi.org/10.1007/s11306-014-0628-z.

(22) Yang, L.; Kraemer, M.; Fang, X. F.; Angel, P. M.; Drake, R. R.; Morris, A. J.; Smyth, S. S. LPA Receptor 4 Deficiency Attenuates Experimental Atherosclerosis. *J. Lipid Res.* **2019**, *60* (5), 972–980. https://doi.org/10.1194/jlr.M091066.

(23) Lands, B. Historical Perspectives on the Impact of N-3 and n-6 Nutrients on Health. *Prog. Lipid Res.* **2014**, *55*, 17–29. https://doi.org/10.1016/j.plipres.2014.04.002.
(24) Harayama, T.; Shimizu, T. Roles of Polyunsaturated Fatty Acids, from Mediators to Membranes. *J. Lipid Res.* **2020**, jlr.R120000800. https://doi.org/10.1194/jlr.R120000800.
(25) Harris, W. S.; Von Schacky, C. The Omega-3 Index: A New Risk Factor for Death from Coronary Heart Disease? *Prev. Med.* **2004**, *39* (1), 212–220. https://doi.org/10.1016/j.ypmed.2004.02.030.
(26) Stark, K. D. Applications of Innovative Lipidomic Methods for Blood Lipid Biomarkers. *J. Oleo Sci.* **2019**, *68* (6), 503–510. https://doi.org/10.5650/jos.ess19042.
(27) Stark, K. D.; Van Elswyk, M. E.; Higgins, M. R.; Weatherford, C. A.; Salem, N. Global Survey of the Omega-3 Fatty Acids, Docosahexaenoic Acid and Eicosapentaenoic Acid in the Blood Stream of Healthy Adults. *Prog. Lipid Res.* **2016**, *63*, 132–152. https://doi.org/10.1016/j.plipres.2016.05.001.
(28) Health Canada. Canadian Nutrient File (CNF) https://food-nutrition.canada.ca/cnf-fce/index-eng.jsp.
(29) Fahy, E.; Subramaniam, S.; Murphy, R. C.; Nishijima, M.; Raetz, C. R. H.; Shimizu, T.; Spener, F.; Meer, G. van; Wakelam, M. J. O.; Dennis, E. A. Update of the LIPID MAPS Comprehensive Classification System for Lipids. *J. Lipid Res.* **2009**, *50* (Supplement), S9–S14. https://doi.org/10.1194/jlr.R800095-JLR200.
(30) Siskos, A. P.; Jain, P.; Römisch-Margl, W.; Bennett, M.; Achaintre, D.; Asad, Y.; Marney, L.; Richardson, L.; Koulman, A.; Griffin, J. L.; Raynaud, F.; Scalbert, A.; Adamski, J.; Prehn, C.; Keun, H. C. Interlaboratory Reproducibility of a Targeted Metabolomics Platform for Analysis of Human Serum and Plasma. *Anal. Chem.* **2017**, *89* (1), 656–665. https://doi.org/10.1021/acs.analchem.6b02930.
(31) Zhang, Q.; Xu, H.; Liu, R.; Gao, P.; Yang, X.; Jin, W.; Zhang, Y.; Bi, K.; Li, Q. A Novel Strategy for Targeted Lipidomics Based on LC-Tandem-MS Parameters Prediction, Quantification, and Multiple Statistical Data Mining: Evaluation of Lysophosphatidylcholines as Potential Cancer Biomarkers. *Anal. Chem.* **2019**, *91* (5), 3389–3396. https://doi.org/10.1021/acs.analchem.8b04715.
(32) Alshehry, Z. H.; Mundra, P. A.; Barlow, C. K.; Mellett, N. A.; Wong, G.; McConville, M. J.; Simes, J.; Tonkin, A. M.; Sullivan, D. R.; Barnes, E. H.; Nestel, P. J.; Kingwell, B. A.; Marre, M.; Neal, B.; Poulter, N. R.; Rodgers, A.; Williams, B.; Zoungas, S.; Hillis, G. S.; Chalmers, J.; Woodward, M.; Meikle, P. J. Plasma Lipidomic Profiles Improve on Traditional Risk Factors for the Prediction of Cardiovascular Events in Type 2 Diabetes Mellitus. *Circulation* **2016**, *134* (21), 1637–1650. https://doi.org/10.1161/CIRCULATIONAHA.116.023233.
(33) Liebisch, G.; Vizcaíno, J. A.; Köfeler, H.; Trötzmüller, M.; Griffiths, W. J.; Schmitz, G.; Spener, F.; Wakelam, M. J. O. Shorthand Notation for Lipid Structures Derived from Mass Spectrometry. *J. Lipid Res.* **2013**, *54* (6), 1523–1530. https://doi.org/10.1194/jlr.M033506.
(34) Liebisch, G.; Fahy, E.; Aoki, J.; Dennis, E. A.; Durand, T.; Ejsing, C. S.; Fedorova, M.; Feussner, I.; Griffiths, W. J.; Köfeler, H.; Merrill, A. H.; Murphy, R. C.; O'Donnell, V. B.; Oskolkova, O.; Subramaniam, S.; Wakelam, M. J. O.; Spener, F. Update on LIPID MAPS Classification, Nomenclature, and Shorthand Notation for MS-Derived Lipid Structures. *J. Lipid Res.* **2020**, *61* (12), 1539–1555. https://doi.org/10.1194/jlr.S120001025.

(35) Liebisch, G.; Ekroos, K.; Hermansson, M.; Ejsing, C. S. Reporting of Lipidomics Data Should Be Standardized. *Biochim. Biophys. Acta BBA - Mol. Cell Biol. Lipids* **2017**, *1862* (8), 747–751. https://doi.org/10.1016/j.bbalip.2017.02.013.
(36) Maccarone, A. T.; Duldig, J.; Mitchell, T. W.; Blanksby, S. J.; Duchoslav, E.; Campbell, J. L. Characterization of Acyl Chain Position in Unsaturated Phosphatidylcholines Using Differential Mobility-Mass Spectrometry. *J. Lipid Res.* **2014**, *55* (8), 1668–1677. https://doi.org/10.1194/jlr.M046995.
(37) Steckel, K. E.; Aristizabal Henao, J. J.; Stark, K. D. Medio Level Macrolipidomics for Nutritional Research. *INFORM: AOCS*. July 2020, pp 18–21.
(38) Trufelli, H.; Palma, P.; Famiglini, G.; Cappiello, A. An Overview of Matrix Effects in Liquid Chromatography–Mass Spectrometry. *Mass Spectrom. Rev.* **2011**, *30* (3), 491–509. https://doi.org/10.1002/mas.20298.
(39) Harris, D. C. *Quantitative Chemical Analysis*, 8th ed.; W.H. Freeman Company, 2010.
(40) Lange, M.; Ni, Z.; Criscuolo, A.; Fedorova, M. Liquid Chromatography Techniques in Lipidomics Research. *Chromatographia* **2019**, *82* (1), 77–100. https://doi.org/10.1007/s10337-018-3656-4.
(41) Lange, M.; Fedorova, M. Evaluation of Lipid Quantification Accuracy Using HILIC and RPLC MS on the Example of NIST® SRM® 1950 Metabolites in Human Plasma. *Anal. Bioanal. Chem.* **2020**. https://doi.org/10.1007/s00216-020-02576-x.
(42) Fenn, J. B.; Mann, M.; Meng, C. K.; Wong, S. F.; Whitehouse, C. M. Electrospray Ionization for Mass Spectrometry of Large Biomolecules. *Science* **1989**, *246* (4926), 64–71. https://doi.org/10.1126/science.2675315.
(43) Ho, C.; Lam, C.; Chan, M.; Cheung, R.; Law, L.; Lit, L.; Ng, K.; Suen, M.; Tai, H. Electrospray Ionisation Mass Spectrometry: Principles and Clinical Applications. *Clin. Biochem. Rev.* **2003**, *24* (1), 3–12.
(44) Bruins, A. P. Mechanistic Aspects of Electrospray Ionization. *J. Chromatogr. A* **1998**, *794* (1), 345–357. https://doi.org/10.1016/S0021-9673(97)01110-2.
(45) Paglia, G.; Kliman, M.; Claude, E.; Geromanos, S.; Astarita, G. Applications of Ion-Mobility Mass Spectrometry for Lipid Analysis. *Anal. Bioanal. Chem.* **2015**, *407* (17), 4995–5007. https://doi.org/10.1007/s00216-015-8664-8.
(46) Hinz, C.; Liggi, S.; Griffin, J. L. The Potential of Ion Mobility Mass Spectrometry for High-Throughput and High-Resolution Lipidomics. *Curr. Opin. Chem. Biol.* **2018**, *42*, 42–50. https://doi.org/10.1016/j.cbpa.2017.10.018.
(47) Kanu, A. B.; Dwivedi, P.; Tam, M.; Matz, L.; Hill, H. H. Ion Mobility–Mass Spectrometry. *J. Mass Spectrom.* **2008**, *43* (1), 1–22. https://doi.org/10.1002/jms.1383.
(48) Liu, Y.; Clemmer, D. E. Characterizing Oligosaccharides Using Injected-Ion Mobility/Mass Spectrometry. *Anal. Chem.* **1997**, *69* (13), 2504–2509. https://doi.org/10.1021/ac9701344.
(49) Aristizabal Henao, J. J. Fatty Acyl-Specific Macrolipidomics and Microlipidomics for Nutritional Research. PhD, University of Waterloo, 2019.
(50) Fernandez-Lima, F.; Kaplan, D. A.; Suetering, J.; Park, M. A. Gas-Phase Separation Using a Trapped Ion Mobility Spectrometer. *Int. J. Ion Mobil. Spectrom.* **2011**, *14* (2), 93–98. https://doi.org/10.1007/s12127-011-0067-8.
(51) Ridgeway, M. E.; Lubeck, M.; Jordens, J.; Mann, M.; Park, M. A. Trapped Ion Mobility Spectrometry: A Short Review. *Int. J. Mass Spectrom.* **2018**, *425*, 22–35. https://doi.org/10.1016/j.ijms.2018.01.006.

(52) Gathungu, R. M.; Larrea, P.; Sniatynski, M. J.; Marur, V. R.; Bowden, J. A.; Koelmel, J. P.; Starke-Reed, P.; Hubbard, V. S.; Kristal, B. S. Optimization of Electrospray Ionization Source Parameters for Lipidomics To Reduce Misannotation of In-Source Fragments as Precursor Ions. *Anal. Chem.* **2018**, *90* (22), 13523–13532. https://doi.org/10.1021/acs.analchem.8b03436.
(53) Wood, P. L.; Cebak, J. E. Lipidomics Biomarker Studies: Errors, Limitations, and the Future. *Biochem. Biophys. Res. Commun.* **2018**, *504* (3), 569–575. https://doi.org/10.1016/j.bbrc.2018.03.188.
(54) Burla, B.; Arita, M.; Arita, M.; Bendt, A. K.; Cazenave-Gassiot, A.; Dennis, E. A.; Ekroos, K.; Han, X.; Ikeda, K.; Liebisch, G.; Lin, M. K.; Loh, T. P.; Meikle, P. J.; Orešič, M.; Quehenberger, O.; Shevchenko, A.; Torta, F.; Wakelam, M. J. O.; Wheelock, C. E.; Wenk, M. R. MS-Based Lipidomics of Human Blood Plasma: A Community-Initiated Position Paper to Develop Accepted Guidelines1. *J. Lipid Res.* **2018**, *59* (10), 2001–2017. https://doi.org/10.1194/jlr.S087163.
(55) Murphy, R. C. Challenges in Mass Spectrometry-Based Lipidomics of Neutral Lipids. *TrAC Trends Anal. Chem.* **2018**, *107*, 91–98. https://doi.org/10.1016/j.trac.2018.07.023.
(56) Fahy, E.; Subramaniam, S.; Brown, H. A.; Glass, C. K.; Merrill, A. H.; Murphy, R. C.; Raetz, C. R. H.; Russell, D. W.; Seyama, Y.; Shaw, W.; Shimizu, T.; Spener, F.; Meer, G. van; VanNieuwenhze, M. S.; White, S. H.; Witztum, J. L.; Dennis, E. A. A Comprehensive Classification System for Lipids. *J. Lipid Res.* **2005**, *46* (5), 839–861. https://doi.org/10.1194/jlr.E400004-JLR200.
(57) Schmelzer, K.; Fahy, E.; Subramaniam, S.; Dennis, E. A. The Lipid Maps Initiative in Lipidomics. In *Methods in Enzymology*; Lipidomics and Bioactive Lipids: Mass-Spectrometry–Based Lipid Analysis; Academic Press, 2007; Vol. 432, pp 171–183. https://doi.org/10.1016/S0076-6879(07)32007-7.
(58) Tsugawa, H.; Ikeda, K.; Takahashi, M.; Satoh, A.; Mori, Y.; Uchino, H.; Okahashi, N.; Yamada, Y.; Tada, I.; Bonini, P.; Higashi, Y.; Okazaki, Y.; Zhou, Z.; Zhu, Z.-J.; Koelmel, J.; Cajka, T.; Fiehn, O.; Saito, K.; Arita, M.; Arita, M. A Lipidome Atlas in MS-DIAL 4. *Nat. Biotechnol.* **2020**, 1–5. https://doi.org/10.1038/s41587-020-0531-2.
(59) Lichtman, S. W.; Pisarska, K.; Berman, E. R.; Pestone, M.; Dowling, H.; Offenbacher, E.; Weisel, H.; Heshka, S.; Matthews, D. E.; Heymsfield, S. B. Discrepancy between Self-Reported and Actual Caloric Intake and Exercise in Obese Subjects. *N. Engl. J. Med.* **1992**, *327* (27), 1893–1898. https://doi.org/10.1056/NEJM199212313272701.
(60) Hill, R. J.; Davies, P. S. The Validity of Self-Reported Energy Intake as Determined Using the Doubly Labelled Water Technique. *Br. J. Nutr.* **2001**, *85* (4), 415–430. https://doi.org/10.1079/bjn2000281.
(61) Hodson, L.; Skeaff, C. M.; Fielding, B. A. Fatty Acid Composition of Adipose Tissue and Blood in Humans and Its Use as a Biomarker of Dietary Intake. *Prog. Lipid Res.* **2008**, *47* (5), 348–380. https://doi.org/10.1016/j.plipres.2008.03.003.
(62) Lands, W. E. Long-Term Fat Intake and Biomarkers. *Am. J. Clin. Nutr.* **1995**, *61* (3 Suppl), 721S-725S. https://doi.org/10.1093/ajcn/61.3.721S.
(63) Strawford, A.; Antelo, F.; Christiansen, M.; Hellerstein, M. K. Adipose Tissue Triglyceride Turnover, de Novo Lipogenesis, and Cell Proliferation in Humans Measured with 2H2O. *Am. J. Physiol. Endocrinol. Metab.* **2004**, *286* (4), E577-588. https://doi.org/10.1152/ajpendo.00093.2003.

(64) Liu, X.; Hoene, M.; Wang, X.; Yin, P.; Häring, H.-U.; Xu, G.; Lehmann, R. Serum or Plasma, What Is the Difference? Investigations to Facilitate the Sample Material Selection Decision Making Process for Metabolomics Studies and Beyond. *Anal. Chim. Acta* **2018**, *1037*, 293–300. https://doi.org/10.1016/j.aca.2018.03.009.
(65) Yu, Z.; Kastenmüller, G.; He, Y.; Belcredi, P.; Möller, G.; Prehn, C.; Mendes, J.; Wahl, S.; Roemisch-Margl, W.; Ceglarek, U.; Polonikov, A.; Dahmen, N.; Prokisch, H.; Xie, L.; Li, Y.; Wichmann, H.-E.; Peters, A.; Kronenberg, F.; Suhre, K.; Adamski, J.; Illig, T.; Wang-Sattler, R. Differences between Human Plasma and Serum Metabolite Profiles. *PloS One* **2011**, *6* (7), e21230. https://doi.org/10.1371/journal.pone.0021230.
(66) Havel, R. J.; Eder, H. A.; Bragdon, J. H. The Distribution and Chemical Composition Of Ultracentrifugally Separated Lipoproteins In Human Serum. *J. Clin. Invest.* **1955**, *34* (9), 1345–1353.
(67) Russ, E. M.; Eder, H. A.; D. P. Barr. Protein-Lipid Relationships in Human Plasma: I. In Normal Individuals. *Am. J. Med.* **1951**, *11* (4), 468–479. https://doi.org/10.1016/0002-9343(51)90182-9.
(68) Barr, D. P.; Russ, E. M.; Eder, H. A. Protein-Lipid Relationships in Human Plasma: II. In Atherosclerosis and Related Conditions. *Am. J. Med.* **1951**, *11* (4), 480–493. https://doi.org/10.1016/0002-9343(51)90183-0.
(69) Christinat, N.; Masoodi, M. Comprehensive Lipoprotein Characterization Using Lipidomics Analysis of Human Plasma. *J. Proteome Res.* **2017**, *16* (8), 2947–2953. https://doi.org/10.1021/acs.jproteome.7b00236.
(70) Barboriak, J. J.; Rimm, A. A.; Anderson, A. J.; Tistani, F. E.; Walker, J. A.; Flemma, R. J. Heart Disease Indicators in Patients with Aortocoronary Bypass Operation. *Cardiology* **1976**, *61* (3), 153–161. https://doi.org/10.1159/000169758.
(71) Brenna, J. T.; Plourde, M.; Stark, K. D.; Jones, P. J.; Lin, Y.-H. Best Practices for the Design, Laboratory Analysis, and Reporting of Trials Involving Fatty Acids. *Am. J. Clin. Nutr.* **2018**, *108* (2), 211–227. https://doi.org/10.1093/ajcn/nqy089.
(72) Kritchevsky, D. Atherosclerosis and Cholesterol. *J. Dairy Sci.* **1967**, *50* (5), 776–781. https://doi.org/10.3168/jds.S0022-0302(67)87515-5.
(73) Quehenberger, O.; Dennis, E. A. The Human Plasma Lipidome. *N. Engl. J. Med.* **2011**, *365* (19), 1812–1823. https://doi.org/10.1056/NEJMra1104901.
(74) National Institute of Standards and Technology. *Certificate of Analysis: Standard Reference Material 1950 - Metabolites in Human Plasma*; 2012.
(75) Phinney, K. W.; Ballihaut, G.; Bedner, M.; Benford, B. S.; Camara, J. E.; Christopher, S. J.; Davis, W. C.; Dodder, N. G.; Eppe, G.; Lang, B. E.; Long, S. E.; Lowenthal, M. S.; McGaw, E. A.; Murphy, K. E.; Nelson, B. C.; Prendergast, J. L.; Reiner, J. L.; Rimmer, C. A.; Sander, L. C.; Schantz, M. M.; Sharpless, K. E.; Sniegoski, L. T.; Tai, S. S.-C.; Thomas, J. B.; Vetter, T. W.; Welch, M. J.; Wise, S. A.; Wood, L. J.; Guthrie, W. F.; Hagwood, C. R.; Leigh, S. D.; Yen, J. H.; Zhang, N.-F.; Chaudhary-Webb, M.; Chen, H.; Fazili, Z.; LaVoie, D. J.; McCoy, L. F.; Momin, S. S.; Paladugula, N.; Pendergrast, E. C.; Pfeiffer, C. M.; Powers, C. D.; Rabinowitz, D.; Rybak, M. E.; Schleicher, R. L.; Toombs, B. M. H.; Xu, M.; Zhang, M.; Castle, A. L. Development of a Standard Reference Material for Metabolomics Research. *Anal. Chem.* **2013**, *85* (24), 11732–11738. https://doi.org/10.1021/ac402689t.
(76) Ulmer, C. Z.; Ragland, J. M.; Koelmel, J. P.; Heckert, A.; Jones, C. M.; Garrett, T. J.; Yost, R. A.; Bowden, J. A. LipidQC: Method Validation Tool for Visual Comparison to SRM

1950 Using NIST Interlaboratory Comparison Exercise Lipid Consensus Mean Estimate Values. *Anal. Chem.* **2017**, *89* (24), 13069–13073. https://doi.org/10.1021/acs.analchem.7b04042.
(77) Ulmer, C. Z.; Jones, C. M.; Yost, R. A.; Garrett, T. J.; Bowden, J. A. Optimization of Folch, Bligh-Dyer, and Matyash Sample-to-Extraction Solvent Ratios for Human Plasma-Based Lipidomics Studies. *Anal. Chim. Acta* **2018**, *1037*, 351–357. https://doi.org/10.1016/j.aca.2018.08.004.
(78) Wolrab, D.; Chocholoušková, M.; Jirásko, R.; Peterka, O.; Holčapek, M. Validation of Lipidomic Analysis of Human Plasma and Serum by Supercritical Fluid Chromatography–Mass Spectrometry and Hydrophilic Interaction Liquid Chromatography–Mass Spectrometry. *Anal. Bioanal. Chem.* **2020**. https://doi.org/10.1007/s00216-020-02473-3.
(79) Triebl, A.; Burla, B.; Selvalatchmanan, J.; Oh, J.; Tan, S. H.; Chan, M. Y.; Mellet, N. A.; Meikle, P. J.; Torta, F.; Wenk, M. R. Shared Reference Materials Harmonize Lipidomics across MS-Based Detection Platforms and Laboratories. *J. Lipid Res.* **2020**, *61* (1), 105–115. https://doi.org/10.1194/jlr.D119000393.
(80) Schwaiger, M.; Schoeny, H.; El Abiead, Y.; Hermann, G.; Rampler, E.; Koellensperger, G. Merging Metabolomics and Lipidomics into One Analytical Run. *The Analyst* **2019**, *144* (1), 220–229. https://doi.org/10.1039/C8AN01219A.
(81) Schoeny, H.; Rampler, E.; Hermann, G.; Grienke, U.; Rollinger, J. M.; Koellensperger, G. Preparative Supercritical Fluid Chromatography for Lipid Class Fractionation—a Novel Strategy in High-Resolution Mass Spectrometry Based Lipidomics. *Anal. Bioanal. Chem.* **2020**, *412* (10), 2365–2374. https://doi.org/10.1007/s00216-020-02463-5.
(82) Koelmel, J. P.; Li, X.; Stow, S. M.; Sartain, M. J.; Murali, A.; Kemperman, R.; Tsugawa, H.; Takahashi, M.; Vasiliou, V.; Bowden, J. A.; Yost, R. A.; Garrett, T. J.; Kitagawa, N. Lipid Annotator: Towards Accurate Annotation in Non-Targeted Liquid Chromatography High-Resolution Tandem Mass Spectrometry (LC-HRMS/MS) Lipidomics Using a Rapid and User-Friendly Software. *Metabolites* **2020**, *10* (3). https://doi.org/10.3390/metabo10030101.
(83) Koelmel, J. P.; Cochran, J. A.; Ulmer, C. Z.; Levy, A. J.; Patterson, R. E.; Olsen, B. C.; Yost, R. A.; Bowden, J. A.; Garrett, T. J. Software Tool for Internal Standard Based Normalization of Lipids, and Effect of Data-Processing Strategies on Resulting Values. *BMC Bioinformatics* **2019**, *20*. https://doi.org/10.1186/s12859-019-2803-8.
(84) Avanti Polar. *SPLASH LIPIDOMIX Quantitative Mass Spec Internal Standard*; Technical Data Sheet.
(85) Folch, J.; Lees, M.; Stanley, G. H. S. A Simple Method for the Isolation and Purification of Total Lipides from Animal Tissues. *J. Biol. Chem.* **1957**, *226* (1), 497–509.
(86) Kind, T.; Liu, K.-H.; Lee, D. Y.; DeFelice, B.; Meissen, J. K.; Fiehn, O. LipidBlast in Silico Tandem Mass Spectrometry Database for Lipid Identification. *Nat. Methods* **2013**, *10* (8), 755–758. https://doi.org/10.1038/nmeth.2551.
(87) Hsu, F.-F.; Turk, J. Electrospray Ionization with Low-Energy Collisionally Activated Dissociation Tandem Mass Spectrometry of Glycerophospholipids: Mechanisms of Fragmentation and Structural Characterization. *J. Chromatogr. B* **2009**, *877* (26), 2673–2695. https://doi.org/10.1016/j.jchromb.2009.02.033.
(88) Murphy, R. C.; Axelsen, P. H. Mass Spectrometric Analysis of Long-Chain Lipids. *Mass Spectrom. Rev.* **2011**, *30* (4), 579–599. https://doi.org/10.1002/mas.20284.

(89) López-Bascón, M. A.; Calderón-Santiago, M.; Díaz-Lozano, A.; Camargo, A.; López-Miranda, J.; Priego-Capote, F. Development of a Qualitative/Quantitative Strategy for Comprehensive Determination of Polar Lipids by LC–MS/MS in Human Plasma. *Anal. Bioanal. Chem.* **2019**. https://doi.org/10.1007/s00216-019-02261-8.
(90) Koivusalo, M.; Haimi, P.; Heikinheimo, L.; Kostiainen, R.; Somerharju, P. Quantitative Determination of Phospholipid Compositions by ESI-MS: Effects of Acyl Chain Length, Unsaturation, and Lipid Concentration on Instrument Response. *J. Lipid Res.* **2001**, *42* (4), 663–672.
(91) Pulfer, M.; Murphy, R. C. Electrospray Mass Spectrometry of Phospholipids. *Mass Spectrom. Rev.* **2003**, *22* (5), 332–364. https://doi.org/10.1002/mas.10061.
(92) Triebl, A.; Trötzmüller, M.; Hartler, J.; Stojakovic, T.; Köfeler, H. C. Lipidomics by Ultrahigh Performance Liquid Chromatography-High Resolution Mass Spectrometry and Its Application to Complex Biological Samples. *J. Chromatogr. B Analyt. Technol. Biomed. Life. Sci.* **2017**, *1053*, 72–80. https://doi.org/10.1016/j.jchromb.2017.03.027.
(93) Meier, F.; Brunner, A.-D.; Koch, S.; Koch, H.; Lubeck, M.; Krause, M.; Goedecke, N.; Decker, J.; Kosinski, T.; Park, M. A.; Bache, N.; Hoerning, O.; Cox, J.; Räther, O.; Mann, M. Online Parallel Accumulation–Serial Fragmentation (PASEF) with a Novel Trapped Ion Mobility Mass Spectrometer. *Mol. Cell. Proteomics MCP* **2018**, *17* (12), 2534–2545. https://doi.org/10.1074/mcp.TIR118.000900.
(94) Meier, F.; Beck, S.; Grassl, N.; Lubeck, M.; Park, M. A.; Raether, O.; Mann, M. Parallel Accumulation–Serial Fragmentation (PASEF): Multiplying Sequencing Speed and Sensitivity by Synchronized Scans in a Trapped Ion Mobility Device. *J. Proteome Res.* **2015**, *14* (12), 5378–5387. https://doi.org/10.1021/acs.jproteome.5b00932.
(95) Vasilopoulou, C. G.; Sulek, K.; Brunner, A.-D.; Meitei, N. S.; Schweiger-Hufnagel, U.; Meyer, S. W.; Barsch, A.; Mann, M.; Meier, F. Trapped Ion Mobility Spectrometry and PASEF Enable In-Depth Lipidomics from Minimal Sample Amounts. *Nat. Commun.* **2020**, *11*. https://doi.org/10.1038/s41467-019-14044-x.
(96) Pettit, M. E.; Harper, B.; Brantley, M. R.; Solouki, T. Collision-Energy Resolved Ion Mobility Characterization of Isomeric Mixtures. *Analyst* **2015**, *140* (20), 6886–6896. https://doi.org/10.1039/C5AN00940E.
(97) Fenn, L. S.; Kliman, M.; Mahsut, A.; Zhao, S. R.; McLean, J. A. Characterizing Ion Mobility-Mass Spectrometry Conformation Space for the Analysis of Complex Biological Samples. *Anal. Bioanal. Chem.* **2009**, *394* (1), 235–244. https://doi.org/10.1007/s00216-009-2666-3.
(98) Bowden, J. A.; Ulmer, C. Z.; Jones, C. M.; Koelmel, J. P.; Yost, R. A. NIST Lipidomics Workflow Questionnaire: An Assessment of Community-Wide Methodologies and Perspectives. *Metabolomics* **2018**, *14* (5), 53. https://doi.org/10.1007/s11306-018-1340-1.
(99) Stark, K. Analytical Implications of Routine Clinical Testing for Omega-3 Fatty Acid Biomarkers. *Lipid Technol.* **2008**, *20* (8), 177–179. https://doi.org/10.1002/lite.200800037.
(100) Aristizabal-Henao, J. J.; Jones, C. M.; Lippa, K. A.; Bowden, J. A. Nontargeted Lipidomics of Novel Human Plasma Reference Materials: Hypertriglyceridemic, Diabetic, and African-American. *Anal. Bioanal. Chem.* **2020**, *412* (27), 7373–7380. https://doi.org/10.1007/s00216-020-02910-3.

Appendices

Appendix A.1. Top 85% Abundance within positive Quadrupole-Orbitrap.

Feature #	m/z	Retention time (min)	Brutto	Medio	Abundance	Relative Abundance (%)	Cumulative Abundance (%)
1	758.5718	17.30	PC 34:2	PC 16:0_18:2	11095238329	8.79	8.79
2	786.6032	21.18	PC 36:2	PC 18:0_18:2	7757229785	6.15	14.94
3	874.7902	33.19	TG 52:3	TG 16:0_18:1_18:2 | TG 16:1_18:0_18:2	6755514626	5.35	20.30
4	782.5714	16.69	PC 36:4	PC 16:0_20:4	6245966578	4.95	25.25
5	760.5871	20.45	PC 34:1	PC 16:0_18:1	6157050332	4.88	30.13
6	876.8070	34.07	TG 52:2	TG 16:0_18:1_18:1 | TG 16:1_18:0_18:1	5374244660	4.26	34.39
7	810.6032	20.69	PC 38:4	PC 18:0_20:4	4229686186	3.35	37.74
8	753.6151	18.29	ISTD	PC 15:0-18:1(d7)	2938294870	2.33	40.07
9	806.5714	15.68	PC 38:6	PC 16:0_22:6	2837468206	2.25	42.32
10	900.8066	33.22	TG 54:4	TG 18:1_18:1_18:2 | TG 16:0_18:2_20:2 | TG 18:0_18:2_18:2	2638397522	2.09	44.41
11	848.7746	33.05	TG 50:2	TG 16:0_16:0_18:2 | TG 16:1_16:0_18:1 | TG 14:0_18:1_18:1	2638191807	2.09	46.50
12	902.8225	34.19	TG 54:3	TG 18:0_18:1_18:2	2433358199	1.93	48.43
13	850.7901	34.07	TG 50:1	TG 16:0_16:0_18:1	1783051390	1.41	49.84
14	898.7893	32.26	TG 54:5	TG 18:1_18:2_18:2 | TG 18:1_18:1_18:3	1755869884	1.39	51.23
15	784.5870	17.68	PC 36:3	PC 18:1_18:2	1530315473	1.21	52.44
16	846.7580	32.07	TG 50:3	TG 16:1_16:1_18:1 | TG 16:0_16:1_18:2 | TG 14:0_18:1_18:2	1436977936	1.14	53.58
17	703.5748	16.02	SM 34:1	SM d18:1_16:0	1418752560	1.12	54.71
18	496.3404	4.24	LPC 16:0	LPC 16:0	1278331536	1.01	55.72
19	788.6179	22.77	PC 36:1	PC 18:0_18:1	1224767431	0.97	56.69
20	812.6184	21.84	PC 38:3	PC 18:0_20:3	1181769604	0.94	57.63
21	666.6175	33.57	CE 18:2	CE 18:2	1161106672	0.92	58.55
22	822.7561	33.04	TG 48:1	TG 14:0_16:0_18:1 | TG 16:0_16:0_16:1	1003693694	0.80	59.34
23	808.5869	16.85	PC 38:5	PC 16:0_22:5 | PC 18:1_20:4	943085744.5	0.75	60.09
24	878.8215	34.97	TG 52:1	TG 16:0_18:0_18:1	875647961.9	0.69	60.78
25	829.8010	32.97	ISTD	TG 15:0-18:1(d7)-15:0	854193200.6	0.68	61.46
26	904.8369	34.97	TG 54:2	TG 18:0_18:1_18:1	834557294.3	0.66	62.12
27	813.6864	24.34	SM 42:2	SM d18:1_24:1	682571627.7	0.54	62.66
28	924.8048	32.85	TG 56:6	TG 18:1_18:1_20:4 | TG 16:0_18:1_22:5 | TG 18:1_18:2_20:3 | TG 16:0_18:2_22:4 | TG 18:0_18:2_20:4 | TG 16:0_20:3_20:3	661804744.5	0.52	63.19

29	960.8998	34.02	TG 58:2		628084340.7	0.50	63.69
30	958.8847	33.17	TG 58:3		590041004.7	0.47	64.15
31	956.8684	32.22	TG 58:4		584686731.5	0.46	64.62
32	820.7403	32.05	TG 48:2	TG 16:0_16:1_16:1 | TG 14:0_16:1_18:1 | TG 14:0_16:0_18:2 | TG 14:1_16:0_18:1 | TG 12:0_18:1_18:1	583834293.8	0.46	65.08
33	690.6181	32.88	CE 20:4	CE 20:4	507201429	0.40	65.48
34	898.7894	32.86	TG 54:5	TG 16:0_18:1_20:4	505845060.2	0.40	65.88
35	870.7563	31.32	TG 42:5	TG 16:0_18:2_18:3 | 16:1_18:1_18:3	490709698.4	0.39	66.27
36	834.6015	19.65	PC 40:6	PC 18:0_22:6	481050010.6	0.38	66.65
37	787.6698	24.45	SM 40:1	SM d18:1_22:0	448910639.1	0.36	67.01
38	824.7706	34.09	TG 48:0	TG 16:0_16:0_16:0 | TG 14:0_16:0_18:0	447634667.8	0.35	67.36
39	922.7875	31.85	TG 56:7	TG 18:1_18:2_20:4 | TG 16:0_18:2_22:5	425891852.2	0.34	67.70
40	369.3519	33.56			417293663.9	0.33	68.03
41	524.3731	5.62	LPC 18:0	LPC 18:0	407439989.7	0.32	68.35
42	732.5535	16.54	PC 32:1	PC 16:0_16:1	404726300.7	0.32	68.68
43	946.8839	34.05	TG 57:2		388349257.1	0.31	68.98
44	794.6057	19.40	PC O-38:5	PC P-18:0_20:4	383257292.8	0.30	69.29
45	811.6700	22.84	SM 42:3	SM d18:2_24:1	380034348.2	0.30	69.59
46	808.5859	18.25	PC 38:5	PC 16:0_22:5 | PC 18:0_20:5	376765583.4	0.30	69.89
47	520.3418	3.66	LPC 18:2	LPC 18:2	360108982.6	0.29	70.17
48	944.8689	33.19	TG 57:3		345111803.7	0.27	70.45
49	862.7878	33.62	TG 51:2	TG 16:0_17:1_18:1 | TG 16:0_17:0_18:2 | TG 17:0_17:1_17:1 | TG 16:1_17:0_18:1 | TG 15:0_18:0_18:2 | TG 15:0_18:1_18:1	343523314.2	0.27	70.72
50	930.8515	32.07	TG 56:3		341835611.2	0.27	70.99
51	852.8031	34.99	TG 50:0	TG 16:0_16:0_18:0	338511807.8	0.27	71.26
52	369.3519	34.64			336743340.2	0.27	71.52
53	932.8678	33.05	TG 56:2		334586774.3	0.27	71.79
54	794.7240	31.89	TG 46:1	TG 14:0_16:0_16:1	329204004.9	0.26	72.05
55	836.7719	33.63	TG 49:1	TG 15:0_16:0_18:1 | TG 16:0_16:1_17:0 | TG 16:0_16:0_17:1 | TG 15:0_17:0_17:1 | TG 14:0_17:0_18:1	309666476.2	0.25	72.30
56	896.7719	31.29	TG 54:6	TG 18:1_18:2_18:3	302327445.4	0.24	72.54
57	529.4013	4.39	ISTD	LPC 18:1(d7)	288981049.6	0.23	72.76
58	768.5898	19.17	PC O-36:4	PC O-16:0_20:4	288518206.9	0.23	72.99
59	808.5866	17.53	PC 38:5		284284408.8	0.23	73.22
60	522.3574	4.44	LPC 18:1	LPC 18:1	283057581.6	0.22	73.44
61	962.9129	34.97	TG 58:1	TG 16:0_18:1_24:0 | TG 15:0_18:1_25:0 |	279630353.6	0.22	73.66

				TG 14:0_18:1_26:0 | TG 16:0_16:1_26:0 | TG 18:0_18:1_22:0			
62	766.5756	18.41	PC O-36:5	PC P-16:0_20:4	278458184.4	0.22	73.89
63	896.7735	31.87	TG 54:6	TG 16:0_18:2_20:4	278021208.3	0.22	74.11
64	986.9155	34.21	TG 60:3		268330437	0.21	74.32
65	684.2024	22.01			267769639.6	0.21	74.53
66	796.7402	33.04	TG 46:0	TG 14:0_16:0_16:0	267469554.7	0.21	74.74
67	942.8527	32.22	TG 57:4		266741436.3	0.21	74.95
68	734.5686	20.12	PC 32:0	PC 16:0_16:0	266629129.8	0.21	75.16
69	808.7393	32.49	TG 47:1		265877068.2	0.21	75.38
70	934.8830	34.04	TG 56:1		265644284.5	0.21	75.59
71	780.5531	14.32	PC 46:5	PC 16:0_20:5	258622406.9	0.20	75.79
72	982.8829	32.29	TG 60:5		250373101.1	0.20	75.99
73	888.8036	33.72	TG 53:3	TG 17:0_18:1_18:2 | TG 17:1_18:1_18:1	243569959.7	0.19	76.18
74	758.2219	23.61			237989696.1	0.19	76.37
75	815.7000	26.12	SM 42:1	SM d18:1_24:0	234833774.9	0.19	76.56
76	836.6192	20.79	PC 40:5	PC 18:0_22:5	231959971.1	0.18	76.74
77	988.9285	34.97	TG 60:2		221066162.7	0.18	76.92
78	926.8198	33.65	TG 56:5	TG 16:0_18:1_22:4 | TG 18:1_18:1_20:3	219639557.8	0.17	77.09
79	731.6057	20.18	SM 36:1		216314721.8	0.17	77.26
80	860.7728	32.64	TG 51:3	TG 15:0_18:1_18:2 | 16:0_17:1_18:2 | 16:1_17:1_18:1	213818005.2	0.17	77.43
81	932.8675	34.04	TG 56:2		209565784.2	0.17	77.60
82	785.6537	22.93	SM 40:2		209090570.7	0.17	77.76
83	810.7552	33.60	TG 47:0	TG 13:0_16:0_18:0 | TG 14:0_16:0_17:0 | TG 15:0_16:0_16:0 | TG 14:0_15:0_18:0 | TG 15:0_15:0_17:0 | TG 13:0_17:0_17:0	205322013.1	0.16	77.93
84	984.9002	33.30	TG 60:4		196153786	0.16	78.08
85	918.8524	33.07	TG 55:2		193751291.2	0.15	78.24
86	738.6462	16.44	ISTD	SM d18:1-18:1(d9)	192895907.3	0.15	78.39
87	844.7408	31.00	TG 50:4	TG 16:1_16:1_18:2 | TG 14:0_18:2_18:2	192882538.1	0.15	78.54
88	954.8500	31.32	TG 58:5		192778614.9	0.15	78.69
89	980.2795	27.34			191001484.2	0.15	78.84
90	904.8346	32.04	TG 54:2	TG 18:0_18:1_18:1	190102399.4	0.15	79.00
91	832.2409	25.03			187771621.5	0.15	79.14
92	813.6838	24.67	SM 42:2		185776806.3	0.15	79.29
93	906.2611	26.24			183243277.9	0.15	79.44
94	610.1827	19.42			179760297	0.14	79.58
95	759.6380	22.71	SM 38:1		179262882.4	0.14	79.72
96	930.8528	33.19	TG 56:3		178034096.5	0.14	79.86
97	920.8669	34.05	TG 55:1		174647158.9	0.14	80.00
98	893.7035	32.22	PS 42:0		173962012.3	0.14	80.14
99	972.9002	34.21	TG 59:3		168749788.6	0.13	80.27

100	926.8203	33.93	TG 56:5	TG 18:0_18:1_20:4	165052091.5	0.13	80.40
101	928.8362	32.25	TG 56:4		163045525.1	0.13	80.53
102	916.8359	32.08	TG 55:3	TG 16:1_19:0_20:2 | TG 17:2_19:0_19:1	161564551.5	0.13	80.66
103	906.8504	33.05	TG 54:1		159104103.1	0.13	80.79
104	796.6210	22.23	PC O-38:4	PC O-18:0_20:4	155468296.2	0.12	80.91
105	668.6320	34.63	CE 18:1	CE 18:1	145244059.7	0.12	81.03
106	780.5534	17.44	PC 46:5	PC 16:0_20:5	145107155.7	0.12	81.14
107	834.7556	32.52	TG 49:2	TG 16:0_16:1_17:1 | TG 16:1_16:1_17:0 | TG 15:0_16:0_18:2 | TG 15:0_16:1_18:1 | TG 15:1_16:0_18:1 | TG 14:0_17:1_18:1 | TG 14:0_17:0_18:2 | TG 15:0_17:1_17:1 | TG 15:1_17:0_17:1	145068420.8	0.11	81.26
108	742.5734	19.22	PC O-34-3	PC P-16:0_18:2	144818976.7	0.11	81.37
109	877.7289	32.23	TG 54:7		143703701	0.11	81.48
110	930.8510	34.95	TG 56:3	TG 18:1_18:1_20:1	139775263.7	0.11	81.59
111	895.7198	33.16	MGDG 44:2		137249337.8	0.11	81.70
112	808.5840	21.26	PC 38:5	PC 18:0_20:5	136305539.3	0.11	81.81
113	922.7909	32.41	TG 56:7	TG 16:0_18:1_22:6	135247999.8	0.11	81.92
114	818.7233	30.84	TG 48:3	TG 14:0_16:1_18:2 | TG 14:1_16:1_18:1 | TG 14:1_16:0_18:2	134689473.4	0.11	82.03
115	879.7437	33.19	TG 54:6		132688483.2	0.11	82.13
116	980.8665	31.25	TG 60:6		127066371.9	0.10	82.23
117	772.5851	19.40	PC 35:2	PC 17:0_18:2	126668051.7	0.10	82.33
118	729.5905	16.60	SM 36:2		126340841.7	0.10	82.43
119	782.7236	32.47	TG 45:0	TG 14:0_15:0_16:0	126325687.5	0.10	82.53
120	834.7553	32.94	TG 49:2	TG 16:0_16:1_17:1 | TG 16:1_16:1_17:0 | TG 15:0_16:0_18:2 | TG 15:0_16:1_18:1 | TG 15:1_16:0_18:1 | TG 14:0_17:1_18:1 | TG 14:0_17:0_18:2 | TG 15:0_17:1_17:1 | TG 15:1_17:0_17:1	125450817.4	0.10	82.63
121	804.5528	16.64	PC 38:7		124411496.2	0.10	82.73
122	908.2389	22.15			123284259.9	0.10	82.83
123	760.2011	15.98			122701922.6	0.10	82.92
124	768.7074	31.85	TG 44:0	TG 14:0_14:0_16:0 | TG 12:0_16:0_16:0 | TG 14:0_15:0_15:0	122116178.7	0.10	83.02
125	886.7884	32.80	TG 53:4	TG 17:0_18:2_18:2 | TG 17:1_18:1_18:2	121631234	0.10	83.12
126	801.6831	25.30	SM 41:1	SM d18:1_23:0	118916099.6	0.09	83.21
127	834.2200	19.67			118877421.8	0.09	83.31

128	970.8850	33.25	TG 59:4		117698924.6	0.09	83.40
129	982.2576	23.45			117671196.7	0.09	83.49
130	913.8962	32.97			116331703.4	0.09	83.59
131	686.1800	12.79			116280984.4	0.09	83.68
132	897.7350	34.00	TG 57:9		115965667.2	0.09	83.77
133	756.5526	14.78	PC 34:3	PC 16:0_18:3	114234240.5	0.09	83.86
134	492.4043	41.06	ST 30:2		113918270.3	0.09	83.95
135	974.9130	34.96	TG 59:2	TG 16:1_18:1_25:0 | TG 18:1_18:1_23:0 | TG 17:1_18:1_24:0 | TG 17:0_18:2_24:0 | TG 16:0_18:2_25:0	111426485.8	0.09	84.04
136	701.5571	13.05	SM 34:2	SM d16:1_18:1	111230272.2	0.09	84.13
137	948.8973	34.97	TG 57:1		110690439.6	0.09	84.21
138	836.6173	21.79	PC 40:5	PC 18:0_22:5	109654565.8	0.09	84.30
139	522.5985	20.28			108720410.6	0.09	84.39
140	752.6092	18.29	HexCer 38:3		105999561.3	0.08	84.47
141	814.6297	22.96	PC 40:2	PC 18:0_20:2	105677149	0.08	84.56
142	968.8690	32.26	TG 59:5		105571711.2	0.08	84.64
143	881.7590	34.01	TG 54:5		103799175.8	0.08	84.72
144	928.8361	34.17	TG 56:4		102289378.8	0.08	84.80
145	369.3516	32.87			101402904.9	0.08	84.88
146	612.1609	10.26			101024450.3	0.08	84.96
147	792.7076	30.81	TG 46:2		100396051.9	0.08	85.04

CE, cholesterol ester; Cho, cholesterol; DG, diacylglycerol; HexCer, hexosylceramide; ISTD, internal standard; LPC, lysophosphatidylcholine; MGDG, Monogalactosyldiacylglycerol; PC, phosphatidylcholine; SM, sphingomyelin; ST, sterol; TG, triacylglycerol.

Appendix A.2 Top 85% Abundance within negative Quadrupole-Orbitrap.

Feature #	m/z	Retention time (min)	Brutto	Medio	Abundance	Relative Abundance (%)	Cumulative Abundance (%)
1	802.5564	17.30	PC 34:2	PC 16:0_18:2	366008553	9.05	9.05
2	830.5875	21.19	PC 36:2	PC 18:0_18:2	254319919	6.29	15.34
3	804.5723	20.47	PC 34:1	PC 16:0_18:1	216511965	5.35	20.69
4	826.5566	16.71	PC 36:4	PC 16:0_20:4	184024933	4.55	25.24
5	747.5628	16.02	SM 34:1	SM d18:1_16:0	141772000	3.50	28.74
6	828.5724	18.37	PC 36:3	PC 16:0_20:3	112808812	2.79	31.53
7	854.5876	20.68	PC 38:4	PC 18:0_20:4	99899428	2.47	34.00
8	797.6011	18.30	ISTD	PC 15:0_18:1(d7)	98788092	2.44	36.44
9	540.3288	4.25	LPC 16:0	LPC 16:0	79267382	1.96	38.40
10	339.2306	5.46			77755296	1.92	40.33
11	857.6715	24.34	SM 42:2	SM d18:1_24:1	74752044	1.85	42.17
12	828.5725	17.69	PC 36:3	PC 18:1_18:2	55022944	1.36	43.53
13	856.6037	21.84	PC 38:3	PC 18:0_20:3	53601164	1.33	44.86
14	831.6561	24.46	SM 40:1	SM d18:1_22:0	51390289	1.27	46.13
15	832.6031	22.78	PC 36:1	PC 18:0_18:1	46366715	1.15	47.28
16	859.6872	26.13	SM 42:1	SM d18:1_24:0	40417389	1.00	48.28
17	826.5564	14.79	PC 36:4	PC 18:2_18:2	39689250	0.98	49.26
18	850.5569	15.70	PC 38:6	PC 16:0_22:6	38137933	0.94	50.20
19	568.3598	5.62	LPC 18:0	LPC 18:0	37162223	0.92	51.12
20	852.5726	16.89	PC 38:5	PC 18:1_20:4 | PC 16:0_22:5	35748074	0.88	52.00
21	855.6561	22.85	SM 42:3	SM d18:2_24:1	34448418	0.85	52.85
22	885.5456	16.71	PI 38:4	PI 18:0_20:4	33882409	0.84	53.69
23	857.6717	24.69	PC 42:2	PC 18:1_24:1	30116016	0.74	54.44
24	564.3287	3.65	LPC 18:2	LPC 18:2	30035957	0.74	55.18
25	878.5878	19.69	PC 40:6	PC 18:0_22:6	27344398	0.68	55.85
26	782.6349	16.44	ISTD	SM d18:1-18:1(d9)	22767313	0.56	56.42
27	812.5777	19.17	PC O-36:4	PC O-16:0_20:4	21873667	0.54	56.96
28	775.5945	20.16			21839672	0.54	57.50
29	745.5474	13.07	SM 34:2	SM d18:1_16:1	21546937	0.53	58.03
30	829.6406	22.95	SM 40:2	SM d18:1_22:1	21534428	0.53	58.56
31	845.6712	25.32	SM 41:1		21480782	0.53	59.09
32	854.5892	19.63	PC 38:4	PC 16:0_22:4	21162153	0.52	59.62
33	824.5413	14.36	PC 36:5	PC 16:0_20:5	19649938	0.49	60.10
34	566.3444	4.43	LPC 18:1	LPC 18:1	19165907	0.47	60.58
35	852.5724	18.27	PS 41:4 (H-) | PC 38:5 | PE 41:5		18648274	0.46	61.04
36	573.3883	4.41	ISTD	LPC 18:1(d7)	17954203	0.44	61.48
37	776.5416	16.55	PC 32:1	PC 16:0_16:1	17866344	0.44	61.92
38	898.5751	21.26			17029647	0.42	62.35
39	740.5437	15.43	ISTD	PG 15:0_18:1(d7)	16604818	0.41	62.76
40	838.5936	19.41	PC O-38:5	PC P-18:0_20:4	15908079	0.39	63.15
41	803.6254	22.72	SM 38:1	SM d18:1_20:0	15386526	0.38	63.53

42	778.5557	20.10	PC 32:0	PC 16:0_16:0	15097130	0.37	63.90
43	850.5568	14.25	PE 41:6 | PE 38:6		14671257	0.36	64.27
44	870.5442	17.22	PS 39:4		14610341	0.36	64.63
45	872.5596	20.43	PS 39:3		13619762	0.34	64.96
46	766.5364	21.45	PE 38:4	PE 18:0_20:4	13340091	0.33	65.29
47	609.5556	23.63			12622200	0.31	65.60
48	815.5503	16.01			12608128	0.31	65.92
49	694.6329	28.08	Cer 42:1		12025933	0.30	66.21
50	750.5415	22.42	PE O-38:5	PE P-18:0_20:4	11246555	0.28	66.49
51	800.5416	14.79	PS 37:2 (H-) | PC 34:3 | PE 37:3	PC 16:0_18:3	10614286	0.26	66.75
52	852.5725	17.52	PS 41:4 (H-) | PC 38:5 | PE 41:5	PS 20:4_21:0	10485778	0.26	67.01
53	719.5320	12.64	SM 32:1	SM d18:1_14:0	10283462	0.25	67.27
54	843.6560	23.85	SM 41:2		10262931	0.25	67.52
55	206.9721	0.05			10062756	0.25	67.77
56	581.5241	21.64	FA 36:0		10038984	0.25	68.02
57	773.5785	16.60	SM 36:2		9998132	0.25	68.27
58	786.5625	19.23	PS O-37:2 (H-) | PC O-34:3 | PE O-37:3	PC P-18:1_16:1	9887933	0.24	68.51
59	810.5623	18.45	PC O-36:5	PC P-16:0_20:4	9821037	0.24	68.75
60	925.6582	24.33			9771942	0.24	68.99
61	740.5435	15.68	ISTD	PG 15:0_18:1(d7)	9572948	0.24	69.23
62	684.6042	28.09			9453322	0.23	69.46
63	197.8070	1.37			9332289	0.23	69.70
64	894.5439	16.68			9071296	0.22	69.92
65	828.5587	14.50	ISTD	PI 15:0_18:1(d7)	8993562	0.22	70.14
66	800.5415	14.12	PS 37:2 (H-) | PC 34:3 | PE 37:3		8864637	0.22	70.36
67	861.5459	17.22	PI 32:2	PI 18:0_18:2	8844451	0.22	70.58
68	742.5367	21.85	PE 32:2	PE 18:0_18:2	8611787	0.21	70.79
69	840.6088	22.24	PC O-38:4	PC O-18:0_20:4	8502967	0.21	71.00
70	854.5880	18.78	PS 41:3 (H-) | PC 38:4 | PE 41:4	PC 16:0_22:4	8298796	0.21	71.21
71	896.5587	18.43	PS 41:5		8044617	0.20	71.41
72	747.5631	15.34	SM 34:1		7579250	0.19	71.59
73	195.8103	1.37			7344908	0.18	71.78
74	599.5266	23.63			7167296	0.18	71.95
75	829.6406	22.65	SM 40:2	SM d18:1_22:1	7113324	0.18	72.13
76	722.5106	19.66	PE O-36:5	PE P-16:0_20:4	6984841	0.17	72.30
77	922.5743	20.72			6845797	0.17	72.47
78	927.6734	26.13			6840436	0.17	72.64
79	924.5900	21.84			6778942	0.17	72.81

80	816.5730	19.39	PS 38:1(H-) | PC 35:2 | PE 38:2		6662364	0.16	72.97
81	880.6034	20.80	PS 43:4 (H-) | PC 40:5 | PE 43:3		6652632	0.16	73.14
82	748.5258	19.98	PE O-38:6		6562440	0.16	73.30
83	899.6428	24.46			6454007	0.16	73.46
84	733.5477	14.22	SM 33:1		6317790	0.16	73.62
85	865.5882	18.31	PI 36:0		6269811	0.16	73.77
86	588.3288	3.54	LPC 20:4	LPC 20:4	6239644	0.15	73.92
87	882.6190	22.38	PS 43:3 (H-) | PC 40:4 | PE 43:4		6111985	0.15	74.08
88	817.6408	23.63	SM 39:1		5906234	0.15	74.22
89	640.6229	22.70			5792111	0.14	74.36
90	174.9555	43.06			5697701	0.14	74.51
91	857.5149	13.33	PI 36:4		5646683	0.14	74.65
92	170.8328	42.55			5344489	0.13	74.78
93	833.5149	13.75	PI 34:2		5288457	0.13	74.91
94	858.6164	22.98	PS 41:1(H-) | PC 38:2 | PE 41:2		5269454	0.13	75.04
95	790.5936	22.13	PS O-37:0 | PC O-34:1 | PE O-37:1		5006558	0.12	75.16
96	465.3029	7.24			4998560	0.12	75.29
97	788.5782	19.89	PS O-37:0 | PC O-34:2 | PE O-37:2		4892830	0.12	75.41
98	571.4955	21.65			4873477	0.12	75.53
99	792.5283	17.22			4690690	0.12	75.64
100	835.5309	16.40	PI 34:1		4679255	0.12	75.76
101	925.6579	24.69			4613874	0.11	75.87
102	880.6029	21.80	Hex2Cer 32:0		4555796	0.11	75.99
103	199.8043	1.37			4550955	0.11	76.10
104	900.5894	22.77	PS 41:3		4533875	0.11	76.21
105	820.5591	21.12			4527290	0.11	76.32
106	682.5886	26.36			4508554	0.11	76.43
107	896.5594	17.69			4349514	0.11	76.54
108	923.6425	22.86			4322307	0.11	76.65
109	256.9545	43.74			4286245	0.11	76.75
110	843.6562	23.52	SM 41:2		4252667	0.11	76.86
111	637.5868	25.41			4221259	0.10	76.96
112	774.5259	13.75	PS 35:1(H-) | PC 32:2 | PE 35:2		4176458	0.10	77.07
113	794.5444	20.49			4175209	0.10	77.17
114	666.6021	26.48	Cer 40:1	Cer d18:1_22:0	4154303	0.10	77.27
115	887.5609	18.26	PI 38:3		4102815	0.10	77.37
116	749.5791	17.51	SM 34:0		4092610	0.10	77.48

117	711.6230	28.09			4068061	0.10	77.58
118	906.6122	16.17	Hex2Cer 34:1		4067706	0.10	77.68
119	836.5777	18.78			4039286	0.10	77.78
120	172.8300	42.54			4005162	0.10	77.88
121	801.6099	20.68	SM 38:2		3986403	0.10	77.97
122	800.5420	15.39	PS 37:2 (H-) | PC 34:3 | PE 37:3		3935322	0.10	78.07
123	816.5732	18.78	PS 38:1 (H-) | PC 35:2 | PE 38:2		3930945	0.10	78.17
124	692.6174	26.37	Cer 42:1	Cer d18:1_24:1	3914826	0.10	78.26
125	796.5947	18.32	HexCer 38:3		3716721	0.09	78.36
126	656.5733	26.49			3699869	0.09	78.45
127	856.6847	26.59	HexCer 43:1 (H-) | HexCer 42:1 (FA-)		3681382	0.09	78.54
128	178.9773	44.99			3666499	0.09	78.63
129	709.5496	19.37	ISTD	PE 15:0_18:1(d7)	3595777	0.09	78.72
130	818.5889	21.88	PS 38:0 (H-) | PC 35:1 | PE 38:1		3581442	0.09	78.81
131	838.5933	21.89	PC O-38:5		3563556	0.09	78.90
132	680.6174	27.29	Cer 41:1	Cer d18:1_23:0	3549211	0.09	78.98
133	626.5458	23.63			3540094	0.09	79.07
134	737.5347	15.98			3505609	0.09	79.16
135	863.5620	20.24	PI 36:1		3466373	0.09	79.24
136	608.3161	4.25			3438167	0.09	79.33
137	670.5886	27.30			3387641	0.08	79.41
138	178.9773	0.07			3368587	0.08	79.50
139	913.6581	25.31			3360878	0.08	79.58
140	840.5732	18.73	PS 40:3 (H-) | PC 37:4 | PE 40:4		3340463	0.08	79.66
141	316.9470	33.58			3295248	0.08	79.74
142	918.5435	15.70			3268256	0.08	79.82
143	847.6435	24.32	PG 41:0	PG 15:0_26:0	3243306	0.08	79.90
144	180.9730	42.30			3227790	0.08	79.98
145	806.5863	22.61			3175654	0.08	80.06
146	840.5280	15.67			3161729	0.08	80.14
147	894.5436	14.80			3123121	0.08	80.22
148	538.3140	3.43	LPC 16:1	LPC 16:1	3096885	0.08	80.29
149	888.5339	20.43			3077260	0.08	80.37
150	593.4761	8.94			3054335	0.08	80.45
151	726.5418	22.76	PE O-36:3	PE P-18:0_18:2	2999737	0.07	80.52
152	205.8392	1.40			2872197	0.07	80.59
153	682.5882	26.69			2865941	0.07	80.66
154	816.5283	16.66			2865856	0.07	80.73
155	774.5416	21.89	PE O-40:2		2855807	0.07	80.80

156	828.6535	24.98	HexCer 40:1		2853357	0.07	80.87
157	723.5324	23.63			2847867	0.07	80.94
158	180.9730	0.06			2777858	0.07	81.01
159	814.5936	22.26	PS 0-39:2 (H-) | PC O-36:3		2772011	0.07	81.08
160	871.6866	24.89	SM 43:2		2762149	0.07	81.15
161	808.6099	28.09			2750342	0.07	81.22
162	692.6174	26.68	Cer 42:2	Cer d18:1_24:1 1	2739951	0.07	81.28
163	750.5215	16.06			2711652	0.07	81.35
164	627.5579	25.41			2697972	0.07	81.42
165	915.6231	24.45			2691193	0.07	81.49
166	897.6275	22.95			2689369	0.07	81.55
167	838.5935	20.03	PC O-38:5	PC P-18:0_20:4	2686118	0.07	81.62
168	883.5297	14.05			2674889	0.07	81.68
169	206.9722	15.67			2640301	0.07	81.75
170	178.9773	1.78			2623442	0.06	81.81
171	946.5754	19.70			2589632	0.06	81.88
172	920.5594	16.97			2548669	0.06	81.94
173	854.6692	24.88	HexCer 42:2		2510956	0.06	82.00
174	636.3477	5.63			2474962	0.06	82.06
175	883.5375	16.01	PI 38:5	PI 18:2_20:3	2451921	0.06	82.13
176	362.9398	32.24			2395210	0.06	82.18
177	687.5293	16.02	PA O-36:1		2329919	0.06	82.24
178	843.5824	20.16			2295391	0.06	82.30
179	738.5054	17.73	PE 36:4 | PE O-36:5	PE 18:2_18:2	2272790	0.06	82.35
180	761.5790	18.06	PE-Cer 38:1 | SM 35:1	SM d18:1_17:0	2256081	0.06	82.41
181	598.5144	21.63			2235357	0.06	82.47
182	940.5471	20.36			2217507	0.05	82.52
183	316.9470	34.12			2210288	0.05	82.58
184	866.6240	22.24	PC O-40:5	PC O-20:1_20:4	2206099	0.05	82.63
185	831.5248	16.01			2202440	0.05	82.68
186	294.9524	32.24			2193194	0.05	82.74
187	316.9470	34.64			2184470	0.05	82.79
188	813.5343	13.07			2148900	0.05	82.85
189	256.9544	0.23			2142830	0.05	82.90
190	134.8651	44.99			2116117	0.05	82.95
191	590.3446	3.96	LPC 20:3	LPC 20:3	2103824	0.05	83.00
192	583.2538	5.76			2090051	0.05	83.05
193	215.8679	42.48			2084496	0.05	83.11
194	132.8676	44.93			2067976	0.05	83.16
195	764.5783	21.95	PC O-32:0 | PE O-35:0	PC O-16:0_16:0	2057089	0.05	83.21
196	846.6560	26.58	PS O-41:0 (H-) | PC		2040796	0.05	83.26

			O-38:1 | PE O-41:1				
197	844.5592	20.73			2019300	0.05	83.31
198	993.6460	24.35	PI 46:6 (H-)		2012318	0.05	83.36
199	850.6229	16.44	PS O-38:0		1988885	0.05	83.41
200	914.5475	21.27			1987112	0.05	83.46
201	922.6854	25.49	PC O-44:5		1977476	0.05	83.51
202	790.5580	18.46	PS 36:0 | PC 33:1 | PE 36:1		1951256	0.05	83.55
203	767.5547	16.17	PA 41:3 (H-)		1949312	0.05	83.60
204	485.3368	4.57	ISTD	LPE 18:1(d7)	1927487	0.05	83.65
205	746.5105	18.46	PE O-38:7	PE P-16:0_22:6	1921406	0.05	83.70
206	207.8362	1.40			1917135	0.05	83.74
207	632.3167	3.65			1913033	0.05	83.79
208	941.6327	24.34			1909054	0.05	83.84
209	966.5631	21.32			1894198	0.05	83.89
210	846.5749	21.83			1887887	0.05	83.93
211	818.5441	17.70			1884915	0.05	83.98
212	894.6552	23.87	PC O-42:5		1864675	0.05	84.03
213	995.6615	26.13	PI 46:5	PI 20:5_26:0	1863574	0.05	84.07
214	859.5303	14.58	PI 36:3	PI 18:1_18:2	1808608	0.04	84.12
215	248.9597	33.58			1795399	0.04	84.16
216	695.5018	21.63			1787469	0.04	84.20
217	814.5927	20.10	PS O-39:2 (H-) | PC O-36:3		1782777	0.04	84.25
218	849.6582	26.14			1780653	0.04	84.29
219	459.2891	7.00			1762815	0.04	84.34
220	762.5052	16.62	PE 38:6 | PE O-38:7;O		1759112	0.04	84.38
221	911.6428	23.85			1732994	0.04	84.42
222	951.2302	16.55			1716368	0.04	84.46
223	876.5736	16.03	PS 43:6 (H-) | PC 40:7		1710441	0.04	84.51
224	818.5435	18.42			1693500	0.04	84.55
225	821.6275	24.46			1661719	0.04	84.59
226	808.5304	15.43	PS 34:0		1655086	0.04	84.63
227	697.6072	27.31			1640858	0.04	84.67
228	876.5725	16.48	PS 43:6 (H-) | PC 40:7	PC 18:1_22:6	1639378	0.04	84.71
229	816.6091	22.54	PS O-39:1 (H-) | PC O-36:2	PC P-18:1_18:0	1630687	0.04	84.75
230	938.5314	17.48			1600740	0.04	84.79
231	871.6121	22.70			1592623	0.04	84.83
232	847.6428	24.69	PG 41:0 | PA 43:0	PG 17:0_24:0	1586337	0.04	84.87
233	787.5734	18.25			1585844	0.04	84.91

234	859.5303	14.06	PI 36:3	PI 18:1_18:2	1582238	0.04	84.95
235	992.5777	21.81			1528835	0.04	84.99
236	788.5417	15.43	PS 36:1 (H-) | PC 33:2 | PE 36:2		1502934	0.04	85.02

Cer, ceramide; FFA, free fatty acyl; HexCer, hexosylceramide; ISTD, internal standard; LPA, lysophosphatidic acid; LPG, lysophosphatidylglycerol; LPC lysophosphatidylcholine; PA, phosphatidic acid; PC, phosphatidylcholine; PE, phosphatidylethanolamine; PG, phosphatidylglycerol; PI, phosphatidylinositol; PS, phosphatidylserine; SM, sphingomyelin.

Appendix A.3. Top 85% Abundance within positive Quadrupole-Time-of-Flight.

Feature #	m/z	Retention time (min)	Brutto	Medio	Abundance	Relative Abundance (%)	Cumulative Abundance (%)
1	758.5757	15.47	PC 34:2	PC 16:0_18:2	127506786.8	4.57	4.57
2	550.6285	21.43			110954605.1	3.98	8.55
3	786.6028	19.25	PC 36:2	PC 18:0_18:2	89453753.19	3.21	11.76
4	760.5868	18.34	PC 34:1	PC 16:0_18:1	75030783.54	2.69	14.45
5	782.5712	14.92	PC 36:4	PC 16:0_20:4	73871253.98	2.65	17.10
6	153.1384	41.56			73397097.98	2.63	19.73
7	874.7896	30.77	TG 52:3	TG 16:0_18:1_18:2	69881397.27	2.51	22.24
8	876.8053	31.51	TG 52:2	TG 16:0_18:1_18:1	65417982.19	2.35	24.59
9	810.6013	18.59	PC 38:4	PC 18:0_20:4	48620066.52	1.74	26.33
10	958.8792	30.77	TG 58:3		39664607.15	1.42	27.75
11	784.5850	16.39	PC 36:3	PC 16:0_20:3	38221540.82	1.37	29.12
12	753.6139	16.34	ISTD	PC 15:0_18:1(d7)	37850386.46	1.36	30.48
13	960.8945	31.55	TG 58:2		35136890.97	1.26	31.74
14	806.5702	14.07	PC 38:6	PC 16:0_22:6	35102812.82	1.26	33.00
15	369.3546	31.13			34337064.94	1.23	34.23
16	848.7698	30.65	TG 50:2	TG 16:0_16:1_18:1 | TG 14:0_18:1_18:1	32424612.84	1.16	35.39
17	900.8006	30.77	TG 54:4	TG 18:1_18:1_18:2 | TG 18:0_18:2_18:2 | TG 16:0_18:1_20:3	31380002.92	1.13	36.52
18	902.8165	31.55	TG 54:3	TG 18:0_18:1_18:2	28136963.52	1.01	37.53
19	850.7859	31.55	TG 50:1	TG 16:0_16:0_18:1	27707584.55	0.99	38.52
20	149.0229	32.08			25192101.93	0.90	39.43
21	872.7697	29.97	TG 52:4	TG 16:0_18:2_18:2 | TG 16:1_18:1_18:2	23432840.86	0.84	40.27
22	956.8631	29.92	TG 58:4		22510977.99	0.81	41.07
23	369.3524	32.08			21479535.62	0.77	41.84
24	666.6190	31.13	CE 18:2	CE 18:2	21050589.73	0.75	42.60
25	703.5750	14.36	SM 34:1	SM d18:1_16:0	19572398.1	0.70	43.30
26	944.8629	30.77	TG 57:3		19418078.14	0.70	44.00
27	142.1588	36.91			19399246.07	0.70	44.69
28	684.2027	20.50			19196629.19	0.69	45.38
29	784.5845	15.78	PC 36:3	PC 18:1_18:2	17727488.24	0.64	46.02
30	758.2220	22.36			17577245.84	0.63	46.65
31	898.7845	29.97	TG 54:5	TG 18:1_18:2_18:2 | TG 16:0_18:2_20:3 | TG 16:0_18:1_20:4 | TG 16:0_18:3_20:2	17542853.29	0.63	47.28
32	496.3410	3.84	LPC 16:0	LPC 16:0	17488556.1	0.63	47.90
33	946.8789	31.55	TG 57:2		17256270.18	0.62	48.52
34	932.8618	30.65	TG 56:2		16814904.36	0.60	49.13
35	699.5954	26.48	DG 42:5		15766523.6	0.57	49.69
36	800.7142	26.48			15578798.89	0.56	50.25
37	808.5844	15.08	PC 38:5	PC 16:0_22:5	14855821.28	0.53	50.78
38	788.6156	21.55	PC 36:1	PC 18:0_18:1	14081178.21	0.51	51.29
39	156.1741	36.91			13913377.26	0.50	51.79

40	934.8773	31.55	TG 56:1		13317999.58	0.48	52.26
41	832.2403	23.76			12963588.35	0.46	52.73
42	170.1897	39.17			12802118.89	0.46	53.19
43	812.6158	20.26	PC 38:3	PC 18:0_20:3	12610067.84	0.45	53.64
44	786.6989	26.48			12479589.6	0.45	54.09
45	984.8945	30.84	TG 60:4		12276802.82	0.44	54.53
46	369.3516	30.54			12207201.47	0.44	54.97
47	986.9107	31.62	TG 60:3		12170477.95	0.44	55.40
48	168.1733	40.86			12089417.96	0.43	55.84
49	982.8775	29.97	TG 60:5		11856775.04	0.43	56.26
50	942.8470	29.92	TG 57:4		11543961.09	0.41	56.68
51	565.5664	22.36			11509056.31	0.41	57.09
52	980.2779	25.85			11099602.5	0.40	57.49
53	906.2589	24.87			11055809.43	0.40	57.88
54	930.8460	29.82	TG 56:3		10968958.2	0.39	58.28
55	524.3711	5.01	LPC 18:0	LPC 18:0	10121984.88	0.36	58.64
56	930.8467	30.77	TG 56:3	TG 16:0_20:1_20:2	10111959.72	0.36	59.00
57	610.1844	17.36			10060910.51	0.36	59.36
58	813.6842	23.06	SM 42:2	SM d16:1_26:11	10039414.29	0.36	59.72
59	760.2012	14.18			9831319.641	0.35	60.08
60	846.7538	29.82	TG 50:3	TG 16:0_16:1_18:2 | TG 14:0_18:1_18:2	9590274.094	0.34	60.42
61	834.2192	17.47			9520623.808	0.34	60.76
62	829.7976	30.60	ISTD	TG 15:0_18:1 (d7)_15:0	9487143.221	0.34	61.10
63	879.7407	30.77	TG 54:6		9115080.777	0.33	61.43
64	750.5575	23.17			8953888.834	0.32	61.75
65	686.1818	11.44			8932320.946	0.32	62.07
66	908.2377	20.79			8907824.33	0.32	62.39
67	932.8629	31.55	TG 56:2		8825750.748	0.32	62.71
68	918.8460	30.65	TG 55:2		8194536.494	0.29	63.00
69	881.7565	31.55	TG 54:5	TG 16:0_18:1_20:4	8116778.663	0.29	63.29
70	972.8927	31.62	TG 59:3		8022782.577	0.29	63.58
71	822.7542	30.65	TG 48:1	TG 14:0_16:0_18:1	7941839.812	0.28	63.86
72	982.2570	22.31			7850656.339	0.28	64.14
73	172.2054	37.60			7710083.965	0.28	64.42
74	182.1883	38.19			7572282.669	0.27	64.69
75	808.5838	16.29	PC 38:5	PC 16:0_22:5	7499283.236	0.27	64.96
76	537.5346	19.92			7141686.335	0.26	65.22
77	877.7251	29.92	TG 54:7	TG 16:0_18:2_20:5	6849636.26	0.25	65.46
78	962.9094	32.37	TG 58:1		6844304.031	0.25	65.71
79	920.8616	31.55	TG 55:1		6741166.831	0.24	65.95
80	924.8004	30.49	TG 56:6	TG 18:1_18:1_20:4 | TG 16:0_18:1_22:5	6611919.515	0.24	66.19
81	906.8450	31.55	TG 54:1		6598487.211	0.24	66.42
82	968.8618	29.97	TG 59:5		6309918.8	0.23	66.65
83	690.6184	30.54	CE 20:4	CE 20:4	6293341.985	0.23	66.88
84	184.2052	39.70			6122422.134	0.22	67.10
85	954.8469	29.11	TG 58:5		6035918.272	0.22	67.31
86	671.5736	31.13	CE 20:5	CE 20:5	5979755.626	0.21	67.53

87	520.3399	3.31	LPC 18:2	LPC 18:2	5897280.675	0.21	67.74
88	928.8310	29.92	TG 56:4		5885092.193	0.21	67.95
89	878.8165	32.37	TG 52:1	TG 16:0_18:0_18:1	5872069.648	0.21	68.16
90	916.8296	29.82	TG 55:3		5792334.698	0.21	68.37
91	732.5535	14.76	PC 32:1	PC 16:0_16:1	5747347.049	0.21	68.57
92	988.9262	32.32	TG 60:2		5530576.829	0.20	68.77
93	980.8629	29.17	TG 60:6		5428527.271	0.19	68.97
94	228.1047	38.54			5422677.389	0.19	69.16
95	834.6001	17.53	PC 40:6	PC 18:2_22:4	5402057.982	0.19	69.36
96	904.8319	32.37	TG 54:2	TG 18:0_18:1_18:1 | TG 16:0_18:1_20:1	5357773.947	0.19	69.55
97	577.5193	31.55			5261671.515	0.19	69.74
98	787.6679	23.17	SM 40:1		5173731.304	0.19	69.92
99	140.1416	37.03			5073123.653	0.18	70.10
100	906.8452	30.65	TG 54:1		5048278.397	0.18	70.28
101	824.7695	31.55	TG 48:0		5028901.41	0.18	70.46
102	916.8296	30.77	TG 55:3		5010153.432	0.18	70.64
103	918.8450	31.55	TG 55:2		4935477.75	0.18	70.82
104	209.1639	40.22			4863108.233	0.17	71.00
105	904.8303	29.75	TG 54:2		4814136.483	0.17	71.17
106	913.8910	30.60	TG 57:1		4771532.19	0.17	71.34
107	780.5512	15.47	PC 36:5	PC 16:0_20:5	4709465.163	0.17	71.51
108	970.8783	30.84	TG 59:4		4691656.231	0.17	71.68
109	200.2001	41.50			4612123.429	0.17	71.84
110	905.7555	30.89	TG 56:7	TG 18:1_18:2_20:4	4488372.558	0.16	72.00
111	740.6749	24.75	TG 42:0	TG 16:0_16:0_10:0	4485211.629	0.16	72.16
112	926.8153	31.13	TG 56:5	TG 16:0_18:1_22:4	4430462.372	0.16	72.32
113	207.1843	41.56			4412284.224	0.16	72.48
114	768.5894	17.13	PC O-36:4	PC O-16:0_20:4	4376712.919	0.16	72.64
115	811.6676	21.60	SM 42:3	SM d22:0_20:3	4356193.386	0.16	72.79
116	612.1635	9.15			4338743.247	0.16	72.95
117	794.6042	17.30	PC O-38:5	PC P-18:0_20:4	4252719.04	0.15	73.10
118	904.8296	30.65	TG 54:2		4214046.852	0.15	73.25
119	522.3554	3.95	LPC 18:1	LPC 18:1	4190468.631	0.15	73.40
120	529.3992	3.95	ISTD	LPC 18:1 (d7)	4186977.075	0.15	73.55
121	171.1390	1.57			4133039.888	0.15	73.70
122	223.2155	41.56			3907966.816	0.14	73.84
123	808.5819	19.25	PC 38:5	PC 18:0_20:5	3905774.911	0.14	73.98
124	922.7841	29.63	TG 56:7	TG 18:1_18:2_20:4 | TG 16:0_18:2_22:5	3881750.836	0.14	74.12
125	903.7403	29.97	TG 56:8		3848721.698	0.14	74.26
126	948.8935	32.32	TG 57:1		3832324.986	0.14	74.40
127	223.1799	36.79			3788641.472	0.14	74.53
128	870.7536	29.17	TG 52:5	TG 16:1_18:2_18:2	3722140.994	0.13	74.67
129	603.5347	31.55			3721445.107	0.13	74.80
130	734.5691	18.00	PC 32:0	PC 16:0_16:0	3708470.942	0.13	74.93
131	853.7251	30.65			3698834.6	0.13	75.07
132	785.6526	21.72	SM 40:2		3648977.203	0.13	75.20
133	766.5736	16.43	PC O-36:5	PC P-16:0_20:4	3606385.853	0.13	75.33

134	820.7379	29.75	TG 48:2	TG 16:0_16:1_16:1 | TG 14:0_16:1_18:1 | TG 14:1_16:0_18:1 | TG 12:0_18:1_18:1 | TG 14:0_16:0_18:2	3587233.993	0.13	75.45
135	890.8155	31.96	TG 53:2	TG 17:0_18:1_18:1 | TG 16:0_18:1_19:1	3552116.153	0.13	75.58
136	768.7060	26.14	TG 44:0	TG 10:0_16:0_18:0	3522945.774	0.13	75.71
137	780.5530	12.81	PC 36:5	PC 16:0_20:5	3508337.482	0.13	75.83
138	928.8305	28.93	TG 56:4		3506543.287	0.13	75.96
139	815.6994	24.75	SM 42:1	SM d18:1_24:0	3376285.689	0.12	76.08
140	914.8125	29.92	TG 55:4		3376029.378	0.12	76.20
141	184.0730	15.47			3358084.43	0.12	76.32
142	601.5190	30.77			3351652.921	0.12	76.44
143	758.9519	15.47			3304808.545	0.12	76.56
144	936.8929	32.37	TG 56:0		3264611.024	0.12	76.68
145	940.8305	29.17	TG 57:5		3244256.448	0.12	76.79
146	782.5672	18.34	PC 36:4	PC 16:0_20:4	3185227.613	0.11	76.91
147	756.5532	13.22	PC 34:3	PC 16:0_18:3	3181602.178	0.11	77.02
148	896.7692	29.17	TG 54:6	TG 18:1_18:2_18:3	3175069.935	0.11	77.14
149	279.1586	32.08			3172162.371	0.11	77.25
150	907.7722	31.67	TG 56:6		3129642.58	0.11	77.36
151	237.1955	40.80			3097980.332	0.11	77.47
152	956.8623	30.84	TG 58:4		3078418.484	0.11	77.58
153	215.1745	32.02			3057769.406	0.11	77.69
154	279.1585	31.07			3056409.636	0.11	77.80
155	954.8467	29.97	TG 58:5		2996943.116	0.11	77.91
156	804.5505	14.92	PC 38:7	PC 16:0_22:7	2932602.194	0.11	78.02
157	862.7847	31.13	TG 51:2	TG 16:0_17:1_18:1	2927893.895	0.11	78.12
158	758.8708	15.47			2916494.915	0.10	78.23
159	851.7090	29.82	TG 52:6	TG 16:0_18:3_18:3	2776383.451	0.10	78.33
160	149.0595	0.99			2748810.356	0.10	78.42
161	738.6464	14.70	ISTD	SM d18:1_18:1(d9)	2687844.307	0.10	78.52
162	536.1655	14.07			2672399.639	0.10	78.62
163	731.6055	18.06	SM 36:1	SM d16:1_20:0	2650865.74	0.10	78.71
164	668.6340	32.08	CE 18:1	CE 18:1	2649482.504	0.10	78.81
165	892.8296	30.65	TG 53:1		2604859.327	0.09	78.90
166	899.8755	30.60			2572635.234	0.09	78.99
167	974.9100	32.32	TG 59:2		2549204.498	0.09	79.08
168	575.5034	30.77			2502279.772	0.09	79.17
169	205.1686	40.92			2473344.483	0.09	79.26
170	577.5180	30.77			2434588.967	0.09	79.35
171	836.6152	18.69	PC 40:5	PC 18:0_22:5	2357757.357	0.08	79.43
172	774.2523	18.00			2323119.652	0.08	79.52
173	184.0728	19.25			2317329.397	0.08	79.60
174	966.8467	29.17	TG 59:6		2308683.816	0.08	79.68
175	888.7999	31.19	TG 53:3	TG 17:0_18:1_18:2	2307435.305	0.08	79.77
176	759.3409	15.47			2290908.754	0.08	79.85
177	261.1097	1.39			2288696.876	0.08	79.93
178	855.7407	31.55	TG 50:1		2275821.672	0.08	80.01

179	890.8138	29.75	TG 53:2		2266107.497	0.08	80.09
180	896.7688	29.63	TG 54:6	TG 16:0_18:2_20:4 | 18:1_18:2_18:3	2266052.397	0.08	80.17
181	848.2708	21.08			2260754.696	0.08	80.26
182	149.0593	1.65			2225495.915	0.08	80.34
183	890.8131	30.65	TG 53:2		2199113.875	0.08	80.41
184	796.7379	30.65	TG 46:0		2177664.384	0.08	80.49
185	852.8002	32.37	TG 50:0	TG 16:0_16:0_18:0	2152266.186	0.08	80.57
186	700.2342	14.65			2149848.047	0.08	80.65
187	875.7087	29.17	TG 52:5		2136867.85	0.08	80.72
188	964.9251	33.12	TG 58:0		2103544.247	0.08	80.80
189	695.5734	30.54	CE 20:4		2098054.503	0.08	80.87
190	894.8447	31.55	TG 53:0		2095874.783	0.08	80.95
191	902.8150	29.82	TG 54:3		2079807.758	0.07	81.02
192	759.6364	21.49	SM 38:1	SM d18:1_20:0	2073737.439	0.07	81.10
193	922.2899	22.54			2072164.046	0.07	81.17
194	712.6449	24.75	TG 40:0		2047086.148	0.07	81.25
195	796.6203	20.85	PC O-38:4	PC O-18:0_20:4	2015266.849	0.07	81.32
196	901.7246	29.63	TG 56:9		1997450.624	0.07	81.39
197	750.5521	18.75			1980627.893	0.07	81.46
198	801.6841	23.99	SM 41:1		1979141.605	0.07	81.53
199	834.7530	30.60	TG 49:2		1946015.125	0.07	81.60
200	219.1838	41.56			1943475	0.07	81.67
201	279.1584	7.01			1936187.323	0.07	81.74
202	290.1384	1.47			1926472.293	0.07	81.81
203	774.7117	30.54			1924750.218	0.07	81.88
204	742.5737	17.13	PC O-34:3	PC P-16:0_18:2	1921166.571	0.07	81.95
205	796.7365	27.42			1912013.453	0.07	82.02
206	832.5821	18.64	PC 40:7	PC 20:3_20:4	1902505.839	0.07	82.08
207	140.1416	40.74			1867199.325	0.07	82.15
208	666.6858	22.36			1848228.79	0.07	82.22
209	203.1516	37.96			1832457.305	0.07	82.28
210	832.5835	14.18	PC 40:7	PC 18:1_22:6	1822490.282	0.07	82.35
211	952.8310	29.17	TG 58:6		1808425.561	0.06	82.41
212	712.6435	23.29			1763774.33	0.06	82.48
213	926.8146	29.17	TG 56:5		1757069.398	0.06	82.54
214	844.7375	28.93	TG 50:4	TG 18:2_18:2_14:0 | 16:1_16:1_18:2	1748116.846	0.06	82.60
215	940.8278	29.97	TG 57:5		1747353.485	0.06	82.67
216	684.6140	23.29			1733860.754	0.06	82.73
217	864.7999	31.96	TG 51:1	TG 16:0_17:0_18:1	1718050.285	0.06	82.79
218	701.5585	11.73	SM 34:2		1713453.018	0.06	82.85
219	934.8780	32.37	TG 56:1		1712836.442	0.06	82.91
220	215.1745	30.54			1707371.606	0.06	82.97
221	914.8131	28.93	TG 55:4	TG 18:1_18:2_19:1	1701531.462	0.06	83.03
222	522.5966	18.18			1697731.56	0.06	83.10
223	878.8149	29.69	TG 52:1	TG 16:1_18:0_18:0 | 16:0_18:0_18:1 | TG 16:0_16:1_20:0	1676662.679	0.06	83.16
224	652.6704	22.36			1675974.362	0.06	83.22

225	772.6834	26.48			1675284.166	0.06	83.28
226	893.6996	29.92			1663391.228	0.06	83.34
227	684.6138	26.14			1656249.219	0.06	83.39
228	883.7717	32.37	TG 52:1		1648693.487	0.06	83.45
229	214.9170	42.14			1646324.848	0.06	83.51
230	729.5897	14.82	SM 36:2		1645413.759	0.06	83.57
231	909.7890	32.37	TG 54:2		1627136.582	0.06	83.63
232	942.8439	30.89	TG 57:4		1623941.959	0.06	83.69
233	626.2151	11.73			1613637.546	0.06	83.75
234	895.7157	30.81			1601061.068	0.06	83.80
235	656.5823	24.75			1551877.684	0.06	83.86
236	184.0729	18.34			1541741.921	0.06	83.91
237	369.3512	14.13	Cho	Cholesterol	1526824.974	0.05	83.97
238	772.5844	17.30	PC 35:2	PC 17:0_18:2	1517503.349	0.05	84.02
239	270.2785	3.48			1514762.594	0.05	84.08
240	978.8466	28.30	TG 60:7		1513848.662	0.05	84.13
241	752.6064	16.34			1509704.263	0.05	84.19
242	150.0262	31.07			1509002.053	0.05	84.24
243	888.7962	29.82			1500446.009	0.05	84.29
244	922.8768	32.37	TG 55:0		1495180.264	0.05	84.35
245	996.3088	23.64			1493071.511	0.05	84.40
246	994.8781	30.43	TG 61:6		1477767.776	0.05	84.45
247	217.1677	40.34			1475286.861	0.05	84.51
248	880.8295	30.65	TG 52:0		1469787.007	0.05	84.56
249	673.5889	32.08	CE 18:1	CE 18:1	1463373.999	0.05	84.61
250	788.8935	29.35			1460976.284	0.05	84.67
251	799.6690	22.59	SM 41:2		1450789.11	0.05	84.72
252	281.0509	9.15			1439508.815	0.05	84.77
253	186.2212	41.68			1437607.758	0.05	84.82
254	814.6342	21.72	PC 38:2	PC 18:0_20:2	1418190.393	0.05	84.87
255	880.8313	33.12	TG 52:0	TG 16:0_18:0_18:0	1417946.098	0.05	84.92
256	399.2498	2.59			1412725.051	0.05	84.97
257	775.5941	16.34			1406618.843	0.05	85.02

CE, cholesterol ester; Cho, cholesterol; DG, diacylglycerol; HexCer, hexosylceramide; ISTD, internal standard; LPC, lysophosphatidylcholine; MGDG, Monogalactosyldiacylglycerol; PC, phosphatidylcholine; SM, sphingomyelin; ST, sterol; TG, triacylglycerol.

Appendix A.4. Top 85% Abundance within negative Quadrupole-Time-of-Flight.

Feature #	m/z	Retention time (min)	Brutto	Medio	Abundance	Relative Abundance (%)	Cumulative Abundance (%)
1	206.9714	0.03			21342165.92	7.17	7.17
2	206.9715	0.96			13694968.9	4.60	11.76
3	802.5602	15.46	PC 34:2	PC 16:0_18:2	12351106.59	4.15	15.91
4	830.5915	19.35	PC 36:2	PC 18:0_18:2	10760738.6	3.61	19.52
5	804.5759	18.39	PC 34:1	PC 16:0_18:1	7400572.104	2.48	22.01
6	197.8069	1.36			5700185.129	1.91	23.92
7	180.9722	44.92			5692126.273	1.91	25.83
8	826.5604	14.92	PC 36:4	PC 16:0_20:4	5337604.339	1.79	27.63
9	162.9815	0.10			4916967.365	1.65	29.28
10	195.8103	1.36			4477735.202	1.50	30.78
11	339.2327	4.88			4259743.744	1.43	32.21
12	180.9722	0.03			3750917.004	1.26	33.47
13	828.5757	16.33	PC 36:3	PC 16:0_20:3	3686184.954	1.24	34.71
14	854.5921	18.70	PC 38:4	PC 18:0_20:4	3333662.631	1.12	35.83
15	540.3305	3.79	LPC 16:0	LPC 16:0	3331822.597	1.12	36.95
16	797.6038	16.33	ISTD	PC 15:0_18:1(d7)	3218593.305	1.08	38.03
17	857.6753	23.11	SM 42:2	SM d18:1_24:1	3209216.987	1.08	39.10
18	747.5650	14.36	SM 34:1	SM d18:1_16:0	3183140.884	1.07	40.17
19	856.6072	20.29	PC 38:3	PC 18:0_20:3	3134763.565	1.05	41.22
20	178.9765	0.06			3112182.861	1.04	42.27
21	162.9816	0.96			3077789.533	1.03	43.30
22	160.8409	1.36			2786954.751	0.94	44.24
23	199.8039	1.36			2653675.487	0.89	45.13
24	162.8381	1.36			2585388.824	0.87	46.00
25	444.1042	8.49			2098019.237	0.70	46.70
26	828.5758	15.78	PC 36:3	PC 18:1_18:2	2076607.745	0.70	47.40
27	977.1535	17.55			2067486.977	0.69	48.09
28	178.9764	0.95			1855421.385	0.62	48.72
29	859.6912	24.76	SM 42:1	SM d18:1_24:0	1752017.149	0.59	49.30
30	829.1155	11.44			1696610.993	0.57	49.87
31	607.3274	21.29			1620783.792	0.54	50.42
32	850.5601	14.02	PC 38:6	PC 16:0_22:6	1569851.195	0.53	50.95
33	755.0958	9.18			1551990.549	0.52	51.47
34	568.3614	5.01	LPC 18:0	LPC 18:0	1549231.596	0.52	51.99
35	826.5598	13.22	PC 36:4	PC 18:2_18:2	1540602.169	0.52	52.50
36	852.5752	15.10	PC 38:5	PC 18:1_20:4 | PC 16:0_22:5	1526497.291	0.51	53.02
37	832.6072	21.59	PC 36:1	PC 18:0_18:1	1479842.893	0.50	53.51
38	445.2375	8.52			1447361.19	0.49	54.00
39	797.6535	23.11	SM 41:2	SM d18:1_23:1	1444398.422	0.48	54.48
40	564.3299	3.31	LPC 18:2	LPC 18:2	1418422.633	0.48	54.96
41	607.3273	17.05			1347011.673	0.45	55.41
42	831.6591	23.22	SM 40:1	SM d18:1_22:0	1245244.762	0.42	55.83
43	855.6592	21.63	SM 42:3	SM d18:2_24:1	1241510.74	0.42	56.25

44	829.6430	21.79	SM 40:2	SM d18:1_22:1	1066447.723	0.36	56.61
45	885.5494	14.92	PI 38:4	PI 18:0_20:4	975290.8623	0.33	56.93
46	740.5454	13.84	ISTD	PG 15:0_18:1(d7)	974731.0365	0.33	57.26
47	493.2408	0.95			972914.4786	0.33	57.59
48	799.6695	24.78	SM 41:1	SM d18:1_23:0	952458.6308	0.32	57.91
49	845.6745	24.04	SM 41:1	SM d18:1_23:0	931654.4639	0.31	58.22
50	467.2417	3.79			832137.478	0.28	58.50
51	444.1043	9.04			790553.0881	0.27	58.76
52	742.5384	15.46	PC 34:2	PC 16:0_18:2	776865.6206	0.26	59.03
53	770.5684	19.30	PC 36:2	PC 18:0_18:2	729297.8669	0.24	59.27
54	299.0005	0.90			725982.4436	0.24	59.51
55	480.3087	3.82			689769.2748	0.23	59.75
56	775.5966	18.14	SM 36:1	SM d18:1_18:0	688494.4045	0.23	59.98
57	566.3458	3.99	LPC 18:1	LPC 18:1	649381.2697	0.22	60.20
58	812.5806	17.08	PC O-36:4	PC O-16:0_20:4	644786.914	0.22	60.41
59	681.0764	7.21			623144.9288	0.21	60.62
60	903.1341	14.40			612606.1399	0.21	60.83
61	824.5441	12.84	PC 36:5	PC 16:0_20:5	611919.0023	0.21	61.03
62	687.5438	14.36	SM 34:1	SM d18:1_16:0	611413.0939	0.21	61.24
63	917.1862	18.10			606102.0222	0.20	61.44
64	840.6112	20.86	PC O-38:4	PC O-18:0_20:4	594079.0765	0.20	61.64
65	750.5428	21.10	PE O-38:5	PE P-18:0_20:4	588783.1868	0.20	61.84
66	609.5568	22.39			568675.1529	0.19	62.03
67	164.8354	1.36			556382.422	0.19	62.22
68	795.6369	21.68	SM 42:3		554015.1438	0.19	62.40
69	873.1593	9.77			552588.7616	0.19	62.59
70	988.0475	17.55			550928.5004	0.18	62.77
71	769.1484	11.78			549464.3604	0.18	62.96
72	799.1406	7.87			548512.4965	0.18	63.14
73	991.2048	21.10			547774.2868	0.18	63.32
74	852.5755	16.18	PC 38:5	PC 18:0_20:5 | PC 16:0_22:5	539149.3126	0.18	63.51
75	201.8007	1.36			528124.3103	0.18	63.68
76	843.6592	22.59	SM 41:2	SM d18:2_23:0	528019.4756	0.18	63.86
77	803.6273	21.48	SM 38:1	SM d18:1_20:0	512998.1156	0.17	64.03
78	695.1292	9.38			509005.0779	0.17	64.20
79	898.5783	19.35	PS 41:4		507758.4532	0.17	64.37
80	465.3035	6.46			503994.4451	0.17	64.54
81	573.3899	3.93	ISTD	LPC 18:1(d7)	503184.7951	0.17	64.71
82	725.1217	6.21			493171.3866	0.17	64.88
83	771.6380	23.22	SM 40:1	SM d18:1_22:0	488189.6716	0.16	65.04
84	168.9880	0.83			487628.7867	0.16	65.21
85	782.6375	14.69	ISTD	SM d18:1-18:1(d9)	487569.7557	0.16	65.37
86	745.5493	11.70	SM 34:2	SM d18:1_16:1	481882.9305	0.16	65.53
87	161.8477	1.35			481428.9071	0.16	65.69
88	778.5603	18.04	PC 32:0	PC 16:0_16:0	476056.1324	0.16	65.85
89	878.5908	17.61	PC 40:6	PC 18:0_22:6	470348.9139	0.16	66.01

90	828.5621	13.02	ISTD	PI 15:0_18:1(d7)	456490.0907	0.15	66.16
91	694.6344	26.45	Cer 42:1	Cer d18:1_24:0	448811.2973	0.15	66.31
92	744.5538	18.39	PC 34:1	PC 16:0_18:1	447390.5273	0.15	66.46
93	843.1677	14.64			433624.6914	0.15	66.61
94	785.6534	23.99	SM 41:1	SM d18:1_23:0	431697.7891	0.14	66.75
95	747.5646	13.76	SM 34:1	SM d18:1_16:0	413743.8472	0.14	66.89
96	768.5409	19.53			410023.8244	0.14	67.03
97	857.6746	22.83	SM 42:2	SM d18:1_24:1	409655.4884	0.14	67.17
98	467.2414	15.46	LPG 15:1 (H-) | LPA 17:1		395512.1879	0.13	67.30
99	870.5470	15.46			395161.8857	0.13	67.43
100	840.0090	11.44			388685.5345	0.13	67.57
101	466.1599	5.04			387624.9637	0.13	67.70
102	146.9636	0.77			382251.0701	0.13	67.82
103	446.1017	8.49			382046.0939	0.13	67.95
104	947.1792	11.98			381363.7495	0.13	68.08
105	180.9721	14.14			379552.7374	0.13	68.21
106	776.5440	14.75	PC 32:1	PC 16:0_16:1 | PC 14:0_18:1	377495.9619	0.13	68.33
107	547.3210	14.14			377117.1798	0.13	68.46
108	872.5638	18.39			368269.716	0.12	68.58
109	417.2093	6.91			368258.2263	0.12	68.71
110	548.1856	14.14			366303.7511	0.12	68.83
111	838.5959	17.32	PC O-38:5	PC P-18:0_20:4	366003.2385	0.12	68.95
112	325.1829	32.02			363867.6744	0.12	69.08
113	769.6219	21.84	SM 40:2		361998.4478	0.12	69.20
114	556.2182	14.14			360311.9756	0.12	69.32
115	197.8065	0.83			358756.0919	0.12	69.44
116	465.2456	4.33			356956.7686	0.12	69.56
117	833.5181	12.35	PI 34:2	PI 16:0_18:2	356055.4798	0.12	69.68
118	766.5385	14.92	PC 36:4	PC 16:0_20:4	350429.6195	0.12	69.80
119	719.5337	11.31	SM 32:1	SM d18:1_14:0	350365.6403	0.12	69.91
120	800.5435	12.65	PC 34:3	PC 16:1_18:2	341742.3832	0.11	70.03
121	794.5628	18.70	PC 38:4	PC 18:0_20:4	335421.1241	0.11	70.14
122	742.5378	20.29	PE 36:2	PE 18:0_18:2	326486.1354	0.11	70.25
123	766.5383	19.69	PE 38:4	PE 18:0_20:4	324324.7231	0.11	70.36
124	446.1016	9.03			322108.1483	0.11	70.47
125	800.5436	13.22	PC 34:3	PC 16:0_18:3	321007.4955	0.11	70.58
126	747.3837	22.14			320814.565	0.11	70.68
127	609.5566	31.98			313491.0839	0.11	70.79
128	581.5251	32.15			312251.7889	0.10	70.89
129	416.0731	6.91			308279.0323	0.10	71.00
130	581.5251	31.19			307516.9974	0.10	71.10
131	141.8667	0.77			306094.1846	0.10	71.20
132	843.6583	22.26	SM 41:2	SM d18:2_23:0	304884.0424	0.10	71.31
133	581.5252	19.98			304599.2535	0.10	71.41
134	749.3817	22.14			302131.9157	0.10	71.51
135	854.5900	17.55	PC 38:4	PC 16:0_22:4	294760.5624	0.10	71.61

136	249.9764	30.54			293803.9506	0.10	71.71
137	786.5643	17.17	PC O-34:3	PC P-16:0_18:2	286411.143	0.10	71.80
138	546.1880	14.14			286189.3144	0.10	71.90
139	223.0270	30.72			286068.8063	0.10	71.99
140	325.1829	2.99			284584.5306	0.10	72.09
141	861.5483	15.35	PI 36:2	PI 18:0_18:2	284090.6639	0.10	72.19
142	850.5595	12.74	PC 38:6	PC 18:2_20:4	282516.251	0.09	72.28
143	418.0701	6.88			281295.7398	0.09	72.38
144	790.5955	20.71	PS O-37:O (H-) | PC O-34:1 | PE O-37:1		276251.4059	0.09	72.47
145	445.2375	9.03			276247.2266	0.09	72.56
146	848.0399	11.44			275193.1482	0.09	72.65
147	355.0272	2.05			273111.4574	0.09	72.74
148	223.0270	30.00			272980.1689	0.09	72.84
149	162.9815	14.14			272124.6804	0.09	72.93
150	817.6428	22.42	SM 39:1	SM d18:1_21:0	271875.6807	0.09	73.02
151	558.2150	14.14			264427.7149	0.09	73.11
152	197.8065	16.87			263148.9576	0.09	73.20
153	803.1163	11.44			259994.6919	0.09	73.28
154	281.2475	7.07	FFA 18:1	FFA 18:1	259597.8687	0.09	73.37
155	684.6053	26.45	Cer 42:1		258063.487	0.09	73.46
156	882.6211	21.02	PC 40:4	PC 18:0_22:4	257444.1327	0.09	73.54
157	609.5565	31.18			255371.4254	0.09	73.63
158	588.3296	3.21	LPC 20:4		253666.3512	0.09	73.71
159	810.5646	16.44	PC O-36:5	PC P-16:0_20:4	252490.5331	0.08	73.80
160	838.0112	11.44			246289.2201	0.08	73.88
161	508.3398	5.01			246181.3039	0.08	73.96
162	951.1542	17.55			243052.2784	0.08	74.05
163	599.5274	22.39			242440.6006	0.08	74.13
164	456.1311	5.38			238488.1325	0.08	74.21
165	607.3274	8.84			238285.4753	0.08	74.29
166	223.0268	29.61			233700.559	0.08	74.37
167	854.5906	16.69	PC 38:4	PC 18:1_20:3	229956.0651	0.08	74.44
168	163.1117	4.85			226685.7669	0.08	74.52
169	441.2062	5.75			225868.2228	0.08	74.60
170	978.0183	17.55			224251.742	0.08	74.67
171	783.6381	22.59			223823.4299	0.08	74.75
172	680.6186	25.82	Cer 41:1;O2	Cer 18:1_23:0	222688.1243	0.07	74.82
173	442.0887	7.07			220258.645	0.07	74.89
174	223.0269	29.24			219422.4904	0.07	74.97
175	504.3087	3.31			216740.4313	0.07	75.04
176	856.6876	25.16	HexCer 43:1;O4	HexCer d18:1_24:0	215688.5139	0.07	75.11
177	443.2215	7.07			215487.3868	0.07	75.19
178	176.9781	1.49			215331.8573	0.07	75.26

179	692.9966	31.50			215146.9932	0.07	75.33
180	193.8145	1.36			213871.902	0.07	75.40
181	416.0684	5.36			211996.5722	0.07	75.47
182	568.3612	4.72	LPC 18:0	LPC 18:0	211660.8394	0.07	75.54
183	666.6030	25.08	Cer 40:1	Cer d18:1_22:0	210924.8806	0.07	75.62
184	765.9893	9.18			209853.194	0.07	75.69
185	796.5852	20.29			209629.309	0.07	75.76
186	454.1334	5.38			209307.0186	0.07	75.83
187	465.2451	5.54			209225.6713	0.07	75.90
188	223.0267	28.80			209072.6854	0.07	75.97
189	311.1674	2.65			208878.2565	0.07	76.04
190	626.5466	22.39			207077.5436	0.07	76.11
191	996.0784	17.55			205373.3566	0.07	76.18
192	223.0269	22.07			205160.5583	0.07	76.24
193	466.1604	5.38			205079.3658	0.07	76.31
194	894.5466	14.92			204161.0253	0.07	76.38
195	223.0269	25.45			204121.7273	0.07	76.45
196	159.0071	1.47			202652.2762	0.07	76.52
197	773.5807	14.81	SM 36:2	SM d18:1_18:1	200784.2276	0.07	76.59
198	857.5176	11.95	PI 36:4	PI 16:0_20:4	198719.6855	0.07	76.65
199	440.0732	5.75			198187.9775	0.07	76.72
200	223.0268	26.73			197969.0364	0.07	76.79
201	222.9845	0.87			197636.0767	0.07	76.85
202	444.0862	7.07			196311.2772	0.07	76.92
203	279.2316	5.75	FFA 18:2		196242.5901	0.07	76.98
204	223.0268	26.12			192938.5182	0.06	77.05
205	223.0270	31.58			191817.5138	0.06	77.11
206	293.1750	32.10			189552.444	0.06	77.18
207	729.0968	9.18			187984.3497	0.06	77.24
208	816.5754	17.35	PC 35:2	PC 17:0_18:2	186912.4258	0.06	77.30
209	223.0268	27.83			186902.9357	0.06	77.36
210	223.0269	27.31			186359.0952	0.06	77.43
211	205.8383	1.35			186113.4415	0.06	77.49
212	207.8354	1.38			185954.7702	0.06	77.55
213	163.8442	1.35			182971.0044	0.06	77.61
214	607.3271	9.46			182227.8485	0.06	77.68
215	223.0268	28.34			180325.9139	0.06	77.74
216	715.5749	18.16			178101.1378	0.06	77.80
217	748.5275	17.85	PE O-38:6	PE P-18:1_20:4 | PE P-16:0_22:5	176970.9061	0.06	77.85
218	442.0704	5.75			176929.6675	0.06	77.91
219	768.5541	16.38			173129.3035	0.06	77.97
220	465.2457	4.82			171817.8577	0.06	78.03
221	815.5528	14.36			171645.055	0.06	78.09
222	743.6061	21.48			170883.9107	0.06	78.15
223	253.0816	2.26			169936.5971	0.06	78.20
224	297.1513	32.03			167215.3157	0.06	78.26
225	998.0771	17.55			166684.4958	0.06	78.31
226	223.0269	30.36			164149.3384	0.06	78.37
227	774.0210	9.18			163619.0791	0.05	78.42

228	692.6187	25.23	Cer 42:2		162682.6804	0.05	78.48
229	829.9801	11.50			162250.2624	0.05	78.53
230	986.0486	17.55			162170.6015	0.05	78.59
231	621.1097	7.34			161926.7159	0.05	78.64
232	925.6620	23.11			161299.3164	0.05	78.70
233	880.6070	20.18	PS 43:4 (-H) | PC 40:5		158936.5136	0.05	78.75
234	467.2416	19.30			156433.7778	0.05	78.80
235	316.9466	41.65			155087.9422	0.05	78.85
236	429.0461	2.52			154876.0131	0.05	78.91
237	454.1331	9.03			154595.1379	0.05	78.96
238	748.5166	22.13	PS 33:0 (-H) | PC 30:1 | PE 33:1		154007.8666	0.05	79.01
239	711.6242	26.45			153515.9829	0.05	79.06
240	737.5820	16.27			152966.7203	0.05	79.11
241	733.5486	12.77	SM 33:1	SM d18:1_15:0	152553.7497	0.05	79.16
242	880.6063	18.80	PC 40:5	PC 18:0_22:5	151855.2499	0.05	79.22
243	806.5926	21.35	PC 34:0	PC 16:0_18:0	150350.6412	0.05	79.27
244	581.5253	30.51			148558.1741	0.05	79.32
245	442.0888	7.36			148375.5991	0.05	79.37
246	763.9917	9.18			148331.3105	0.05	79.41
247	256.9539	0.78			148319.3782	0.05	79.46
248	922.5776	18.70	PS 43:6		147081.513	0.05	79.51
249	792.5359	15.46	PS O-34:1		145374.8738	0.05	79.56
250	325.1828	0.97			145186.0025	0.05	79.61
251	223.0267	20.72			143543.9824	0.05	79.66
252	203.1184	29.81			143208.3579	0.05	79.71
253	213.0549	0.86			142870.6988	0.05	79.76
254	367.1572	1.52			141738.5134	0.05	79.80
255	466.1599	16.33			141211.7026	0.05	79.85
256	466.1590	5.75			140306.9261	0.05	79.90
257	651.1030	4.92			139679.1693	0.05	79.94
258	919.7093	32.01			139309.8575	0.05	79.99
259	426.1023	6.91			138697.5999	0.05	80.04
260	521.3214	14.14			137024.8468	0.05	80.08
261	480.1488	5.56			133065.8671	0.04	80.13
262	685.5282	11.70			132281.5034	0.04	80.17
263	800.5428	13.73	PS 37:2 (-H) | PC 34:3 | PE 37:3		132157.842	0.04	80.22
264	191.0757	32.05			131506.7671	0.04	80.26
265	538.3141	3.11	LPC 16:1	LPC 16:1	130035.5087	0.04	80.31
266	845.6681	23.71			129974.0927	0.04	80.35
267	503.0653	3.09			128795.0052	0.04	80.39
268	223.0271	31.04			128319.3204	0.04	80.44
269	609.5570	30.54			127322.8065	0.04	80.48

270	722.6155	14.69			125080.983	0.04	80.52
271	790.5385	14.02			124578.8245	0.04	80.56
272	223.0267	31.33			123065.4686	0.04	80.60
273	820.5621	19.30			121342.1208	0.04	80.64
274	512.2979	2.97	LPC 14:0	LPC 14:0	121173.8745	0.04	80.68
275	598.5151	19.98			121125.0081	0.04	80.73
276	858.6261	21.89			120865.1929	0.04	80.77
277	480.3081	5.24	LPC 15:0 | LPE 18:0 | LPE O-18:1 (H-) | PC O-16:0 (CH3-)		120558.4518	0.04	80.81
278	626.5462	22.17			120082.3584	0.04	80.85
279	884.0537	9.77			119061.9718	0.04	80.89
280	865.5910	16.33			119056.4621	0.04	80.93
281	456.1307	9.03			118989.2029	0.04	80.97
282	443.2220	7.37			118134.0918	0.04	81.01
283	768.5539	15.78			117962.3953	0.04	81.05
284	987.0493	17.55			117214.7546	0.04	81.09
285	179.9267	43.43			116498.8446	0.04	81.12
286	325.1828	0.84			115667.2516	0.04	81.16
287	828.6560	23.69	HexCer 40:1	HexCer d18:1_22:0	113859.8828	0.04	81.20
288	279.0095	1.50			112162.8716	0.04	81.24
289	452.1173	7.07			111214.386	0.04	81.28
290	927.6777	24.78			111065.9421	0.04	81.31
291	220.9851	1.47			110425.4972	0.04	81.35
292	303.2319	5.44	FFA 20:4	FFA 20:4	109961.6657	0.04	81.39
293	566.2486	14.14			108985.6759	0.04	81.42
294	158.8455	1.36			108849.8999	0.04	81.46
295	504.1338	20.32			108522.6115	0.04	81.50
296	493.3353	7.68			108328.1752	0.04	81.53
297	203.1182	32.19			106627.6051	0.04	81.57
298	553.2318	14.01			105743.1634	0.04	81.61
299	191.1171	31.94			105580.3512	0.04	81.64
300	305.0805	0.89			105543.4928	0.04	81.68
301	369.1723	1.58			105358.5867	0.04	81.71
302	637.5876	24.04			105252.7677	0.04	81.75
303	896.5629	16.33	PS 41:5		104353.3464	0.04	81.78
304	249.9763	32.10			103845.563	0.03	81.82
305	924.5933	20.32			103113.6458	0.03	81.85
306	863.5633	18.16	PI 36:1	PI 18:0_18:1	102624.4744	0.03	81.89
307	450.1016	5.72			102297.015	0.03	81.92
308	801.6113	18.70	SM 38:2		102097.2422	0.03	81.95
309	341.0477	0.95			101863.0504	0.03	81.99
310	506.3245	3.99			101807.9379	0.03	82.02
311	203.0179	1.46			99575.62758	0.03	82.06

312	856.6110	21.16	PS 41:2 (-H) | PC 38:3 | PE 41:3		99299.58582	0.03	82.09
313	485.3366	4.12	ISTD	LPE 18:1(d7)	99098.96399	0.03	82.12
314	774.5281	12.35	PS 35:1 (-H) | PC 32:2 | PE 35:2		98829.24861	0.03	82.16
315	609.5565	23.22			98630.60456	0.03	82.19
316	599.5267	22.17			97998.54416	0.03	82.22
317	283.2631	9.06	FFA 18:0	FFA 18:0	97921.09535	0.03	82.25
318	887.5633	16.22	PI 38:3	PI 18:0_20:3	97753.11522	0.03	82.29
319	464.0968	4.83			96894.69792	0.03	82.32
320	749.5800	15.63	SM 34:0	SM d20:0_14:0	96453.92943	0.03	82.35
321	465.2449	6.65			96451.17512	0.03	82.39
322	887.6714	14.14	PG 44:1		96144.43059	0.03	82.42
323	482.1485	5.58			95226.46559	0.03	82.45
324	221.8409	0.78			95163.58442	0.03	82.48
325	722.5119	17.61	PE O-36:5	PE P-16:0_20:4	95076.85576	0.03	82.51
326	476.2767	3.41	LPE 18:2	LPE 18:2	94886.83896	0.03	82.55
327	590.3454	3.55	LPC 20:3	LPC 20:3	94666.95981	0.03	82.58
328	339.1987	33.08			93937.67481	0.03	82.61
329	293.1752	31.15			93676.17521	0.03	82.64
330	217.8634	20.06			93461.01321	0.03	82.67
331	492.1076	5.38			93199.83179	0.03	82.70
332	581.5250	19.43			92505.77514	0.03	82.73
333	918.5464	14.05			92220.31082	0.03	82.76
334	810.0348	7.88			91262.30271	0.03	82.80
335	446.0838	7.07			90747.83546	0.03	82.83
336	239.0592	22.07			90634.83278	0.03	82.86
337	478.1330	4.56			90568.20927	0.03	82.89
338	563.2590	14.01			89835.4716	0.03	82.92
339	966.5655	19.30			89557.53691	0.03	82.95
340	796.5969	16.33			89088.36665	0.03	82.98
341	255.2318	6.88	FFA 16:0	FFA 16:0	88381.78355	0.03	83.01
342	783.6375	22.23			87381.44011	0.03	83.04
343	223.0268	32.11			87158.37491	0.03	83.06
344	692.6186	24.94	Cer 42:2		86733.7028	0.03	83.09
345	482.1644	7.07			85686.16895	0.03	83.12
346	838.5959	20.36	PC O-38:5		85663.25685	0.03	83.15
347	341.0480	1.66			85174.53901	0.03	83.18
348	554.3644	14.02			83408.21244	0.03	83.21
349	491.3581	33.06			83357.14561	0.03	83.24
350	772.5859	21.59			82822.82277	0.03	83.26
351	293.1751	30.52			82627.3854	0.03	83.29
352	607.3269	23.73			82492.62756	0.03	83.32
353	583.2552	5.11			82361.46773	0.03	83.35
354	755.9611	9.18			82104.27496	0.03	83.37

355	900.5947	21.53			81759.99298	0.03	83.40
356	884.5103	19.53			81672.88124	0.03	83.43
357	899.6472	23.22			81597.12765	0.03	83.46
358	223.0268	23.91			81387.79302	0.03	83.48
359	466.1601	18.23			81321.69896	0.03	83.51
360	487.1929	5.54			81318.90229	0.03	83.54
361	165.0393	29.99			81221.16837	0.03	83.57
362	279.0092	0.97			81176.29262	0.03	83.59
363	221.8408	41.73			81008.03503	0.03	83.62
364	466.0944	4.83			80816.78676	0.03	83.65
365	571.4962	19.98			80346.95833	0.03	83.67
366	474.1253	4.83			80207.93971	0.03	83.70
367	467.2414	21.59			78859.05004	0.03	83.73
368	502.1369	30.80			78709.16301	0.03	83.75
369	179.9263	43.12			78251.95105	0.03	83.78
370	312.1710	32.04			78112.58768	0.03	83.81
371	158.0108	1.46			77413.70852	0.03	83.83
372	928.0797	18.10			76867.43954	0.03	83.86
373	502.1367	21.25			76793.34041	0.03	83.88
374	256.9537	43.00			76592.14311	0.03	83.91
375	417.2064	5.04			76370.73433	0.03	83.94
376	896.5631	15.78			76365.50602	0.03	83.96
377	445.2377	5.38			76166.24085	0.03	83.99
378	774.5441	20.33			75528.67889	0.03	84.01
379	177.0332	0.98			75107.79755	0.03	84.04
380	195.8097	0.83			74920.51191	0.03	84.06
381	726.5432	21.53	PE O-36:3	PE P-18:0_18:2	74777.96522	0.03	84.09
382	252.9953	0.93			74398.76663	0.02	84.11
383	199.8029	7.51			74362.80605	0.02	84.14
384	882.0559	9.77			74226.6962	0.02	84.16
385	788.5799	17.82	PC O-34:2 | PE O-37:2		73993.06861	0.02	84.19
386	149.0084	30.00			73952.80201	0.02	84.21
387	235.9249	41.66			73919.95173	0.02	84.24
388	692.9957	31.15			73677.32274	0.02	84.26
389	454.1161	7.07			73462.35408	0.02	84.29
390	191.0754	31.15			73006.98823	0.02	84.31
391	535.2879	6.49			72862.05277	0.02	84.34
392	607.3277	7.93			71392.87179	0.02	84.36
393	612.3295	3.07	LPC 22:6	LPC 22:6	70856.57959	0.02	84.38
394	936.1109	18.10			70703.96389	0.02	84.41
395	859.6865	23.68	SM 42:1		70683.27703	0.02	84.43
396	835.5338	14.64	PI 34:1	PC 16:0_18:1	70462.78839	0.02	84.45
397	883.3762	19.61			70267.28867	0.02	84.48
398	992.0709	21.10			69830.27643	0.02	84.50
399	205.0946	30.49			69606.44249	0.02	84.52
400	555.2286	14.01			69531.4832	0.02	84.55
401	316.9466	1.43			69427.41476	0.02	84.57

402	229.0939	30.48		69385.13838	0.02	84.59
403	239.0588	20.73		69193.72379	0.02	84.62
404	190.0498	1.62		68894.17204	0.02	84.64
405	416.0728	6.29		68559.67555	0.02	84.66
406	670.5902	25.82		68417.82868	0.02	84.69
407	656.5743	25.07		68320.94412	0.02	84.71
408	329.0281	2.05		68088.6403	0.02	84.73
409	736.0152	6.21		67982.81254	0.02	84.76
410	819.5506	15.46		67975.27304	0.02	84.78
411	428.0997	6.91		67857.16572	0.02	84.80
412	191.0749	31.04		67803.98182	0.02	84.82
413	245.9822	0.97		67682.70675	0.02	84.85
414	223.0268	32.36		67674.02732	0.02	84.87
415	682.5890	24.94		67467.82515	0.02	84.89
416	418.0694	6.30		67181.25066	0.02	84.91
417	281.0086	1.68		67127.67784	0.02	84.94
418	816.5755	16.74	PS 38:1 (-H) | PC 35:2 | PE 38:2	66779.80983	0.02	84.96
419	204.9732	1.48		66458.94621	0.02	84.98
420	502.1369	13.22		65918.7653	0.02	85.00

Cer, ceramide; FFA, free fatty acyl; HexCer, hexosylceramide; ISTD, internal standard; LPA, lysophosphatidic acid; LPG, lysophosphatidylglycerol; LPC lysophosphatidylcholine; PA, phosphatidic acid; PC, phosphatidylcholine; PE, phosphatidylethanolamine; PG, phosphatidylglycerol; PI, phosphatidylinositol; PS, phosphatidylserine; SM, sphingomyelin.

Appendix A.5. Top 85% Abundance within positive Trapped Ion Mobility-Quadrupole-Time-of-Flight.

Feature #	m/z	Retention time (min)	Brutto	Medio	Abundance	Relative Abundance (%)	Cumulative Abundance (%)
1	758.57066	21.10	PC 34:2	PC 16:0_18:2	198505498.2	6.44	6.44
2	666.61958	42.08	CE 18:2	CE 18:2	170869753.8	5.55	11.99
3	430.91365	0.12			124301100.6	4.03	16.02
4	362.92606	0.12			107337090.2	3.48	19.50
5	786.60167	24.74	PC 36:2	PC 18:0_18:2	104136099.4	3.38	22.88
6	566.8882	0.12			99248718.5	3.22	26.10
7	760.58583	23.91	PC 34:1	PC 16:0_18:1	89039909.7	2.89	28.99
8	702.86288	0.11			86540819.96	2.81	31.80
9	634.87575	0.10			80771666.49	2.62	34.42
10	782.57011	20.46	PC 36:4	PC 16:0_20:4	76522937.33	2.48	36.91
11	498.90093	0.11			74131752.72	2.41	39.31
12	770.85007	0.11			72690795.33	2.36	41.67
13	226.95132	0.11			61843381.7	2.01	43.68
14	838.83769	0.11			56049679.17	1.82	45.50
15	874.78519	41.84	TG 52:3	TG 16:0_18:1_18:2	43933127.2	1.43	46.92
16	784.58507	22.10	PC 36:3	PC 16:0_20:3	43190222.54	1.40	48.33
17	753.614	22.01	ISTD	PC 15:0_18:1(d7)	43080438.21	1.40	49.72
18	369.35157	42.08			41503899.54	1.35	51.07
19	810.60118	24.17	PC 38:4	PC 18:0_20:4	40831828.83	1.33	52.40
20	496.33922	4.57	LPC 16:0	LPC 16:0	37198688.57	1.21	53.60
21	690.61869	41.83	CE 20:4	CE 20:4	36690618.82	1.19	54.79
22	906.82543	0.12			36067835.75	1.17	55.96
23	876.80227	42.18	TG 52:2	TG 16:0_18:1_18:1	31792582.34	1.03	57.00
24	668.63424	42.55	CE 18:1	CE 18:1	30004003.42	0.97	57.97
25	537.39483	24.43			29085640.5	0.94	58.91
26	872.76985	41.48	TG 52:4	TG 16:1_18:1_18:2	25644132.11	0.83	59.75
27	369.35152	42.54			23788092.66	0.77	60.52
28	784.58508	21.46	PC 36:3	PC 18:1_18:2	22475725.9	0.73	61.25
29	703.57535	19.49	SM 34:1	SM d18:1_16:0	22394689.11	0.73	61.97
30	974.81329	0.12			20639220.78	0.67	62.64
31	1042.8012	0.12			19699614.76	0.64	63.28
32	848.77069	41.82	TG 50:2	TG 16:0_16:1_18:1	18301886.1	0.59	63.88
33	806.57004	19.21	PC 38:6	PC 16:0_22:6	17920567.36	0.58	64.46
34	693.63018	42.08			17454036.89	0.57	65.03
35	900.80163	41.86	TG 54:4	TG 18:1_18:1_18:2 | TG 18:0_18:2_18:2 | TG 16:0_18:1_20:3	16775328.89	0.54	65.57
36	940.81907	0.12			15430123.82	0.50	66.07
37	788.61677	27.61	PC 36:1	PC 18:0_18:1	14879658.12	0.48	66.55
38	846.7538	41.41	TG 50:3	TG 16:0_16:1_18:2 | TG 16:1_16:1_18:1	14075265.88	0.46	67.01
39	812.61658	25.67	PC 38:3	PC 18:0_20:3	13773725.41	0.45	67.46
40	524.37095	6.30	LPC 18:0	LPC 18:0	12982288.32	0.42	67.88

41	902.81766	42.18	TG 54:3	TG 18:1_18:1_18:1 | TG 16:1_18:1_20:1 | TG 16:0_18:1_20:2 | TG 16:1_18:0_20:2	12978979.72	0.42	68.30
42	675.67779	42.52	ISTD	CE 18:1 (d7)	12859201.7	0.42	68.72
43	1110.7892	0.12			12684028.06	0.41	69.13
44	808.58496	20.66	PC 38:5	PC 16:0_22:5	12542903.16	0.41	69.54
45	850.7865	42.18	TG 50:1	TG 16:0_16:0_18:1	12395567.37	0.40	69.94
46	736.85636	0.12			12091429.16	0.39	70.33
47	565.56644	29.43			11673495.87	0.38	70.71
48	1008.807	0.11			11021466.79	0.36	71.07
49	537.53521	25.35			10996045.35	0.36	71.42
50	369.35151	41.82			10977553.14	0.36	71.78
51	520.33933	3.70	LPC 18:2	LPC 18:2	10706981.94	0.35	72.13
52	369.35162	18.52	Cho	Cholesterol	10151353.37	0.33	72.46
53	294.93893	0.12			10035718.15	0.33	72.78
54	804.84391	0.11			9740729.294	0.32	73.10
55	782.56924	18.03	PC 36:4	PC 18:2_18:2	8981258.545	0.29	73.39
56	872.83103	0.10			8965973.003	0.29	73.68
57	664.60237	41.65	CE 18:3	CE 18:3	8701885.617	0.28	73.96
58	1076.7954	0.11			8584258.496	0.28	74.24
59	522.35554	4.87	LPC 18:1	LPC 18:1	8508472.514	0.28	74.52
60	899.78444	41.48			8498411.329	0.28	74.79
61	559.45023	24.42			8018784.866	0.26	75.05
62	1178.7775	0.12			7748384.214	0.25	75.31
63	870.75355	41.10	TG 52:5	TG 16:0_18:2_18:3 | TG 16:1_18:1_18:3 | TG 16:1_18:2_18:2	7638329.551	0.25	75.55
64	529.399	4.82	ISTD	LPC 18:1 (d7)	7246553.612	0.24	75.79
65	717.62962	41.80			6865861.597	0.22	76.01
66	732.55333	20.19	PC 32:1	PC 16:0_16:1	6750644.934	0.22	76.23
67	813.68455	31.11	SM 42:2	SM d18:1_24:1	6331814.358	0.21	76.44
68	820.73884	41.39	TG 48:2	TG 14:0_16:1_18:1 | TG 14:0_16:0_18:2 | TG 12:0_18:1_18:1	6177388.465	0.20	76.64
69	768.58992	22.70	PC O-36:4	PC O-16:0_20:4	6140182.963	0.20	76.84
70	695.64477	42.55			6104123.83	0.20	77.03
71	834.60094	23.19	PC 40:6	PC 18:0_22:6	6089863.539	0.20	77.23
72	805.34551	0.11			6050470.134	0.20	77.43
73	338.34177	11.30			5908619.155	0.19	77.62
74	879.74181	41.86	TG 52:3	TG 16:0_18:1_18:2	5869428.632	0.19	77.81
75	1144.7834	0.10			5822073.588	0.19	78.00
76	822.75496	41.81	TG 48:1	TG 14:0_16:0_18:1	5800597.109	0.19	78.19
77	640.6027	42.03	CE 16:1	CE 16:1	5647993.969	0.18	78.37
78	829.79872	41.78	ISTD	TG 15:0_18:1 (d7)_15:0	5610703.732	0.18	78.55
79	702.8627	46.85			5506883.719	0.18	78.73
80	903.74185	41.50	TG 54:5		5499253.328	0.18	78.91
81	734.5692	23.53	PC 32:0	PC 16:0_16:0	5294126.247	0.17	79.08
82	684.20234	26.38			5036214.213	0.16	79.24

83	680.48003	24.27			4949120.655	0.16	79.41
84	737.35814	0.11			4732245.406	0.15	79.56
85	1065.463	0.12			4636210.957	0.15	79.71
86	811.66873	27.80	SM 42:3	SM d18:2_24:1	4626303.625	0.15	79.86
87	794.60552	22.88	PC O 38:5	PC P-18:0_20:4	4587495.598	0.15	80.01
88	413.26627	9.10	ST 24:2;O4		4584283.097	0.15	80.16
89	881.75747	42.18	TG 52:2	TG 16:0_18:1_18:1	4543588.238	0.15	80.30
90	707.49096	24.27			4497901.646	0.15	80.45
91	668.86915	0.12			4451635.782	0.14	80.60
92	691.61317	41.65			4450089.185	0.14	80.74
93	780.55331	17.46	PC 36:5	PC 16:0_20:5	4373174.975	0.14	80.88
94	609.60407	29.43			4345576.288	0.14	81.02
95	975.31499	0.10			4259670.006	0.14	81.16
96	642.6184	42.57	CE 16:0	CE 16:0	4215518.162	0.14	81.30
97	844.73903	40.96	TG 50:4	TG 14:0_18:2_18:2 | TG 16:1_16:1_18:2	4206658.178	0.14	81.43
98	787.66871	31.37	SM 40:1		4189126.377	0.14	81.57
99	738.64654	20.03	ISTD	SM d18:1_18:1(d9)	3968388.219	0.13	81.70
100	581.57252	25.35			3944004.615	0.13	81.83
101	654.33191	5.54			3911353.7	0.13	81.95
102	810.60055	23.13	PC 38:4	PC 18:0_20:4	3886020.05	0.13	82.08
103	758.22096	29.99			3811419.431	0.12	82.20
104	731.60571	23.60	SM 36:1	SM d20:1_16:0	3715932.222	0.12	82.32
105	808.58453	21.33	PC 38:5	PC 18:0_20:5	3650226.081	0.12	82.44
106	315.25297	6.33	FA 18:1;O2		3647942.239	0.12	82.56
107	878.8177	42.53	TG 52:1	TG 16:0_18:0_18:1	3640160.182	0.12	82.68
108	901.72573	41.09	TG 56:9	TG 18:2_18:2_20:5 | TG 18:2_18:3_20:4 | TG 16:0_18:3_22:6	3620927.265	0.12	82.80
109	1043.3029	0.12			3566162.379	0.12	82.91
110	610.18377	23.22			3565510.104	0.12	83.03
111	896.77238	41.34	TG 54:6	TG 16:0_18:2_20:4	3523499.835	0.11	83.14
112	1133.4509	0.11			3510860.391	0.11	83.26
113	1156.1132	0.12			3397203.395	0.11	83.37
114	593.59792	33.49			3351423.375	0.11	83.48
115	916.52725	21.09			3349935.247	0.11	83.58
116	695.57395	41.79	CE 20:4	CE 20:4	3315949.144	0.11	83.69
117	904.83345	42.54	TG 54:2	TG 16:0_18:1_20:1 | TG 18:0_18:1_18:1	3244862.218	0.11	83.80
118	1246.7652	0.10			3210249.809	0.10	83.90
119	360.32361	11.30			3171920.3	0.10	84.00
120	742.57386	22.73	PC O-34:3	PC O-16:0_18:3	3101373.689	0.10	84.10
121	1314.752	0.11			3002698.398	0.10	84.20
122	818.72371	40.87	TG 48:3	TG 14:0_16:1_18:2 | TG 14:1_16:0_18:2 | TG 12:0_18:1_18:2 | TG 14:1_16:1_18:1	2972142.543	0.10	84.30
123	897.76721	41.08			2959637.157	0.10	84.39

124	647.45844	33.89			2943595.526	0.10	84.49
125	756.55328	18.01	PC 34:3	PC 16:0_18:3	2941152.63	0.10	84.59
126	808.58478	22.00	PC 38:5	PC 18:0_20:5	2892222.955	0.09	84.68
127	702.68874	42.49			2847212.118	0.09	84.77
128	905.75768	41.94	TG 54:4	TG 18:1_18:1_18:2	2800625.789	0.09	84.86
129	701.55889	15.67	SM 34:2		2722346.102	0.09	84.95
130	785.65303	27.99	SM 40:2		2667098.994	0.09	85.04

CE, cholesterol ester; Cho, cholesterol; DG, diacylglycerol; HexCer, hexosylceramide; ISTD, internal standard; LPC, lysophosphatidylcholine; MGDG, Monogalactosyldiacylglycerol; PC, phosphatidylcholine; SM, sphingomyelin; ST, sterol; TG, triacylglycerol.

Appendix A.6. Top 85% Abundance within negative Trapped Ion Mobility-Quadrupole-Time-of-Flight.

Feature #	m/z	Retention time (min)	Brutto	Medio	Abundance	Relatie Abundance (%)	Cumulative Abundance (%)
1	540.3294	4.51	LPC 16:0	LPC 16:0	78769679	5.76	5.76
2	802.5591	20.97	PC 34:2	PC 16:0_18:2	62940516	4.60	10.36
3	830.5897	24.57	PC 36:2	PC 18:0_18:2	45979296	3.36	13.71
4	804.5744	23.76	PC 34:1	PC 16:0_18:1	42100958	3.08	16.79
5	339.2319	6.22			37737832	2.76	19.55
6	281.2482	8.89	FFA 18:1	FFA 18:1	36295056	2.65	22.20
7	826.5584	20.26	PC 36:4	PC 16:0_20:4	35851569	2.62	24.82
8	747.5642	19.33	SM 34:1	SM d18:1_16:0	34698045	2.54	27.36
9	588.8961	0.11			34326969	2.51	29.86
10	568.3598	6.24	LPC 18:0	LPC 18:0	29836019	2.18	32.05
11	520.9084	0.11			28028548	2.05	34.09
12	564.3286	3.65	LPC 18:2	LPC 18:2	26431962	1.93	36.02
13	452.9216	0.11			26294687	1.92	37.95
14	384.9346	0.11			24679627	1.80	39.75
15	656.8830	0.11			24330324	1.78	41.53
16	316.9470	0.11			23590407	1.72	43.25
17	724.8699	0.10			22007211	1.61	44.86
18	566.3448	4.80	LPC 18:1	LPC 18:1	21084205	1.54	46.40
19	279.2320	7.16	FFA 18:2	FFA 18:2	20299983	1.48	47.88
20	792.8575	0.12			19868832	1.45	49.34
21	854.5893	23.99	PC 38:4	PC 18:0_20:4	19382754	1.42	50.75
22	828.5728	21.98	PC 36:3	PC 16:0_20:3	19216624	1.40	52.16
23	573.3882	4.75	ISTD	LPC 18:1(d7)	18938071	1.38	53.54
24	797.6023	21.87	ISTD	PC 15:0_18:1(d7)	18647244	1.36	54.90
25	860.8448	0.11			14498298	1.06	55.96
26	828.5733	21.30	PC 36:3	PC 18:1_18:2	13406734	0.98	56.94
27	255.2321	8.60	FFA 16:0	FFA 16:0	12422437	0.91	57.85
28	850.5585	19.01	PC 38:6	PC 16:0_22:6	12103577	0.88	58.73
29	832.6050	27.43	PC 36:1	PC 18:0_18:1	11380936	0.83	59.57
30	745.5480	15.52	SM 34:2	SM d18:2_16:0	10730590	0.78	60.35
31	782.6352	19.83	ISTD	SM d18:1-18:1(d9)	9561626	0.70	61.05
32	248.9595	0.10			9331749	0.68	61.73
33	928.8321	0.11			9316030	0.68	62.41
34	677.5428	29.24	DG 37:3		8989101	0.66	63.07
35	826.5575	17.81	PC 36:4	PC 18:2_18:2	8807128	0.64	63.71
36	856.6050	25.48	PC 38:3	PC 18:0_20:3	8737963	0.64	64.35
37	857.6725	30.94	SM 42:2	SM d18:1_24:1	8690902	0.64	64.98
38	852.5732	20.50	PC 38:5	PC 16:0_22:5 | PC 18:1_20:4	7901727	0.58	65.56
39	855.6568	27.62	SM 42:3	SM d18:2_24:1	6988880	0.51	66.07
40	283.2632	11.44	FFA 18:0	FFA 18:0	6893433	0.50	66.58
41	776.5416	20.01	PC 32:1	PC 16:0_16:1	6784994	0.50	67.07
42	588.3289	3.49	LPC 20:4	LPC 20:4	6624154	0.48	67.56
43	996.8194	0.11			6117103	0.45	68.00

44	824.5421	17.26	PC 36:5	PC 16:0_20:5	6002132	0.44	68.44
45	649.5120	25.17			5817847	0.43	68.87
46	719.5318	14.94	SM 32:1	SM d18:1_14:0	5530418	0.40	69.27
47	740.5440	18.90	ISTD	PG 15:0_18:1(d7)	5190952	0.38	69.65
48	656.8826	46.83			5001152	0.37	70.02
49	894.8379	0.11			4907935	0.36	70.37
50	812.5782	22.53	PC O-36:4	PC O-16:0_20:4	4868409	0.36	70.73
51	1064.8062	0.11			4783591	0.35	71.08
52	829.6410	27.82	SM 40:2	SM d18:2_22:0 | SM d18:1_22:1	4624648	0.34	71.42
53	581.5244	25.17			4490684	0.33	71.75
54	724.8698	46.86			4466284	0.33	72.07
55	778.5568	23.39	PC 32:0	PC 16:0_16:0	4244628	0.31	72.38
56	316.9468	46.88			4121186	0.30	72.68
57	857.6727	31.71	SM 42:2	SM d18:2_24:0	4092866	0.30	72.98
58	773.5783	20.04	SM 36:2	SM d18:1_18:1	4055235	0.30	73.28
59	775.5940	23.47	SM 36:1	SM d18:1_18:0	4032542	0.29	73.57
60	962.8255	0.13			3853604	0.28	73.86
61	878.5888	23.03	PC 40:6	PC 18:0_22:6	3849632	0.28	74.14
62	303.2326	6.80	FFA 20:4	FFA 20:4	3677259	0.27	74.41
63	744.5418	28.73			3587476	0.26	74.67
64	826.8504	0.11			3543762	0.26	74.93
65	800.5417	17.81	PC 34:3	PC 16:0_18:3	3458850	0.25	75.18
66	750.5418	26.78	PE O-38:5	PE P-18:O_20:4	3329218	0.24	75.42
67	852.5732	21.67	PC 38:5	PC 18:0_20:5	3299323	0.24	75.66
68	538.3133	3.27	LPC 16:1	LPC 16:1	3277839	0.24	75.90
69	838.5938	22.73	PC O-38:5	PC P-18:0_20:4	3149944	0.23	76.13
70	766.5366	25.02	PE 38:4	PE 18:0_20:4	2902298	0.21	76.35
71	609.5555	29.24			2843000	0.21	76.55
72	465.3036	8.21			2803520	0.20	76.76
73	854.5886	22.95	PC 38:4	PC 16:0_22:4	2784708	0.20	76.96
74	850.5577	17.15	PC 38:6	PC 18:2_20:4	2762411	0.20	77.16
75	885.5465	20.76	PI 38:4	PI 18:0_20:4	2736133	0.20	77.36
76	480.3081	4.51			2732957	0.20	77.56
77	760.6046	35.62			2590275	0.19	77.75
78	800.5417	16.94	PC 34:3	PC 16:1_18:2	2560900	0.19	77.94
79	786.5629	22.55	PC O-34:3	PC P-16:0_18:2	2555824	0.19	78.13
80	831.6571	31.23	SM 40:1	SM d18:1_22:0	2476070	0.18	78.31
81	705.5736	33.31			2467293	0.18	78.49
82	253.2167	6.70	FFA 16:1	FFA 16:1	2330103	0.17	78.66
83	563.5027	8.89			2285186	0.17	78.82
84	803.6256	27.32	SM 38:1	SM d18:1_20:0	2221512	0.16	78.99
85	485.3360	4.96	ISTD	LPE 18:1(d7)	2206228	0.16	79.15
86	733.5474	17.04	SM 33:1 | CerPE 36:1		2200014	0.16	79.31
87	760.6048	36.43			2195836	0.16	79.47
88	367.1580	1.51	ST 19:2;O2		2130479	0.16	79.62
89	590.3440	4.14	LPC 20:3	LPC 20:3	2080015	0.15	79.78

90	843.6564	29.74	SM 41:2	SM d18:2_23:0	2019541	0.15	79.92
91	1098.7998	0.11			2015461	0.15	80.07
92	768.5385	24.88			1995312	0.15	80.22
93	840.6098	26.19	PC O-38:4	PC O-18:0_20:4	1935049	0.14	80.36
94	593.4765	10.40			1821343	0.13	80.49
95	774.5260	16.46	PC 32:2	PC 14:0_18:2	1803560	0.13	80.62
96	810.5626	21.97	PC O-36:5	PC P-16:0_20:4	1753536	0.13	80.75
97	854.5885	22.24	PC 38:4	PC 18:1_20:3	1703270	0.12	80.88
98	829.6413	27.13	SM 40:2	SM d18:1_22:1	1674658	0.12	81.00
99	775.5129	28.06	PG O-34:3		1663490	0.12	81.12
100	1132.7932	0.11			1633855	0.12	81.24
101	476.2771	3.81			1594586	0.12	81.36
102	852.5729	21.17	PC 38:5	PC 18:1_20:4	1589991	0.12	81.47
103	816.5731	22.79	PC 35:2	PC 17:0_18:2	1574239	0.12	81.59
104	748.5258	23.34	PE O-38:6	PE P-18:1_20:4	1545939	0.11	81.70
105	722.5100	23.07	PE O-36:5	PE P-16:0_20:4	1489541	0.11	81.81
106	1200.7799	0.11			1461984	0.11	81.92
107	397.2740	6.14			1456486	0.11	82.02
108	327.2319	6.39	FFA 22:6	FFA 22:6	1423449	0.10	82.13
109	762.6203	38.83			1408501	0.10	82.23
110	750.5283	19.44	PC 30:0	PC 14:0_16:0	1407448	0.10	82.33
111	1030.8129	0.11			1392455	0.10	82.43
112	790.5941	25.83	PC O-34:1	PC P-18:0_16:0 | PC O-16:0_18:1	1376641	0.10	82.53
113	369.1729	1.53	ST 19:1;O2		1372945	0.10	82.64
114	1166.7869	0.11			1352082	0.10	82.73
115	608.3161	4.56			1344046	0.10	82.83
116	751.5127	30.75	PG O-32:1		1284617	0.09	82.93
117	459.2895	8.05			1268320	0.09	83.02
118	788.5782	23.15	PC O-34:2	PC O-16:0_18:2	1252647	0.09	83.11
119	801.6094	24.01	SM 38:2	SM d18:1_20:1	1214944	0.09	83.20
120	880.6047	24.12	PC 40:5	PC 18:0_22:5 | PC 20:1_20:4	1194783	0.09	83.29
121	777.5286	31.21	PG O-34:2	PG O-16:0_18:2	1192527	0.09	83.37
122	391.2243	4.35			1188079	0.09	83.46
123	742.5364	25.64	PE 36:2	PE 18:0_18:2	1178128	0.09	83.55
124	779.5443	34.85			1154436	0.08	83.63
125	512.2978	2.96	LPC 14:0	LPC 14:0	1154357	0.08	83.71
126	861.5471	21.27	PI 36:2	PI 18:0_18:2	1149949	0.08	83.80
127	475.3589	18.43			1123460	0.08	83.88
128	585.4842	8.89			1107098	0.08	83.96
129	500.2766	3.64	LPE 20:4	LPE 20:4	1104932	0.08	84.04
130	816.5730	22.28	PC 35:2	PC 17:0_18:2	1103720	0.08	84.12
131	854.5872	22.64	PC 38:4	PC 18:1_20:3	1098905	0.08	84.20
132	632.3158	3.65			1088237	0.08	84.28
133	843.6567	29.04	SM 41:2	SM d18:1_23:1	1083606	0.08	84.36
134	277.2164	5.96	FFA 18:3	FFA 18:3	1083199	0.08	84.44
135	612.3282	3.27	LPC 22:6	LPC 22:6	1077869	0.08	84.52
136	676.5538	28.75			1073465	0.08	84.60

137	1065.3078	0.10			1066208	0.08	84.68
138	1035.6596	4.48			1063388	0.08	84.75
139	859.6881	35.10	SM 42:1	SM d18:1_24:0	1054375	0.08	84.83
140	857.5159	16.37	PI 36:4	PI 16:0_20:4	1035343	0.08	84.91
141	845.6725	33.17	SM 41:1	SM d18:1_23:0	1024144	0.07	84.98
142	882.6200	26.54	PC 40:4	PC 18:0_22:4	1023538	0.07	85.06

Cer, ceramide; FFA, free fatty acyl; HexCer, hexosylceramide; ISTD, internal standard; LPA, lysophosphatidic acid; LPG, lysophosphatidylglycerol; LPC lysophosphatidylcholine; PA, phosphatidic acid; PC, phosphatidylcholine; PE, phosphatidylethanolamine; PG, phosphatidylglycerol; PI, phosphatidylinositol; PS, phosphatidylserine; SM, sphingomyelin.

Appendix B.1. % Coefficient of Variation in quantitation in positive polarity across platforms.

Brutto ID	Medio ID	qOrbi (n=4)	QToF (n=3)	timsToF (n=3)
		Confidence of Variation (%)		
PC 34:1	PC 16:0_18:1	0.55	1.17	0.28
PC 34:2	PC 16:0_18:2	0.81	1.15	2.05
PC 36:1	PC 18:0_18:1	0.93	-	1.50
PC 36:2	PC 18:0_18:2	0.39	0.48	0.26
PC 36:3	PC 16:0_20:3	-	3.34	0.48
	PC 18:1_18:2	0.32	-	1.60
PC 36:4	PC 16:0_20:4	0.75	0.52	0.30
PC 38:3	PC 18:0_20:3	1.03	-	-
PC 38:4	PC 18:0_20:4	0.85	2.30	0.59
PC 38:6	PC 16:0_22:6	1.09	0.63	1.57
LPC 16:0	LPC 16:0	3.87		1.61
TG 50:1	TG 16:0_16:0_18:1	3.73	6.26	-
TG 50:2	TG 14:0_18:1_18:1	3.99	2.04	-
	TG 16:0_16:1_18:1			2.28
	TG 16:0_16:0_18:2		-	-
TG 50:3	TG 16:0_16:1_18:2	3.55	-	2.97
	TG 16:1_16:1_18:1	-	-	
TG 52:2	TG 16:0_18:1_18:1	0.40	6.94	0.85
	TG 16:1_18:0_18:1		-	-
TG 52:3	TG 16:0_18:1_18:2	0.38	3.52	1.77
	TG 16:1_18:0_18:2		-	-
TG 52:4	TG 16:0_18:2_18:2	-	3.86	-
	TG 16:1_18:1_18:2	-		1.81
TG 54:3	TG 18:0_18:1_18:2	5.87	3.78	-
TG 54:4	TG 16:0_18:2_20:2	2.34	-	-
	TG 18:0_18:2_18:2			
	TG 18:1_18:1_18:2		2.48	0.34
	TG 16:0_18:1_20:3	-		
TG 54:5	TG 18:1_18:1_18:3	3.35	-	-
	TG 18:1_18:2_18:2		-	-
TG 57:3	-	-	2.81	-
TG 58:2	-	-	4.88	-
TG 58:3	-	-	4.73	-
TG 58:4	-	-	4.70	-
CE 18:1	CE 18:1	-	-	1.77
CE 18:2	CE 18:2	1.40	3.90	3.01
CE 20:4	CE 20:4	-	-	1.76
SM 34:1	SM d18:1_16:0	0.70	2.10	1.34

A dash indicates that the lipid specie was not identified within the top 20 lipids of highest abundance and thus were not quantitated. qOrbi, Quadrupole-Orbitrap; QToF, Quadrupole-Time of Flight; timsToF, Trapped Ion Mobility Spectrometry-Quadrupole-Time of Flight
PC, phosphatidylcholine; LPC, lysophosphatidylcholine; TG, triacylglycerol; CE, cholesterol ester; SM, sphingomyelin.

Appendix B.2. % Coefficient of Variation in quantitation in negative polarity across platforms.

Brutto ID	Medio ID	qOrbi (n=3)	QToF (n=4)	timsToF (n=2)
		Confidence of Variation (%)		
PC 34:1	PC 16:0 _18:1	2.52	1.95	0.40
PC 34:2	PC 16:0_18:2	1.97	2.74	2.99
PC 36:1	PC 18:0_18:1	3.27	1.64	0.19
PC 36:2	PC 18:0_18:2	0.51	2.62	0.09
PC 36:3	PC 16:0 _20:3	2.11	1.88	4.14
	PC 18:1_18:2	2.13	0.81	2.29
PC 36:4	PC 16:0 _20:4	2.38	1.69	0.55
	PC 18:2_18:2	11.31	5.59	0.82
PC 38:3	PC 18:0 _20:3	4.18	2.95	2.35
PC 38:4	PC 18:0_20:4	2.80	1.45	0.25
PC 38:5	PC 16:0_22:5 | PC 18:1_20:4	2.38	1.68	1.91
PC 38:6	PC 16:0_22:6	4.15	1.17	1.89
LPC 16:0	LPC 16:0	1.69	11.03	0.04
LPC 18:0	LPC 18:0	2.80	3.56	2.06
LPC 18:1	LPC 18:1	-	-	0.03
LPC 18:2	LPC 18:2	-	7.14	2.12
PI 38:4	PI 18:0_20:4	3.99	-	-
SM 34:1	SM d18:1_16:0	2.09	2.11	3.00
SM 34:2	-	-	-	2.27
SM 40:1	SM d18:1_22:0	2.38	4.75	-
SM 42:1	SM d18:1_24:0	6.00	2.46	-
SM 42:2	SM d18:1_24:1	2.86	4.63	0.28
SM 42:3	SM d18:2_24:1	2.57	2.53	2.65

A dash indicates that the lipid specie was not identified within the top 20 lipids of highest abundance and thus was not quantitated. qOrbi, Quadrupole-Orbitrap; QToF, Quadrupole-Time of Flight; timsToF, Trapped Ion Mobility Spectrometry-Quadrupole-Time of Flight
PC, phosphatidylcholine; LPC, lysophosphatidylcholine; PI, phosphatidylinositol; SM, sphingomyelin.